DCl and N₂O₅ Chemistry at the Salty Glycerol Surface: Impact of Surfactants on Transport and Reactivity

by

Michael Shaloski

A dissertation submitted in partial fulfillment of the requirements for the degree of

Doctor of Philosophy

(Chemistry)

at the

UNIVERSITY OF WISCONSIN - MADISON

2017

Date of final oral examination: 12/21/2016

Gilbert Nathanson, Professor, Chemistry Edwin Sibert, Professor, Chemistry John Berry, Professor, Chemistry Timothy Bertram, Associate Professor, Chemistry Etienne Garand, Assistant Professor, Chemistry

Abstract

Interfacial reactions between atmospheric gases and sea spray aerosols play an important role by regulating the abundance of species such as O₃, OH, and CH₄. We explore these heterogeneous reactions through gas-liquid scattering experiments that direct gas-phase reagents at a continually-refreshed liquid film in vacuum. The reaction products and their kinetic energies are measured through velocity-resolved electron ionization and quadrupole mass spectrometry.

Chapter 3 of this thesis focuses on the entry and dissociation of DCl into glycerol-based sea spray mimics. DCl molecules react with glycerol, undergoing DCl \rightarrow HCl exchange and desorbing as HCl. The ratio of evaporating HCl to unreacted DCl yields the entry probability into solution. We use sodium dodecyl sulfate (SDS) as a proxy for oceanic surfactants and monitor the change in DCl entry by varying the salt and SDS concentration. The addition of salt (0.25 M NaCl, 0.5 M NaCl, 0.25 M MgCl₂, 0.25 M CaCl₂) enhances the surface concentration of DS⁻, which in turn limits the entry of DCl molecules by blocking their path. We observe that \sim 70% of impinging DCl molecules enter into bare glycerol and dissociate, regardless of salt, while the lowest DCl entry of 11% was found at the most compact monolayer observed (1.8 × 10^{14} cm⁻²), using 0.25 M MgCl₂ and 10.9 mM SDS.

N₂O₅ is a nighttime reservoir species that reacts in numerous ways with sea spray aerosols. In chapter 4, we explore interfacial reactions of N₂O₅ with Br⁻ in salty and surfactant-coated glycerol to produce Br₂. We compare Br₂ production between 2.7 M NaBr and 0.03 M tetrahexylammonium bromide (THABr) and find that the THA⁺ surfactant enhances reactivity by 270%, despite the solutions having similar Br⁻ surface concentrations. This enhancement is attributed to the trapping of an N₂O₅/Br⁻ complex in a charged hydrophobic pocket provided by surface THA⁺ ions. The addition of 0.5 M NaCl, 0.5 M NaBr, or 10 mM SDS lowers this

enhancement (120%, 170%, 110%) but does not eliminate it. 10 mM cetylammonium bromide generates a partial monolayer that produces the least Br_2 , likely because of the tight packing of its hexadecyl chains.

Table of Contents

| Abstract | i |
|--|------|
| Table of Contents | iii |
| List of Tables | vii |
| List of Figures | viii |
| Acknowledgments | x |
| 1. N ₂ O ₅ Chemistry at the Gas-Liquid Interface | |
| 1.1 The Gas-Liquid Interface | 1 |
| 1.2 Sea Spray Aerosols: Types and Production Mechanisms | 1 |
| 1.3 Impact of Aerosols on Climate | 3 |
| 1.4 Impact of Aerosols on the Environment | 4 |
| 1.5 Impact of N ₂ O ₅ on the Environment | 4 |
| 1.6 Previous Studies of Gas Entry and N ₂ O ₅ Reactivity | 6 |
| 1.6.1 N ₂ O ₅ and Sulfuric Acid Surfaces | 6 |
| 1.6.2 DCl Entry and Sulfuric Acid | 7 |
| 1.6.3 N ₂ O ₅ and Artificial Sea Spray Aerosols | 8 |
| 1.6.4 N ₂ O ₅ and Artificial Seawater: Effects of Phenol | 9 |
| 1.7 From Sulfuric Acid and Seawater to Glycerol | 10 |
| 1.7.1 DCl Entry into Glycerol | 10 |
| 1.7.2 Cl ₂ →Br ₂ Conversion with Glycerol – Rates and THABr Enhancements | 11 |
| 1.8 DCl Studies with SDS in Glycerol and Br ₂ Formation from 30 mM THABr | 12 |
| References | 14 |

| 2. | Experimental | Techniques: | Syntheses, | Molecular | Beam Scatt | tering, Liq | uid Film |
|----|--------------|--------------------|------------|-----------|------------|-------------|----------|
| | | | | | | | |

| \sim | | | | | |
|--------|----|----|----|----|----|
| G | PN | ei | ra | Ť١ | nn |

| 2.1 Overview | . 16 |
|--|------|
| 2.2 Synthesis | . 16 |
| 2.2.1 ClNO ₂ Synthesis | . 16 |
| 2.2.2 N ₂ O ₅ Synthesis | . 17 |
| 2.3 Generation of Molecular Beams | . 20 |
| 2.3.1 DCl Beams | . 20 |
| 2.3.2 N ₂ O ₅ Beams | . 21 |
| 2.4 Liquid Reservoirs | . 22 |
| 2.5 Liquid Preparation | . 23 |
| 2.6 Signal Optimization | . 23 |
| 2.6.1 Nozzle Alignment | . 23 |
| 2.6.2 Fenn Source Alignment | . 24 |
| 2.6.3 Detector Optimization | . 25 |
| 2.6.4 Aperture Optimization | . 25 |
| 2.7 Beast Issues | . 26 |
| 2.7.1 Main Chamber | . 26 |
| 2.7.2 Source and Source Differential | . 27 |
| 2.7.3 Detector and Detector Differential | . 28 |
| 2.8 Surface Tension Developments | . 28 |
| 2.9 N ₂ O ₅ Measurements and Dates | . 29 |
| Figures | . 30 |
| Tables | . 38 |
| References | . 41 |

| Ions on Gas Entry | |
|--|-------|
| 3.1 Summary | |
| 3.2 Introduction | |
| 3.3 Experimental Procedure | |
| 3.4 Results and Analysis | ••••• |
| 3.4.1 Surface Tension Measurements and Adsorption of DS on Salty Gly | cerol |
| 3.4.2 High-Energy Argon Scattering as a Probe of DS ⁻ Surface Coverage | |
| 3.4.3 DCl → HCl Exchange and DCl Entry | |
| 3.5 Discussion | |
| 3.5.1 DCl Entry into SDS-Coated Salty Glycerol | |
| 3.5.2 Implications for Gas Uptake into the Ocean and into Sea Spray | |
| 3.6 Acknowledgments | |
| 3.7 Appendix | |
| Tables | |
| References and Notes | |
| Figures | |
| Tables | |
| N ₂ O ₅ Reactions at the Salty Glycerol Surface: Effects of Tetrahexylammo | |
| N ₂ O ₅ Reactions at the Salty Glycerol Surface: Effects of Tetrahexylammo (THABr) | |
| | |
| (THABr) | |
| (THABr) 4.1 Introduction | |
| (THABr) 4.1 Introduction | |
| (THABr) 4.1 Introduction | |

| 4.3.1 Surface Tension Measurements | 2 |
|---|---|
| 4.3.2 High-Energy Argon Scattering | 4 |
| 4.3.3 Conversion of N ₂ O ₅ to Br ₂ in 2.7 M NaBr versus 30 mM THABr | 5 |
| 4.3.4 Salt Mixtures: 30 mM THABr + 0.5 M NaCl and 30 mM THABr + 0.5 M NaBr | |
| 8 | 8 |
| 4.3.5 Surfactant Effects: 30 mM THABr + 10 mM SDS and 10 mM CTAB 8 | 9 |
| 4.3.6 Chemical Ionization Mass Spectrometric detection of reaction products9 | 0 |
| 4.4 Discussion9 | 1 |
| 4.4.1 Enhancement of N ₂ O ₅ reactivity by THA ⁺ 9 | 1 |
| 4.4.2 Influence of the addition of salt to THABr9 | 4 |
| 4.4.3 Surfactant Control of N ₂ O ₅ Reactivity | 6 |
| 4.4.4 Detection of ClNO ₂ , Br ₂ , MNG, and DNG: CIMS versus Molecular Beam | |
| Scattering9 | 7 |
| 4.4.5 Atmospheric Implications 9 | 9 |
| 4.4.6 Conclusion | 0 |
| References 10 | 2 |
| Figures | 6 |
| Tables | 3 |

List of Tables

| 2.1 Incident beam energies | 38 |
|---|-----|
| 2.2 Detector electronic settings | 39 |
| 2.3 Dates of N ₂ O ₅ studies | 40 |
| 3.1 DS ⁻ surface concentrations and f_{exch} values | 60 |
| 4.1 Properties of glycerol and water | 113 |
| 4.2 Summary of surface tension results and slopes | 113 |
| 4.3 Summary of high-energy scattering results | 114 |
| 4.2 Summary of relative Br ₂ signals | 114 |

List of Figures

| 1.1 Snapshot of film droplet formation | 2 |
|--|----|
| 1.2 Snapshot of jet drop formation | 2 |
| 1.3 Depiction of the indirect and direct effects | 3 |
| 1.4 Possible reaction pathways for N ₂ O ₅ | 5 |
| 1.5 Impact of the Reactive Uptake of Aerosols | 6 |
| 1.6 N ₂ O ₅ hydrolysis as a function of butanol and hexanol coverage | 7 |
| 1.7 HCl entry as a function of added surfactant | 8 |
| 1.8 Rate of N ₂ O ₅ loss as a function of surface area concentration | 9 |
| 1.9 Percentage of DCl that enters solution and dissolves into the bulk | 11 |
| 1.10 Reaction scheme proposed by Faust et al | 12 |
| | |
| 2.1 Diagram of the ClNO ₂ synthesis apparatus | 30 |
| 2.2 Diagram of the N ₂ O ₅ synthesis apparatus | 30 |
| 2.3 Photo taken of the N_2O_5 synthesis apparatus | 31 |
| 2.4 Summary of important aperture sizes and distances | 32 |
| 2.5 Vertical slice of the detector umbra and penumbra on the lower reservoir | 33 |
| 2.6 Two main pieces of the detector cold-arm | 34 |
| 2.7 Fully-assembled detector cold-arm | 35 |
| 2.8 Plot of N ₂ O ₅ incident beam energy vs bath temperature | 36 |
| 2.9 Photos taken of the surface tension apparatus | 37 |
| | |
| 3.1 Collisions of gas-phase DCl with sodium dodecyl sulfate (SDS) | 67 |
| 3.2 Experimental setup | 68 |
| 3.3 Surface tension of SDS mixtures | 69 |
| 3.4 High-energy argon scatter with SDS solutions | 70 |

| 3.5 High and low-energy DCl scatter with bare and coated glycerol | 71 |
|--|-------|
| 3.6 DCl entry as a function of DS ⁻ coverage | 72 |
| 3.7 Molecular dynamics snapshots of SDS on water by Rideg et al | 73 |
| 3.A.1 Surface tension of SDS solutions before and after recrystallization | 74 |
| | |
| 4.1 Schematic of the formation of Br ₂ from N ₂ O ₅ | . 106 |
| 4.2 Experimental setup | . 107 |
| 4.3 Summary of surface tension measurements | . 108 |
| 4.4 High-energy argon scattering with glycerol solutions | . 109 |
| 4.5 Low-energy N ₂ O ₅ scatter from pure and 30 mM THABr glycerol | . 110 |
| 4.6 Br ₂ signal comparisons | .111 |
| 4.7 Product distributions of the reaction of N ₂ O ₅ with glycerol solutions | . 112 |

Acknowledgements

I am so thankful for the opportunity to work with Gil Nathanson. I could not have asked for a more thoughtful and dedicated professor. He encouraged me to persevere through many challenging situations. It was a pleasure to work alongside him and the entire CAICE organization to provide the results summarized in this thesis.

I am also thankful for the many lab mates who supported me over the years. T.J. Preston went out of his way to be a mentor when I first started. I enjoyed the many sessions we had going through papers and research ideas together. Jennifer Faust helped me tremendously before I even joined the Nathanson group. I remember the relief I felt as a new pohem lab TA when she gave me her old notes from when she taught the course. More recently, Joe Gord has been exceedingly generous with his time, taking charge of the lab and helping me meet many urgent deadlines. Tom Sobyra and Wen-Tsung Huang must be mentioned as they have been great friends to me. The undergraduates, particularly Matt Melvin, Mara Nevitt, and Sarah Quinn, have been especially helpful, and I simply could not have finished in time without them.

Lastly I want to thank my family, Mike, Gay, and Marisa Shaloski, who always think of me and support me. I appreciate the time they set aside even for the most minor conversations and how they continue to visit despite their fear of driving in snow. Though they are far away, they have helped make my time at UW-Madison enjoyable.

Chapter 1

N₂O₅ Chemistry at the Gas-Liquid Interface

1.1 The Gas-Liquid Interface

Gas-liquid interfaces are found throughout nature. It is common for students in the Nathanson group to discuss such examples as pulmonary surfactants that stabilize alveoli and support gas exchange,¹ molten salts that catalyze the production of gaseous SO₃ from SO₂,² or the formation of acid rain from the capture of SO₂ and NO_x by droplets.³ Our primary mission is to gain a detailed, "blow-by-blow" picture of interfacial chemistry. Many projects within the group have been motivated by understanding the chemistry between atmospheric molecules and aerosol surfaces. In recent years we have had the privilege to work as part of the Center for Aerosol Impacts on Climate and the Environment (CAICE).

The goal of CAICE is to bring the complex chemistry of sea spray aerosols into lab. Previously, Seong-Chan Park's work brought the chemistry between N₂O₅ and stratospheric sulfuric acid aerosols into the lab. Former postdoc Logan Dempsey and student Jennifer Faust mimicked the reactions between Cl₂ and bromide-containing, arctic aerosol particles. My thesis research specifically builds upon what has been learned by our group and extends our knowledge to reactions between N₂O₅ and sea spray aerosols and ocean surface mimics using salty and surfactant-coated glycerol.

1.2 Sea Spray Aerosols: Types and Production Mechanisms

Sea spray are droplets produced from breaking waves and bursting bubbles that range in size from nanometers to millimeters.⁴ The main categories of sea spray are film droplets, jet drops, and spume drops. Spume drops are generated when the wind is able to physically separate

droplets from the crest of the wave. These drops are generally 100 µm in size or greater and spend very little time in the atmosphere, returning quickly to the ocean surface. Our focus in CAICE is instead on the smaller film and jet drops that can reside in the atmosphere for several days, impacting cloud formation and air quality.

Film and jet droplets are formed from bursting bubbles.⁴ Once a wave breaks, air can become trapped within the water column, generating bubbles that rise to the surface. At the surface, the formed bubble caps become thin and eventually burst, generating film droplets, shown in a snapshot from Lhuissier et al. (Figure 1).⁵ After the cap breaks, a jet is formed that falls apart into several droplets a few millimeters above the surface. These are jet droplets shown in Figure 2.⁶

Film droplets are typically submicron in size, with a range between 0.01 μ m to 2 μ m.⁴ The chemical composition of film droplets often mimics the surface region of the ocean, which is enriched with organic molecules.⁷ This upper region is referred to as the sea-surface microlayer,

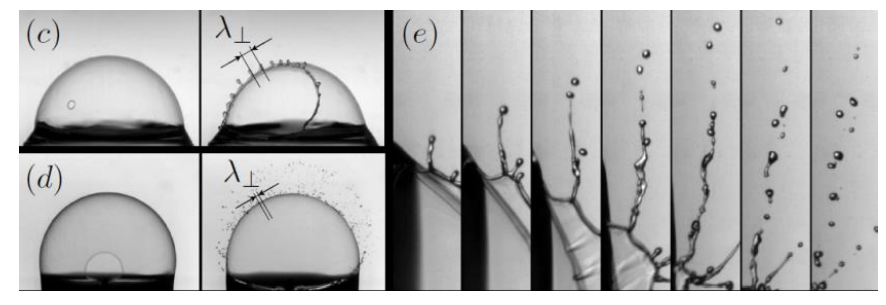


Figure 1. Snapshots of the formation of film droplets. (c) and (d) show 14 and 11.5 mm radius bubbles bursting. (e) provides a close-up.

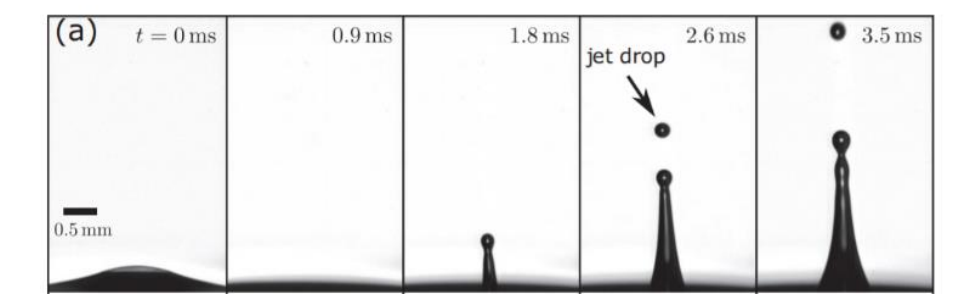


Figure 2. Snapshot of the formation of jet droplets from a glycerol-water solution.

which can contain species such as carbohydrates, lipids, and proteins. Some of these molecules have long hydrocarbon chains, potentially longer than 20 carbons. Some examples found in aerosols include saturated and unsaturated fatty acids, organosulfates, and sulfonates. In contrast, jet droplets are typically $1-50~\mu m$ in size with a chemical composition reflecting the bulk composition of sea water which contains more soluble species.

1.3 Impact of Aerosols on Climate

Aerosols are liquid or solid particles suspended in the air that play an important role in the radiative forcing of the planet, through both direct and indirect effects (Figure 3).^{9,10} The direct effect refers to the direct scattering and absorption of light by individual particles, while the indirect effect

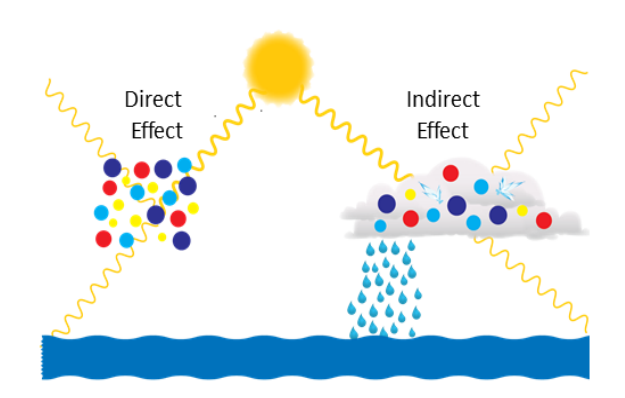


Figure 3. Depiction of the direct and indirect effects.

refers to the change in cloud properties caused by particles that can modify the amount of light reflected. These effects depend on the size and composition of the aerosols. Sub-micron particles can more efficiently reflect light and have longer lifetimes in the atmosphere. Some aerosols, such as carbon particles, are more prone to absorbing light and can potentially warm the atmosphere. Aerosols can also increase the density of smaller cloud particles, increasing cloud albedo. Smaller particles additionally delay precipitation and lead to longer cloud lifetimes, leading to more reflected light. Understanding the complex composition of sea spray aerosols and their impact on radiative forcing is a major goal of the CAICE program.

1.4 Impact of Aerosols on the Environment

Aerosols play an important role in the local environment by providing a surface for heterogeneous chemistry. Heterogeneous or multiphase chemistry includes processes such as interfacial transport, reactions at the interface, and reactions taking place within a droplet or wet surface.¹¹ An example of this is the heterogeneous oxidation of SO₂ to sulfate through water droplets, leading to acid rain.^{3, 12} Some of the most influential heterogeneous reactions in the troposphere are scavenging reactions by aerosols that remove nitrogen oxides (NO₃, HNO₃, N₂O₅, RONO₂) and hydrogen oxides (HO₂, H₂O₂, ROOH), which ultimately influence tropospheric ozone and OH concentrations. These scavenging reactions can be altered by the composition of the aerosol.

1.5 Impact of N₂O₅ on the Environment

A main focus within CAICE is understanding the heterogeneous chemistry of N_2O_5 with sea spray aerosols and ocean surfaces. N_2O_5 acts as a nighttime reservoir for NO_x ($NO_x = NO + NO_2$), a pollutant produced by fossil fuel combustion, and plays an important role in tropospheric chemistry. During the day, N_2O_5 is quickly photolyzed into $NO_2 + NO_3$, leading to the production of tropospheric ozone.¹³

NO₂ + hv (
$$<$$
 420 nm) \rightarrow NO + O(3 P)
O(3 P) + O₂ \rightarrow O₃

Tropospheric ozone is harmful to animal life by damaging cells that line the lungs. ¹⁴ Ozone can also enter crops, damaging them through oxidation that darkens and reddens the leaves. Soybean, cotton, and peanut yields are particularly sensitive and can drop by 20% at heightened ozone levels. ¹⁵

One of the primary routes for removal of N_2O_5 and NO_x is their heterogeneous reaction with aqueous particles and droplets, such as sea spray aerosols. A schematic diagram of potential reactions between N_2O_5 and a lipid (lipid A from a lipopolysaccharide) at the sea spray surface is depicted in Figure 4. N_2O_5

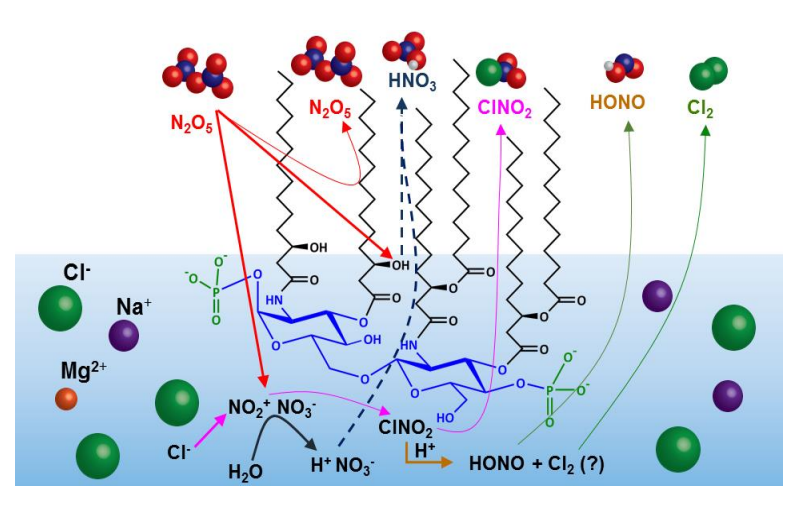


Figure 4. Possible reaction pathways for N_2O_5 at the sea spray aerosol and ocean surface.

is thought to first ionize after solvation into NO_2^+ and NO_3^- .¹⁶ NO_2^+ can react with H_2O to generate H^+ and NO_3^- within a droplet, depositing itself back to the earth surface and removing NO_x from the atmosphere.^{13, 17} Alternatively in the presence of Cl^- (such as in sea spray), N_2O_5 can react to form $ClNO_2$.¹⁸ However the lifetime of $ClNO_2$ is very short, as it quickly photolyzes during the day (over ~ 1 hour) to produce NO_2 and Cl atoms, one of the most reactive species in the atmosphere.¹⁹

Tropospheric ozone can also be photolyzed to produce excited state oxygen, which lead to OH radicals through the following steps:

$$O_3 + hv \rightarrow O(^1D) + O_2$$

$$O(^{1}D) + H_{2}O \rightarrow 2 OH$$

OH radicals, like Cl atoms, are able to react with methane and other alkanes in the atmosphere through hydrogen abstraction. The influence of N_2O_5 on these species is clearly shown by the models performed by Macintyre et al., summarized in Figure 5.²⁰ Macintyre et al. varied the reactive uptake coefficient of N_2O_5 from 10^{-5} to 1 and determined its effect on the concentrations

of ozone and hydroxyl radical and on the lifetime of methane in the atmosphere. This uptake coefficient is the probability that N₂O₅ will undergo an irreversible, heterogeneous reaction upon collision with the aerosol particle. This conversion leads to the removal of N₂O₅ by trapping the species in solution and depositing the products through precipitation. As the reactive uptake coefficient is increased from 10⁻⁵ to 1, their model predicts a dramatic influence in O₃ and OH concentrations in the troposphere (12 % and 18% respectively).

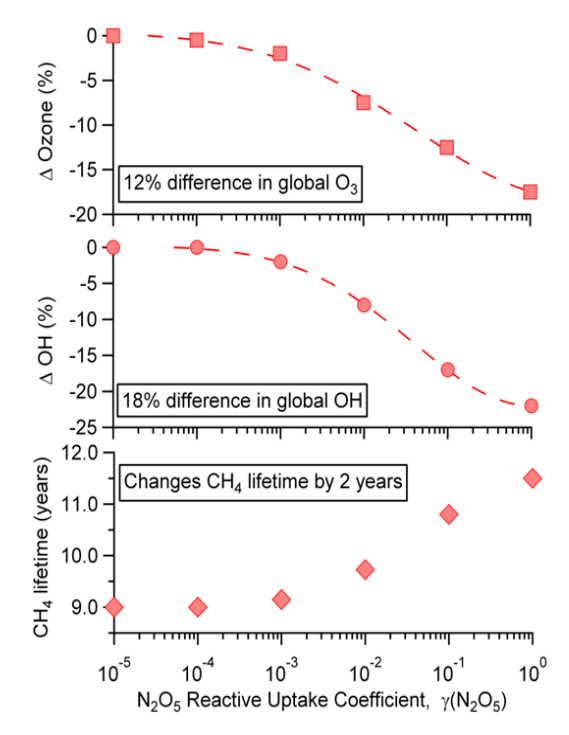


Figure 5. Impact of the Reactive Uptake of Aerosols (Macintyre et al.).

Additionally, the methane lifetime in the troposphere is increased by an additional two years.

These changes demonstrate the dramatic influence that sea spray aerosols can have on the global environment.

1.6 Previous Studies of Gas Entry and N₂O₅ Reactivity

My thesis explores gas entry and N₂O₅ reactivity with sea spray and ocean surface mimics. Our group, as well as many others, have performed similar studies that informed the direction of my research. Below is a summary of key results in the literature.

1.6.1 N₂O₅ and Sulfuric Acid Surfaces

In the lower stratosphere sulfuric acid aerosols influence N_2O_5 concentrations by providing a site for hydrolysis into HNO₃. Seong-Chan Park and Daniel Burden explored this reaction in the

Nathanson group by directing a beam of N₂O₅ molecules at 60 and 68 wt % sulfuric acid solutions.²² Hexanol and butanol were added to the solution to mimic surfactants that could coat the particle. Park reported his findings in terms of the ratio of hydrolysis probabilities between bare and coated sulfuric acid ($\gamma_{\rm film}/\gamma_{\rm bare}$). The result showed a significant linear trend between surface coverage (fraction of a complete monolayer) and $\gamma_{\rm film}/\gamma_{\rm bare}$

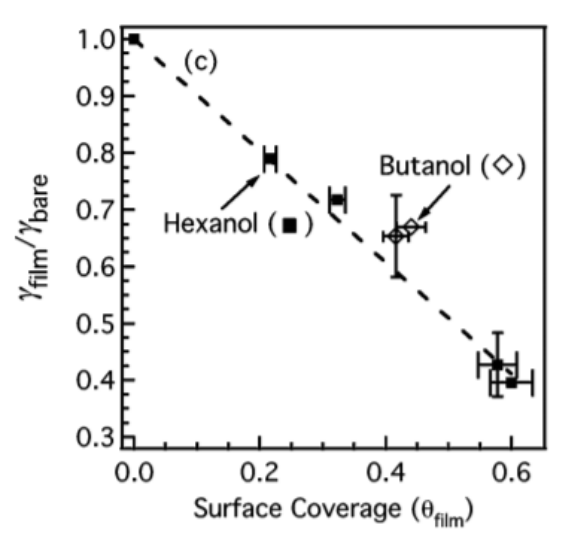


Figure 6. N_2O_5 hydrolysis as a function of butanol and hexanol coverage.

shown in Figure 6. The decrease in hydrolysis from the addition of the alcohols is attributed to blocking by the alkyl chains, which prevents N_2O_5 from reaching the sulfuric acid surface. Though it was not observed, an additional possibility is the production of the alkyl nitrate through ROH + $N_2O_5 \rightarrow RONO_2 + HNO_3$ and ROH + $HNO_3 \rightarrow RONO_2 + H_2O$. Clearly short-chained alcohols can influence the reactivity of N_2O_5 at the surface; however, it is unlikely that the high surface coverages ($\sim 3 \times 10^{14}$ cm⁻²) used in this study are present on stratospheric aerosols.

1.6.2 DCl Entry and Sulfuric Acid

Reactions of gas-phase HCl can also be used to probe the effects of surfactants on interfacial gas transport. HCl molecules that reach the surface of a deuterated solvent and dissociate will reemerge later as DCl. By comparing the DCl/HCl ratio, one can determine the entry probability of HCl into solution. Jennifer Lawrence and Samuel Glass in the Nathanson group found that the addition of hexanol and butanol to 60 - 68 wt % D₂SO₄ at 213 K actually

enhanced HCl entry instead of simply blocking entry as was the case with N₂O₅. This is attributed to the increase in available HCl protonation sites provided by the alcohol surfactants. The only point at which hexanol suppresses HCl entry is when the sulfuric acid concentration is reduced to 56 wt %, where the R-OH₂⁺ concentration is decreased such that the monolayer becomes more compact and blocks HCl transport through the hexyl chains.

Daniel Burden and Alexis Johnson continued these studies in the Nathanson group by adding pentanoic acid as well pentanoic acid/hexanol mixtures to sulfuric acid. The

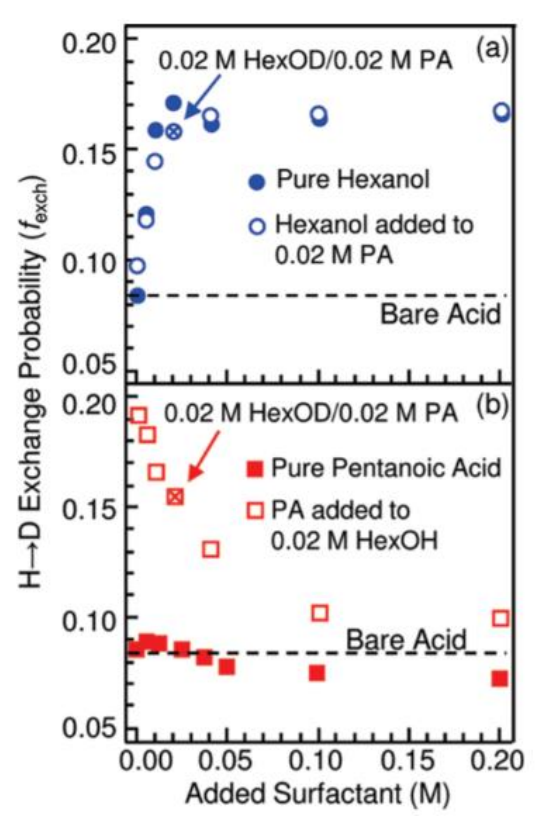


Figure 7. *HCl entry as a function of added surfactant.*

resulting HCl → DCl exchange probabilities with surfactant concentration are shown in Figure 7 for 68 wt % sulfuric acid at 213 K. Pentanoic acid is a weaker base than hexanol and can pack more tightly. For this reason, pentanoic acid enhances HCl uptake at low concentrations (through protonation of –COOH) but has a decreased enhancement at higher concentrations where the more tightly packed chains block the passage of HCl (Figure 7b). Mixing hexanol with pentanoic acid produced results similar to a hexanol-only solution. This is due to hexanol having a higher surface activity and dominating the surface region.

1.6.3 N₂O₅ and Artificial Sea Spray Aerosols

While sulfuric acid is an important subphase to represent stratospheric aerosols, more

neutral aqueous solutions are representative of tropospheric sea spray aerosols. Thornton et al. produced submicron artificial seawater aerosols to better understand N_2O_5 to $ClNO_2$ conversion. Aerosols produced from an atomizer were sent through an N_2O_5 flow reactor, after which products were detected using chemical-ionization mass spectrometry.

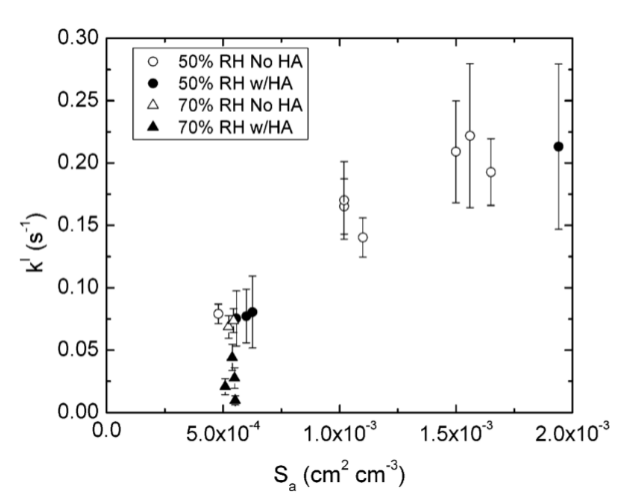


Figure 8. Rate of N_2O_5 loss as a function of surface area concentration.

By adding hexanoic acid vapor, the authors

were able to make the first measurements of a monolayer surfactant restricting the heterogeneous reaction between aerosols and trace atmospheric gases. At a relative humidity of 70% (Figure 7), the addition of hexanoic acid, believed to be one monolayer thick, reduced the reactivity of N_2O_5 by a factor of 3-4. In addition, Alan Bertram and his group have investigated the uptake of N_2O_5 into sulfuric acid coated with straight-chain and branched alcohols and carboxylic acids, both singly and in mixtures. These systematic studies indicate that such surfactants can reduce N_2O_5 uptake by as much as 100-fold.²⁴

1.6.4 N₂O₅ and Artificial Seawater: Effects of Phenol

Ryder et al. in the Bertram group have also studied the influence of surfactants on the conversion of N_2O_5 into $ClNO_2$ with artificial seawater.²⁵ The authors specifically looked at the influence of phenol, which can be enhanced at the surface by a factor of 100 with respect to the bulk solution. N_2O_5 was passed over synthetic seawater solutions, and the products were detected by chemical-ionization mass spectrometry. The addition of phenol provided an additional reaction pathway for N_2O_5 , the nitration of the phenol ring. Adding 8 mM of phenol to the bulk

generates a surface phenol concentration of 2×10^{13} cm⁻². Despite concentrations of Cl⁻ at 0.5 M greatly outnumbering phenol in the bulk, the phenol addition reduced the reaction probability of ClNO₂ from 0.8 to 0.4. The sensitivity of N₂O₅ specifically to the change of phenol at the surface shows the interfacial nature of the reaction.

1.7 From Sulfuric Acid and Seawater to Glycerol

As shown above, surface-active species can play an important role in heterogeneous chemistry, potentially disrupting hydrolysis or providing new reaction sites. These studies focused on artificial seawater for mimicking sea spray aerosols and sulfuric acid for mimicking stratospheric aerosols. The focus of my thesis is on mimicking sea spray aerosols and the ocean surface in a vacuum chamber. While seawater has the potential to be placed in vacuum using microjet techniques in the future, my experiments relied on using glycerol, a low vapor pressure liquid. Glycerol (C₃H₈O₃) is a protic liquid that has a significantly lower vapor pressure than water (10⁻⁴ vs 20 Torr at 20 °C). It also has a high dielectric strength (43) and surface tension (64 dyn/cm) similar to water (68 and 72 dyn/cm). However, glycerol's viscosity is one thousand times larger than that of water (1.4 vs 10⁻³ Pa·s). Glycerol was chosen not only because of its low vapor pressure and similarity to water: it may also be a good mimic of a sea surface microlayer rich in carbohydrates. Though the Nathanson group had not studied N₂O₅ chemistry with glycerol solutions previously, several studies exploring DCl gas entry and Cl₂ reactivity have been performed.

1.7.1 DCl Entry into Glycerol

Similar to the HCl/D₂SO₄ studies before, DCl can also be used to explore the entry of acidic gases into pure and salty glycerol. If DCl enters into solution and ionizes, D→H

exchanged HCl will later reemerge.

These studies were used to explore the dynamics of acid dissociation in the interfacial region of protic liquids and are summarized by Dempsey et al.²⁶

Salts were found to influence the entry of DCl into solution. The

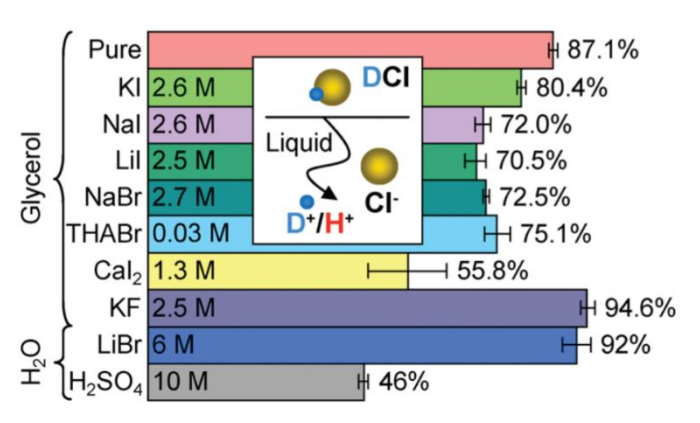


Figure 9. Percentage of DCl that enters solution and dissolves into the bulk.

pathway for DCl is predominantly dissociation into the solvent, as reflected in Figure 9. The addition of salts decreases the fraction of DCl molecules that enter and dissociate by 10 to 30 %. This is likely due to the prebinding of interfacial OH groups of glycerol and water to cations and anions and their removal as reactive sites.

1.7.2 $Cl_2 \rightarrow Br_2$ Conversion with Glycerol – Rates and THABr Enhancements

Bromine chemistry reduces the abundance of tropospheric ozone, where the bromine species are thought to arise from Br^- ions present in sea spray aerosols, snow, and ice surfaces.²⁷ Dempsey et al. studied the conversion of Cl_2 to Br_2 via Br^- by directing Cl_2 molecules at a film of 2.7 M NaBr in glycerol, which generates a Br^- surface concentration of $\sim 7 \times 10^{13}$ cm⁻². Based on their results and kinetics models, the authors determined that Br_2 is formed primarily through the intermediate pathway: $Cl_2Br^- + Br^- \rightarrow Br_2Cl^- + Cl^-$. They found that 23% of the Cl_2 molecules that strike the surface at thermal collision energies proceed to form Br_2 , whereas less than 1% evaporat as BrCl. The reaction to form BrCl and Br_2 takes place in tens of microseconds, indicating that the reaction occurs within the top several monolayers.

Faust et al. expanded this study by exploring the role of surfactants in the reaction of Cl_2 to Br_2 .²⁸ Tetrahexyl ammonium bromide (THABr), a common phase-transfer catalyst, was

chosen as the surfactant. A Cl₂
beam was directed at both 2.7 M
NaBr and 30 mM THABr
solutions in glycerol. These
solutions generate similar
surface concentrations of Br⁻, 7
×10¹³ cm⁻² in NaBr and 8 ×10¹³
cm⁻² in THABr. Surprisingly,

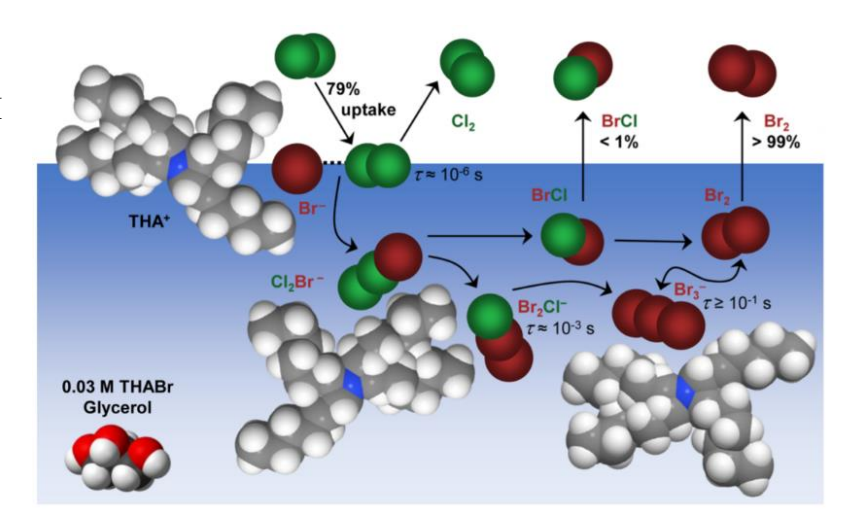


Figure 10. Reaction scheme proposed by Faust et al.

the THABr solution enhanced the reactivity of Cl₂, despite having a similar surface concentration to 2.7 M NaBr and exposing hexyl chains at the surface that could prevent Cl₂ entry. The Cl₂ reaction probability rose from 23% with 2.7 M NaBr to 79% with 30 mM THABr, a 3.4-fold increase.

A schematic of the reaction is shown in Figure 10. The enhancement is attributed to the orientation of the hexyl chains and ammonium headgroup at the surface. Three of the chains are predicted to point upwards from the surface, creating a hydrophobic pocket that may enhance reactivity. Cl_2Br^- is likely formed and stabilized near the pocket, increasing the time to react with an additional Br^- . Remarkably, the THA^+ cation appears to bind strongly enough to Br_3^- (created by $Br_2 + Br^- \leftrightarrow Br_3^-$) to increase the effective solvation time of Br_2 in glycerol from 10 μs to over 0.1 s.

1.8 DCl Studies with SDS in Glycerol and Br₂ Formation from 30 mM THABr

The HCl, DCl, and N_2O_5 studies mentioned above are foundational to the work in this thesis. The next chapter focuses on the experimental procedures, concerns, and recommendations in producing HCl, DCl, and N_2O_5 beams. One of the major works in the thesis

is the development of a large-scale N₂O₅ synthesis and beam generation. This involves careful avoidance of moisture in the synthesis and using specific traps to remove HNO₃ present in the sample. Discussions of the Hal chamber, Beast chamber, and Fenn source are present as well.

Chapter three focuses on the entry of DCl into salty glycerol as a proxy for gas entry into sea spray. Sodium dodecyl sulfate was added to the salty solutions to observe the effect of long alkyl chains on the transfer of gas molecules through the interface. Solutions containing 0.25 M Na $^+$, 0.5 M Na $^+$, 0.25 M Mg $^{2+}$, and 0.25 M Ca $^{2+}$ were studied with SDS concentrations ranging from 0 to 10.9 mM. DCl entry decreased steadily with increasing DS $^-$ coverage. The presence of salt also forced more surfactant to the surface, with divalent cations having the largest impact. The lowest DCl entry probability observed was 0.11 \pm 0.05 using 0.25 M MgCl₂ and 10.9 mM SDS.

Chapter 4 discusses the production of Br₂ from the reaction of N₂O₅ with bromide-rich, glycerol. The main comparison is between 2.7 M NaBr and 30 mM THABr glycerol mixtures. Both solutions have interfacial Br⁻ concentrations of $\sim 7-8\times 10^{13}$ cm⁻². Despite this similarity, the THABr solution enhances the production of Br₂ by a factor of 2.2 over NaBr. This comparison indicates that the hexyl chains of the surfactant do not inhibit the N₂O₅ reaction. It is possible that the cationic headgroup stabilizes N₂O₅ or an intermediate at the surface, allowing more time for reaction. Studies adding NaBr or NaCl salts or the SDS surfactant to 30 mM THABr were performed, reducing the enhancement in all cases.

References

- 1. Sherwood, L., Fundamentals of Human Physiology. 4th ed.; 2012.
- 2. Lantelme, F.; Groult, H., Molten Salts Chemistry: From Lab to Applications. 2013.
- 3. Christensen, E. R.; Li, A., *Physical and Chemical Processes in the Aquatic Environment*. 2014.
- 4. Veron, F., Ocean Spray. *Annu. Rev. Fluid Mech.* **2015,** *47*, 507-538.
- 5. Lhuissier, H.; Villermaux, E., Bursting bubbles. *Phys. Fluids* **2009**, *21*, 091111.
- 6. Walls, P. L. L.; Henaux, L.; Bird, J. C., Jet Drops from Bursting Bubbles: How Gravity and Viscosity Couple to Inhibit Droplet Production. *Phys. Rev. E* **2015**, *92*, 021002-2.
- 7. Cunliffe, M.; Engel, A.; Frka, S.; Gašparovic', B.; Guitart, C.; Murrell, J. C.; Salter, M.; Stolle, C.; Upstill-Goddard, R.; Wurl, O., Sea Surface Microlayers: A Unified Physicochemical and Biological Perspective of the Air–Ocean Interface. *Prog. Oceanogr.* **2014**, *109*, 104–116.
- 8. Cochran, R. E.; Laskina, O.; Jayarathne, T.; Laskin, A.; Laskin, J.; Lin, P.; Sultana, C.; Lee, C.; Moore, K. A.; Cappa, C. D.; Bertram, T. H.; Prather, K. A.; Grassian, V. H.; Stone, E. A., Analysis of Organic Anionic Surfactants in Fine and Coarse Fractions of Freshly Emitted Sea Spray Aerosol. *Environ. Sci. Technol.* **2016**, *50*, 2477-2486.
- 9. Myhre, G.; Shindell, D. 8. Anthropogenic and Natural Radiative Forcing; 2013.
- 10. Andreae, M.; Annegarn, H.; Barrie, L.; Feichter, J.; Hegg, D.; Jayaraman, A.; Leaitch, R.; Murphy, D.; Nganga, J.; Pitari, G. 5. Aerosols, their Direct and Indirect Effects; 2001.
- 11. Molina, M. J.; Molina, L. T.; Kolb, C. E., Gas-Phase and Heterogeneous Chemical Kinetics of the Troposphere and Stratosphere. *Annu. Rev. Phys. Chem.* **1996**, *47*, 327-367.
- 12. Beilke, S.; Gravenhorst, G., Heterogeneous SO₂-Oxidation in the Droplet Phase. In *Sulfur in the Atmosphere*, 1978.
- 13. Finlayson-Pitts, B. J.; Pitts, J. M., *Upper and Lower Atmosphere: Theory, Experiments, and Applications.* 1999.
- 14. EPA The Ozone Problem. https://www3.epa.gov/region1/airquality/oz_prob.html.
- 15. Service, U. A. R. Effects of Ozone Air Pollution on Plants. https://www.ars.usda.gov/southeast-area/raleigh-nc/plant-science-research/docs/climate-changeair-quality-laboratory/ozone-effects-on-plants/.
- 16. Gaston, C. J.; Thornton, J. A., Reacto-Diffusive Length of N₂O₅ in Aqueous Sulfate- and Chloride-Containing Aerosol Particles. *J. Phys. Chem. A* **2016**, *120*, 1039-1045.
- 17. Barker, J. R., *Progress and Problems in Atmospheric Chemistry*. 1995.

- 18. Mielke, L. H.; Furgeson, A.; Osthoff, H. D., Observation of ClNO₂ in a Mid-Continental Urban Environment. **2011**, *45*, 8889-8896.
- 19. Ball, S., Atmospheric chemistry at night. ECG Environmental Briefs **2014**, 3.
- 20. Macintyre, H. L.; Evans, M. J., Sensitivity of a Global Model to the Uptake of N₂O₅ by Tropospheric Aerosol. *Atmos. Chem. Phys.* **2010**, *10*, 7409-7414.
- 21. Wennberg, P. O.; Cohen, R. C.; Stimpfle, R. M.; Koplow, J. P.; Anderson, J. G.; Salawitch, R. J.; Fahey, D. W.; Woodbridge, E. L.; Keim, E. R.; Gao, R. S.; Webster, C. R.; May, R. D.; Toohey, D. W.; Avallone, L. M.; Proffitt, M. H.; Loewenstein, M.; Podolske, J. R.; Chan, K. R.; Wofsy, S. C., Removal of Stratospheric O₃ by Radicals: In Situ Measurements of OH, HO₂, NO, NO₂, ClO, and BrO. *Science* **1994**, 266, 398.
- 22. Park, S.; Burden, D. K.; Nathanson, G. M., The Inhibition of N₂O₅ Hydrolysis in Sulfuric Acid by 1-Butanol and 1-Hexanol Surfactant Coatings. *J. Phys. Chem. A* **2007**, *111*, 2921-2929.
- 23. Thornton, J. A.; Abbatt, J. P. D., N2O5 Reaction on Submicron Sea Salt Aerosol: Kinetics, Products, and the Effect of Surface Active Organics. *J. Phys. Chem. A* **2005**, *109*, 10004-10012.
- 24. Bertram, A. K.; Knopf, D. A.; Cosman, L. M., N₂O₅ Reactive Uptake on Aqueous Sulfuric Acid Solutions Coated with Branched and Straight-Chain Insoluble Organic Surfactants. *J. Phys. Chem. A* **2008**, *112*, 2386-2396.
- 25. Ryder, O. S.; Campbell, N. R.; Shaloski, M. A.; Al-Mashat, H.; Nathanson, G. M.; Bertram, T. H., Role of Organics in Regulating ClNO₂ Production at the Air–Sea Interface. *J. Phys. Chem. A* **2015**, *119*, 8519-8526.
- 26. Dempsey, L. P.; Brastad, S. M.; Nathanson, G. M., Interfacial Acid Dissociation and Proton Exchange Following Collisions of DCl with Salty Glycerol and Salty Water. *J. Phys. Chem. Lett.* **2011**, *2*, 622-627.
- 27. Foster, K. L.; Plastridge, R. A.; Bottenheim, J. W.; Shepson, P. B.; Finlayson-Pitts, B. J.; Spicer, C. W., The Role of Br, and BrCl in Surface Ozone Destruction at Polar Sunrise *Science* **2001**, *291*, 471.
- 28. Faust, J. A.; Dempsey, L. P.; Nathanson, G. M., Surfactant-Promoted Reactions of Cl₂ and Br₂ with Br⁻ in Glycerol. *J. Phys. Chem. B* **2013**, *117*, 12602-12612.

Chapter 2

Experimental Techniques: Syntheses, Molecular Beam Scattering, Liquid Film Generation

2.1 Overview

Experiments discussed in this thesis were primarily performed using the molecular beam scattering machine located in the south side of room 7329. This machine is often referred as Hal, the H₂SO₄ machine, or the AFOSR machine. Hal is composed of 5 chambers: source, source differential, main (including the cube addition), detector differential, and detector. These chambers are discussed in thorough detail in Melissa Antman's and Dan Burden's theses. ¹⁻² This chapter will provide a detailed description of the methods used to synthesize N₂O₅ and ClNO₂. This chapter also includes a description of techniques to optimize the scattering signal, developments in surface tension measurements, preparation of liquid samples and films, and issues with the Beast machine located in 7329.

2.2 Synthesis

2.2.1 ClNO₂ Synthesis

CINO₂ was explored early on as a potential source for NO₂⁺ to look for reaction products with salty and surfactant-coated glycerol. We only used CINO₂ in four experiments in September 2015 and instead focused on N₂O₅ for most experiments. The synthetic method used for CINO₂ was primarily taken from the procedure provided by George Brauer in the *Handbook of Preparative Inorganic Chemistry* with modifications suggested by John Berry.³ Figure 1 depicts the synthesis apparatus. A three-neck round-bottom flask is placed within an ice water bath. The central neck is connected to an addition funnel. The side connections are each occupied with a glass hose adapter. A thin 1/8" Teflon tube is slid through the adapter on the entrance side (depicted on the left) until the tube reaches the bottom of the round-bottom flask. A

hose for N₂ flow runs over the Teflon tubing and connects to the entrance adapter. The exit adapter is connected to a hose that flows into a glass trap cooled by a dry ice/acetone bath.

When the apparatus is assembled, the addition funnel is briefly removed to allow the addition of a stir bar and 60 g of 95-98 wt % sulfuric acid. This is followed by the slow addition of 28 g of fuming nitric acid. The addition funnel is then placed back into the central position and filled with 31 g of chlorosulfonic acid. A hose clamp is placed on the N₂ gas hose on the entrance side, forcing N₂ through the 1/8" Teflon tube. The N₂ gas is adjusted so that the acid solution begins to bubble vigorously. The stir bar should also begin stirring for additional movement in the solution. The addition funnel should be adjusted so that a drop of acid is released every few seconds. The bubbling and stirring must be strong enough to push the ClNO₂ out of solution and into the gas phase and into the trap.

If the collected sample is a yellow liquid at -70 °C, then the product is ClNO₂. However, a solid red sample at this temperature indicates that ClNO has formed, which can come about from H₂O or NO₂ gas. In order to reduce the NO₂ content of aged fuming nitric acid, attempts were made to bubble N₂ through an aliquot of fuming nitric acid before addition to the flask. This may have helped, since the red color was reduced in the solution (white fuming nitric acid is ideal).

$2.2.2 N_2O_5$ Synthesis

The procedure for N₂O₅ synthesis was based on the method developed by Davidson et al.⁴ The apparatus is depicted in Figures 2 and 3 and is comprised of three glass traps, four stainless steel valves, and ½" Teflon tubing connected by ½" stainless steel ultratorr fittings.

The three traps are connected in series, where the central trap contains P₂O₅-coated glass beads (4 mm diameter, soda-lime). Note that buna o-rings will degrade and become brittle over time

and should be replaced periodically. The valves are connected so that the O₃/O₂ inlet shown in Figure 2 can be directed in either direction through the traps. The NO is mixed with the O₃/O₂ through an ultratorr tee that leads to the 1st trap. After being assembled, the O₃/O₂ inlet is replaced with a Baratron pressure transducer and is pumped down using a mechanical pump connected to a LN₂ cold trap to remove moisture and check for leaks. Ideally, the internal pressure reading should remain constant when sealed from the pump and typically reads about 30 Torr (0.3 volts on a 10,000 Torr baratron). The pressure may actually be lower and this is just a baseline issue when at the lower end of the Baratron detection range.

After confirming that there are no leaks, the Baratron is replaced with the O_3/O_2 inlet. The ozone is generated using the department ozonator. UHP oxygen is sent into the ozonator until the ozonator's internal pressure is between 7 and 10 psi with an outgoing flow of \sim 3 slpm. The cooling water inlet of the ozonator is connected to the city water line inside of the hood, while the cooling outlet is run into the liquid drain of the hood. Water should be flowing before any power is turned on. The next step is flipping the two "on" switches of the ozonator followed by slowly ramping the voltage up to 110 V. A chirping is first heard at \sim 60 V indicating that ozone is being formed. The produced ozone is directed towards the NO (cylinder currently closed) tee-connection and flows through the traps before escaping into the hood.

The NO cylinder is opened so that the regulator is delivering ~ 10 psi of gas. The valve between the NO cylinder and the ultratorr-tee connector is adjusted so that the orange/red color just barely disappears and becomes colorless. The orange/red color comes about from NO₂ that is generated from the reaction between O₃/O₂ uand NO. When the NO flow is reduced to the level that the mixture with ozone becomes colorless, then the ozone is at such an excess that no NO₂ is leftover and the product is likely N₂O₅. This colorless mixture is run through the traps for

about 10 minutes without being trapped. This initial run provides an additional method for removing moisture, since any N_2O_5 or NO_2 will react with H_2O and be removed out from the apparatus. After 10 minutes, the final/third trap is placed within a dry ice/acetone bath to collect the generated N_2O_5 .

Overall, the NO and O_3 is mixed just before the 1^{st} trap to generate N_2O_5 . It passes first through an empty trap and then through a trap containing P_2O_5 to reduce moisture. This trap also potentially converts any HNO₃ to N_2O_5 (2 HNO₃ + $P_2O_5 \rightarrow N_2O_5 + 2$ HPO₃). The final trap collects the N_2O_5 , and the uncollected gas exits into the hood. The process is continued for about an hour, producing a bubbler filled with white solid of ~5 g. Note that NO₂ can be deposited at dry ice/acetone temperatures and will create a yellow sample. Ideally the generated gas flow should be colorless.

If NO₂ is collected, there are two methods to remove it. The easiest and recommended method is to remove it during the scattering experiment. When the sample is first warmed to -30 to -15 °C, NO₂ is driven off quickly, generating a brown gas in the beam line. After flowing a carrier gas through the sample \sim 30 minutes, the NO₂ is driven off, and the sample only produces colorless gas. An alternative method can be implemented using the synthesis apparatus. To do this, remove the NO inlet and switch the valves such that the ozone flow is reversed through the traps. The dry ice/acetone bath is then moved to the empty trap, while the trap containing the sample is warmed. Any NO₂ will evaporate and react with the O₃/O₂ mixture, hopefully converting NO₂ to N₂O₅. The sample is then collected in the trap that was originally labeled as the "1st Trap" in Figure 2. This method is not recommended as it allows more time for the sample to be exposed to moisture and produce HNO₃.

Another common issue is clogging in the sample trap (typically the 3rd trap) if the

synthesis is continued for more than one hour, often caused by N_2O_5 filling the stem. In order to correct this, the NO inlet should be removed and the valves should redirect the flow so that ozone will pass from the clogged trap to the empty trap. Be careful that the ozone pressure does not build up by slowly leaking a portion through a valve into the hood. Warm the sample trap until the sample is unclogged and then place the dry ice/acetone bath under the empty trap to collect the sample.

When the synthesis is completed, the NO cylinder should be flushed with N_2 gas for ~ 15 minutes using the purge valve. Additionally, the cooling water and ozonator should be turned off and the ozonator flushed with O_2 for 30 minutes to remove any residual O_3 .

2.3 Generation of Molecular Beams

2.3.1 DCl Beams

DCl beams were generated by passing an HCl gas mixture through a glass bubbler containing 98 wt % D₂SO₄ cooled to 0 °C. With a fresh D₂SO₄ solution, we achieved 90 % DCl with a 10 % HCl impurity. Occasionally, the beam line would need to be completely cleaned, including valves and connections, to obtain a decent DCl/HCl ratio. Filters were also removed from the beamline to improve the ratio.

As the beam is used and D⁺ is replaced by H⁺ in solution, the DCl/HCl content in the beam will drift. To reduce this effect, two consecutive bubblers, each containing D₂SO₄, can be used instead. High-energy, ~90 kJ/mol, DCl beams were generated by flowing a premixed tank of 2% HCl in H₂ through the bubbler. Similarly, ~50 kJ/mol and ~10 kJ/mol DCl beams were generated using a mixture of 2% HCl in He and 10% HCl in N₂ respectively. Generally, these beams were generated with a backing pressure of 1 barr using a 100 micron nozzle heated to 90 °C to reduce DCl dimer formation.

2.3.2 N₂O₅ Beams

 N_2O_5 beam generation has room for improvement. The energy of the beam can change day-to-day based on the shape of the sample in the bubbler and on temperature of the bath. Additionally, the beam flux can drift, requiring quick use of the "double-decker" reservoirs. I begin generating an N_2O_5 beam by collecting a glass bubbler filled with solid N_2O_5 sample. The ideal sample should not have any visible signs of moisture or discoloration. When warmed, some brown NO_2 gas may be produced but can be driven off quickly with a flow of dry gas. The length of the stem as well as the shape of the sample in the bubbler can influence the mixing of the carrier gas and N_2O_5 before exiting the bubbler. Sample containers with a short stem containing sample at the base require the bubbler to be kept at higher temperatures, typically around -15 °C, to force enough N_2O_5 into the carrier gas for reasonable signals. Alternatively, a bubbler with a longer stem with sample collected along the walls and stem will need to be kept at much lower temperature, typically around -30 °C, to generate an N_2O_5 beam of the same composition.

Once a sample is obtained and a bubbler temperature chosen, the carrier gas is sent through the sample to pick up N_2O_5 . The gas mixture is then sent through a trap containing P_2O_5 -coated glass beads followed by a trap lined with nylon mesh to reduce the HNO₃ content in the beam (as recommended to us by Steve Brown). In this case, HNO₃ reacts with the peptide bonds in Nylon, removing the acid from the gas stream. N_2O_5 also reacts for the first few minutes with the Nylon mesh but then passes by it untouched. The gas is then passed through a glass, $100 \, \mu m$ nozzle heated to $90 \, ^{\circ}C$. The P_2O_5 over time will cake and become solid after continued exposure to moisture and will need to be replaced; this could take several experiments before replacement is needed. The nylon trap, however, is swapped out more frequently and will typically only last 1 or 2 experiments. When the nylon mesh reacts with HNO₃, it becomes

yellow and degrades into a sticky, gel-like substance. Used P₂O₅ is often cleaned by slowly reacting it with a large bin of water inside of the hood, generating dilute phosphoric acid. Used nylon is scraped into the solid waste container and is occasionally dipped into the base bath to loosen the nylon before scrapping.

Incident N₂O₅ beam energies were measured by Tom Sobyra and Joe Gord. Using a long-stemmed bubbler with sample collected along the walls and stem, they varied the bubbler temperature from -35 °C to -18 °C and recorded the incident energies produced when mixed with H₂ and Ar. High-energy, H₂ mixtures produced beam energies between 170 and 100 kJ/mol. This data is recorded in Table 1 and displayed in Figure 8. Ar mixtures consistently gave peaks centered at 9.4 kJ/mol at temperatures between -30 and -20 °C.

2.4 Liquid Reservoirs

A single liquid reservoir was used for the DCl studies. In addition, a Teflon block was attached to bottom of the reservoir. This block was attached so that the incident beam could be positioned to strike an inert surface – the scattered DCl and impurity HCl in the beam could then be measured and provide the incident DCl/HCl ratio for comparison with the DCl/HCl ratio when scattering from glycerol. For the N₂O₅ studies, the "double decker" reservoir developed by Annabel Muenter was used instead. This arrangement replaced the Teflon block with a second liquid reservoir. This was useful in the N₂O₅ studies due to the constantly fluctuating N₂O₅ beam. By quickly switching between reservoirs, one can compare signals from two different solutions without worrying about fluctuations from the beam. Typically, the reservoirs were switched every 15 minutes.

Each reservoir is cooled by a recirculating chiller, typically to 289 K, and holds about 50 mL of liquid when full. A 5.0 cm glass wheel rotates within the reservoir driven by a 3-phase

AC synchronous motor. The glass wheel is scraped by a Teflon rod, generating a continuously renewed ~500 µm liquid surface. The liquid film faces a window, the only exit to the reservoir. The reservoirs need to be thoroughly cleaned after the use of surfactants. A thorough cleaning includes dismantling every Teflon and glass piece and placing the pieces in a base bath for cleaning. If this doesn't happen, small amounts of surfactant may be present in the new solution added to the reservoir. The aluminum components are thoroughly washed with deionized water and ethanol. When switching between solutions that contain salty or pure glycerol, additional cleaning of the Teflon pieces may not be necessary.

2.5 Liquid Preparation

Glycerol (99%, Sigma-Aldrich) solutions were prepared by weighing out the desired mass of glycerol, assuming 1.26 g/mL, and adding the desired amount of surfactant and salt to the solution. The solution is mixed via stir bar under mild heat. The solution is pumped using a liquid nitrogen trapped mechanical pump during mixing to ~10 mTorr vacuum. By pumping on the solution, we remove excess gas in solution that would immediately foam up under high-vacuum in the chamber. Additionally, the pumping further dries the glycerol by removing most H₂O that may have been present.

2.6 Signal Optimization

2.6.1 Nozzle Alignment

The general outline of the scattering machine is shown in Figure 4. We used a $100 \,\mu m$ diameter nozzle to generate supersonic expansions of DCl and N_2O_5 studies into vacuum. The nozzle sits within the Source chamber secured by a nozzle holder and "birdcage" assembly. The Source and Source Differential chambers are separated by a conical skimmer. The center of the skimmer has hole with a radius of $0.406 \, mm$, which allows only the center-most region of the

beam to pass from the Source into the Source Differential. In order to generate an expansion with a strong flux, the distance and rotation angle between the nozzle tip and the skimmer must be ideal. The distance between the nozzle and skimmer is typically about 0.214". If the nozzle is removed and later reinserted, the angle of the nozzle must be adjusted in order to maximize signal. We attribute this angle dependence to the fact that the nozzle is made from pulling a glass tube and grinding it until obtaining the desired hole diameter. This method does not guarantee a perfectly symmetric exit. The nozzle is typically rotated very carefully under vacuum while generating a beam by twisting the stainless steel rod attached the glass nozzle. This is done while the detector is open so that counts can be maximized during the rotation.

2.6.2 Fenn Source Alignment

After exiting the skimmer, the molecular beam passes through an aperture in the Source Differential wall into the Main chamber, where the molecules come into contact with the liquid film generated by the reservoir, the "Fenn source" (named after its inventor, John. B. Fenn). The Fenn source is positioned such that the surface provides a 45°, 45° scattering angle into the detector. This is done by placing a right triangle on the backside of the Fenn source and adjusting the Fenn source angle until one leg of the triangle runs parallel with the chamber side, as determined by eye. The manipulator rod is also marked to improve consistency. The manipulator x, y, and z positions of the Fenn source are maximized based on glycerol evaporation and high-energy Ar scattering while under vacuum. The detector is opened to detect either glycerol or Ar. Glycerol is typically detected first followed by the high-energy Ar scattering. Both methods should provide the same optimal position.

For the dual reservoir setup it should be noted that the top reservoir's window to the liquid surface is slightly taller than the reservoir below (8.51 mm above, 6.52 mm below). This

can become an issue when the beam spot is greater than 6.5 mm, as was the case for the N_2O_5 studies. Based on ray diagrams of known apertures, we assume a beam spot of 7.2 mm high with a detector viewing region of 3 mm for the umbra and 8 mm for the penumbra. Using a geometric argument shown in Figure 5, we estimate that 96% of signal that reaches the detector is from collisions with the liquid surface, leaving 4% that could arise from collisions with aluminum. It is worth noting that thermal Ar scattering studies between the two reservoirs showed a \sim 4% smaller signal (in exact agreement!) when scattering from the bottom reservoir. This was accounted for by increasing signals from the bottom reservoir by 4%.

2.6.3 Detector Optimization

The Einzel lenses as well as the grid, extractor, and filament bias within the detector play an important role in directing ions to the conversion dynode. These settings can alter the transmission function through the quad, influencing the detector's sensitivity for heavy and light masses. The experiments for the DCl and N_2O_5 experiments used two different lens settings which are recorded in Table 2. For the DCl study, we used settings similar to those used by Diane Lancaster in the He evaporation studies. However, when switching to the N_2O_5 experiment, the primary product detected was Br_2 at 160 m/z. Due to the much heavier mass and lower signals of the N_2O_5 experiments, the settings were adjusted to maximize the detection of Br_2 at 160 m/z. This adjustment dramatically changed the ion flight time constant α . Before the adjustment α was 7.0 as determined by Diane Lancaster. After the adjustment α became 2.4 based on measurements of SF_6 fragments taken on 1/28/2016. This change most likely arises from a change in ion energy (grid voltage) from 10 to 20 volts.

2.6.4 Aperture Optimization

Between the DCl and N₂O₅ studies, the aperture size after the source differential was

switched from 0.8 mm to 1.7 mm in order to increase the spot and increase signal. A summary table of aperture sizes can be found in Figure 4 along with resulting image sizes on the surface and viewing regions of the detector.

2.7 Beast Issues

When first joining the group in 2012, I worked on the Beast machine located in room 7339. This machine was used for my initial measurements of DCl \rightarrow HCl exchange using glycerol as well as my first measurements of N₂O₅ scattering and HNO₃ production. These experiments were later performed more thoroughly using Hal. There are a few unresolved issues with this machine as well as a cold-arm addition to the detector that should be discussed.

2.7.1 Main Chamber

The Alcatel is the brand of diffusion pump used to bring the main chamber to high vacuum. The Alcatel's gate valve uses a pneumatic design, requiring a N₂ connection for it to open or close fully. In early 2013, a leak was discovered in the N₂ assembly requiring frequent replacement of the high pressure N₂ cylinder. The leak was eventually traced to the solenoid, which had a manual open/close switch. The leak was found to be around the switch itself. It is possibly that constant use wore down an o-ring that prevented N₂ from leaking. The P/N # of the replacement solenoid is N-7501-502. There is only one other issue concerning the Alcatel's gate valve. During the last the time it was used, it was accidentally set to the open position while the bottom of the pump was under rough vacuum and the main chamber above was vented. Due to the design of the gate valve, it could not open under these conditions. It is possible this attempt could have damaged the gate valve.

The main chamber has a potential future issue dealing with the post-chopper assembly.

The post-chopper is held in place by several screws that fit into tapped holes in the main

chamber. Over the years the holes have become worn, and it is difficult to fit screws into several of the holes. I discussed this issue with Rick Pfeiffer in the machine shop and showed him the problem. He did not feel comfortable retapping the holes in the chamber because of the restrictive movement and the possibility of the breaking the tapping tools. To fix the issue, it may require the removal of the detector differential, which would require the use of a crane.

2.7.2 Source and Source Differential

The Source chamber is pumped to high-vacuum by a VHS-10 diffusion pump. Mid-2014, we discovered that the VHS-10 was not reaching proper vacuum under a fully-backed gas nozzle. After checking the temperature, we quickly realized that one of the two heating elements had broken. We raised the diffusion pump using four bolts threaded through the diffusion pump frame and dissembled the bottom. We purchased replacement heating elements and a new crush plate from Duniway stockroom. The crush plate is considered sacrificial and should be replaced anytime the VHS-10 is disassembled. Additionally, the poor condition of the clamp plate required us to salvage a used clamp plate from a VHS-10 in the graveyard. With the replacement pieces in place, the bolts were coated with Milk of Magnesia and the nuts were tightened to the specific torques outlined in the manual. These torques should be followed since the heating elements must make contact with the surface above evenly and tightly. The surface acts as a heatsink for the elements, and if proper contact is not made, the elements will burn out prematurely.

The Source Differential chamber is pumped by a Diffstack diffusion pump. This pump is connected via a right-angle pneumatic valve. The valve is connected to an N_2 cylinder and requires pressure to be open or closed. Unfortunately, when in the open position the pneumatic valve leaks N_2 , requiring the cylinder to be replaced over the course of weeks if left open.

Alternatively, the Diffstack can be only opened during experiments, which will preserve the N_2 cylinder. David Castro also had an issue with leaks in this particular pneumatic valve in 2001.

2.7.3 Detector and Detector Differential

The Detector and Detector Differential chambers are pumped by two turbomolecular pumps, a TMU 260 and TPU 240. Between the turbo pumps and their backing mechanical pumps is a pneumatic valve, which when closed allows the turbo pumps to temporarily run without the support of the mechanical pumps. Unfortunately, this pneumatic valve began to leak in 2015, requiring a constant change of N₂ cylinders if it was to be run continuously. A new pneumatic valve was purchased in 2016 but has yet to be tested.

At the end of 2013 we developed a right angle cold arm that can be attached to the side flange of the detector. This cold arm was made up of two pieces connected via conflat flanges. To attach the cold arm, a support was developed so that the weight of stainless steel would not stress the housing of the detector. This cold arm had been cleaned via phosphoric acid solution and pumped on. However, it has never been confirmed to be leak-free and has never been cooled. Testing will need to be done before use as well as the purchase of a new chicken feeder. Machine drawings of the cold arm are provided in Figures 6 and 7.

2.8 Surface Tension Developments

In early 2015, Tom Sobyra and Keaten Kappes revamped our surface tension methodology. This was in an effort to reduce uncertainty and improve repeatability that had been lacking in measurements at that time. Earlier methods relied on using a thin platinum pin as well as a narrow $\sim 3/4$ " Teflon cup. This was replaced by a 16.5×0.1 mm platinum plate and a ~ 4 " glass dish. The cleaning method was also improved by adding in KOH/isopropanol base bath to the cleaning procedure. This bath is used for cleaning each glass dish after use. The dish

is typically soaked for ~10 minutes before rinsing. If there is a solid buildup on the dish from the bath, the dish is rinsed first with a 1 M HCl solution. Afterwards, the dish is rinsed with DI water and ethanol.

The Cahn 2000 microbalance is used as before and can be seen in photos provided in Figure 9. A thin, light wire is bent and attached to the Cahn setup. The wire is bent such that the plate can be attached and hangs flush with the floor. The N₂ flow is turned on within the enclosed apparatus to reduce sample exposure to moisture. A dish containing the liquid sample is placed below the Pt plate on a lab jack. The plate is first wetted with the liquid by briefly raising the solution to the plate until the plate is pulled into the liquid. Once the plate is wet and the solution is brought away, the solution is raised back up until the solution again pulls the plate in. The solution is then pulled away slowly until the maximum readout voltage is obtained. The maximum voltage is recorded, and the process is repeated six times.

To convert the readout voltage into a surface tension value, a calibration curve needs to be made. This is done by measuring a series of solutions, typically water, glycerol, ethylene glycol, and ethanol. A line is fit between the measured voltages and literature surface tension values. The resulting data is very linear, and the resulting expression provides a simple means of obtaining the final surface tension value. The surface tension measurements were performed primarily by Matt Melvin and Sarah Quinn, two undergraduates in our group.

2.9 N₂O₅ Measurements and Dates

In an effort to improve clarity for future students, I am providing a table that shows the dates of important experiments used for the N_2O_5 manuscript. This can be found in Table 3.

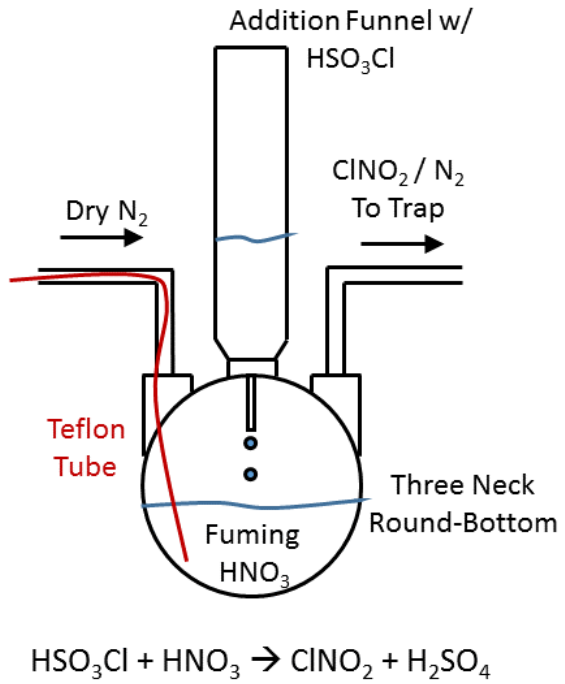


Figure 1. Diagram of the ClNO₂ Synthesis Apparatus.

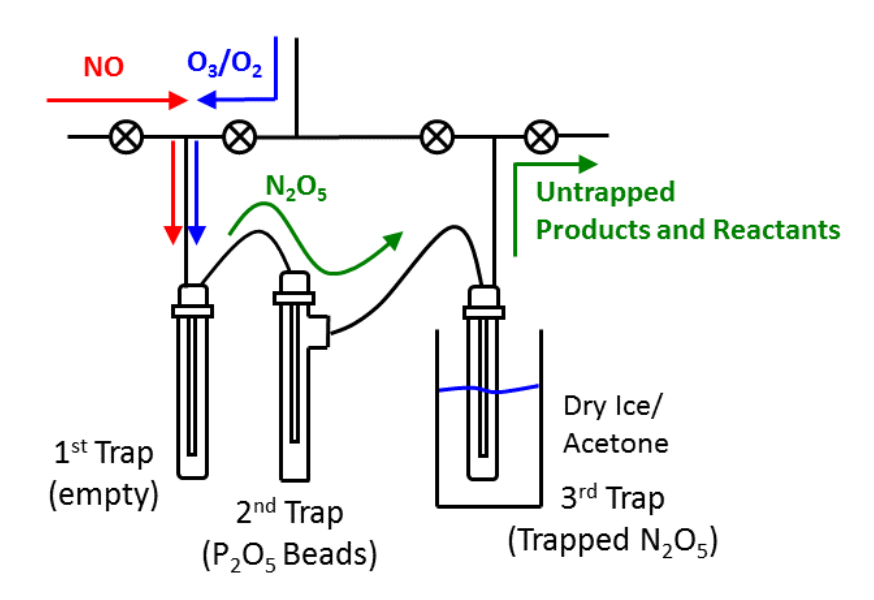


Figure 2. Diagram of the N₂O₅ Synthesis Apparatus.



Figure 3. Photo taken of the N_2O_5 synthesis apparatus.

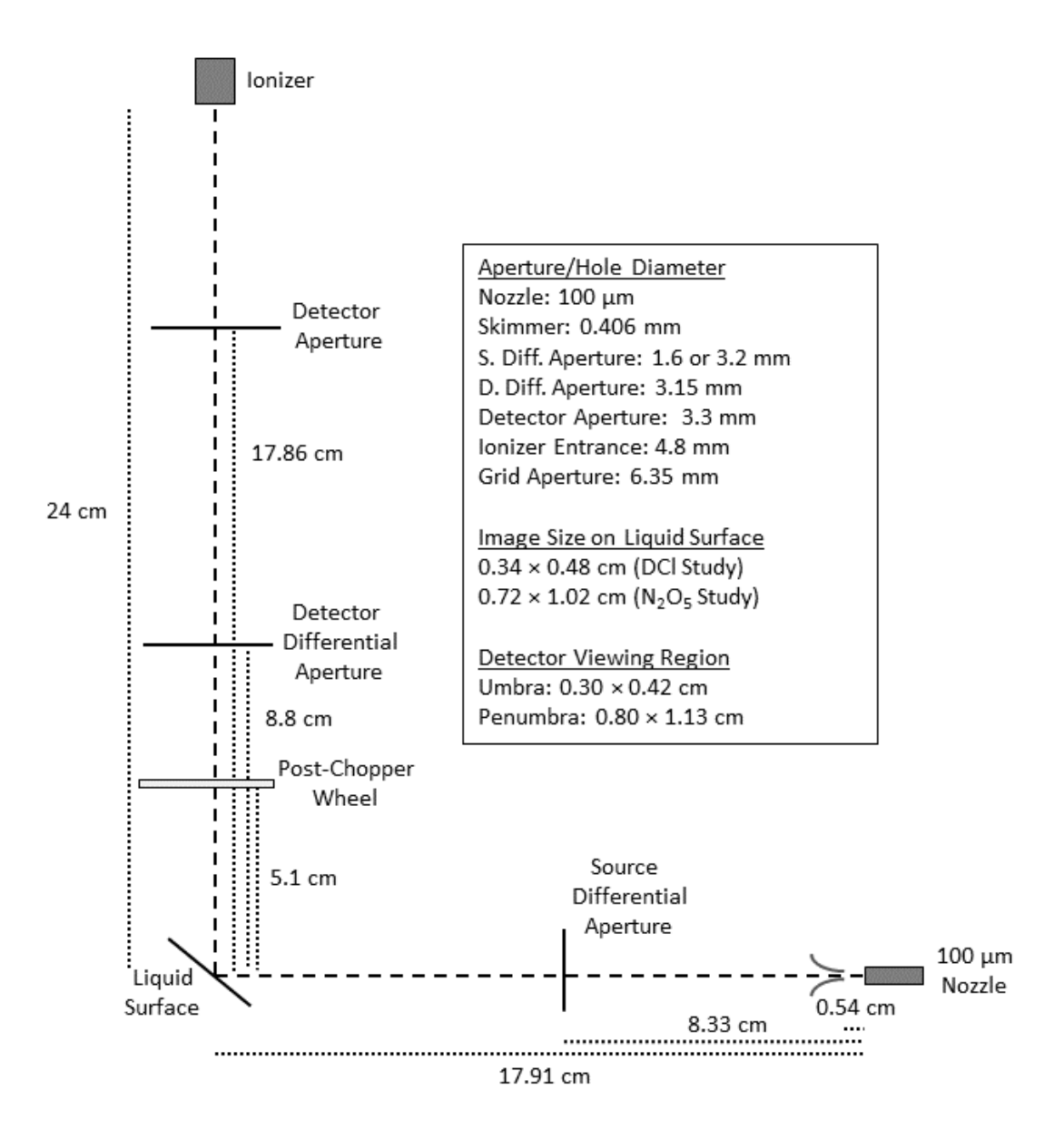


Figure 4. Summary of important aperture sizes and distances. These values were compiled primarily from Annabel Muenter's and Brad Ringeisen's theses. The distance from the liquid surface to the post-chopper wheel was changed from 4.7 to 5.1 to account for Alexis Johnson's change of the flight distance from the post-chopper to the ionizer from 19.3 cm to 18.9 cm. Forward-backward offsets (FBO's) ranged typically from 0 to -7 μs with an electronic offset of 20.5 μs.

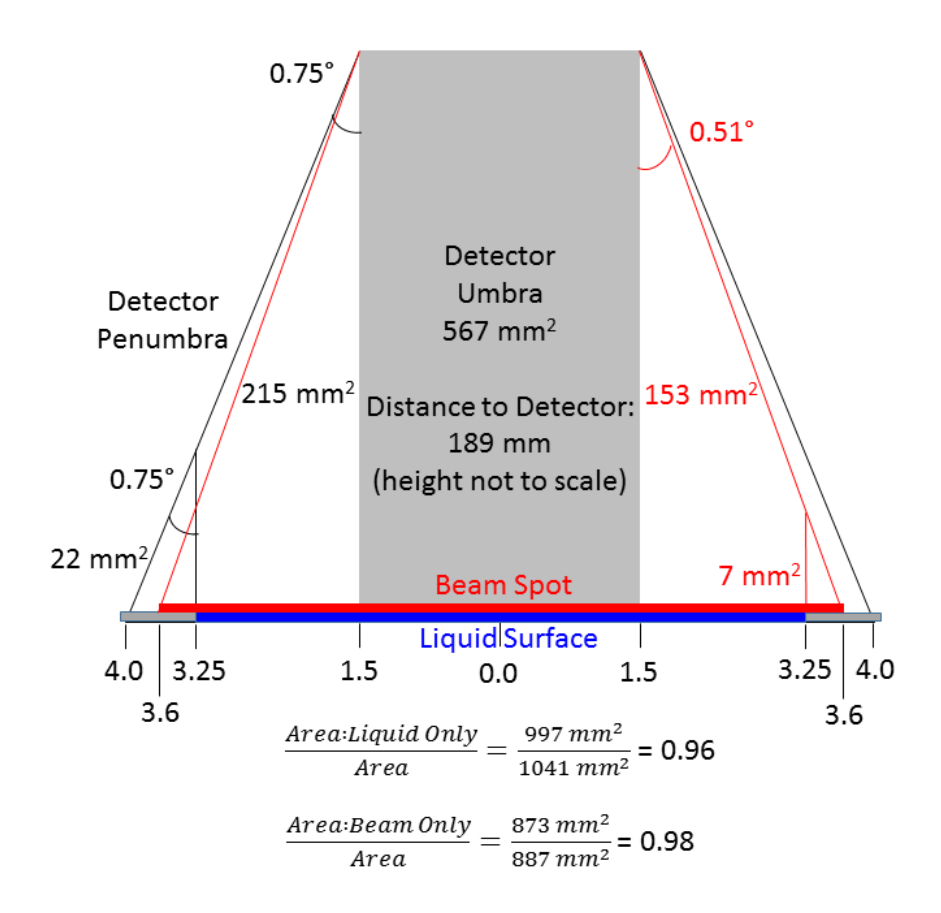


Figure 5. Vertical slice of the detector umbra and penumbra on the lower reservoir. If the beam spot covered the entire penumbra, only 4% of the signal would be due to collisions with the aluminum. Our estimate of beam spot size predicts only 2% of the signal would be from aluminum scatter.

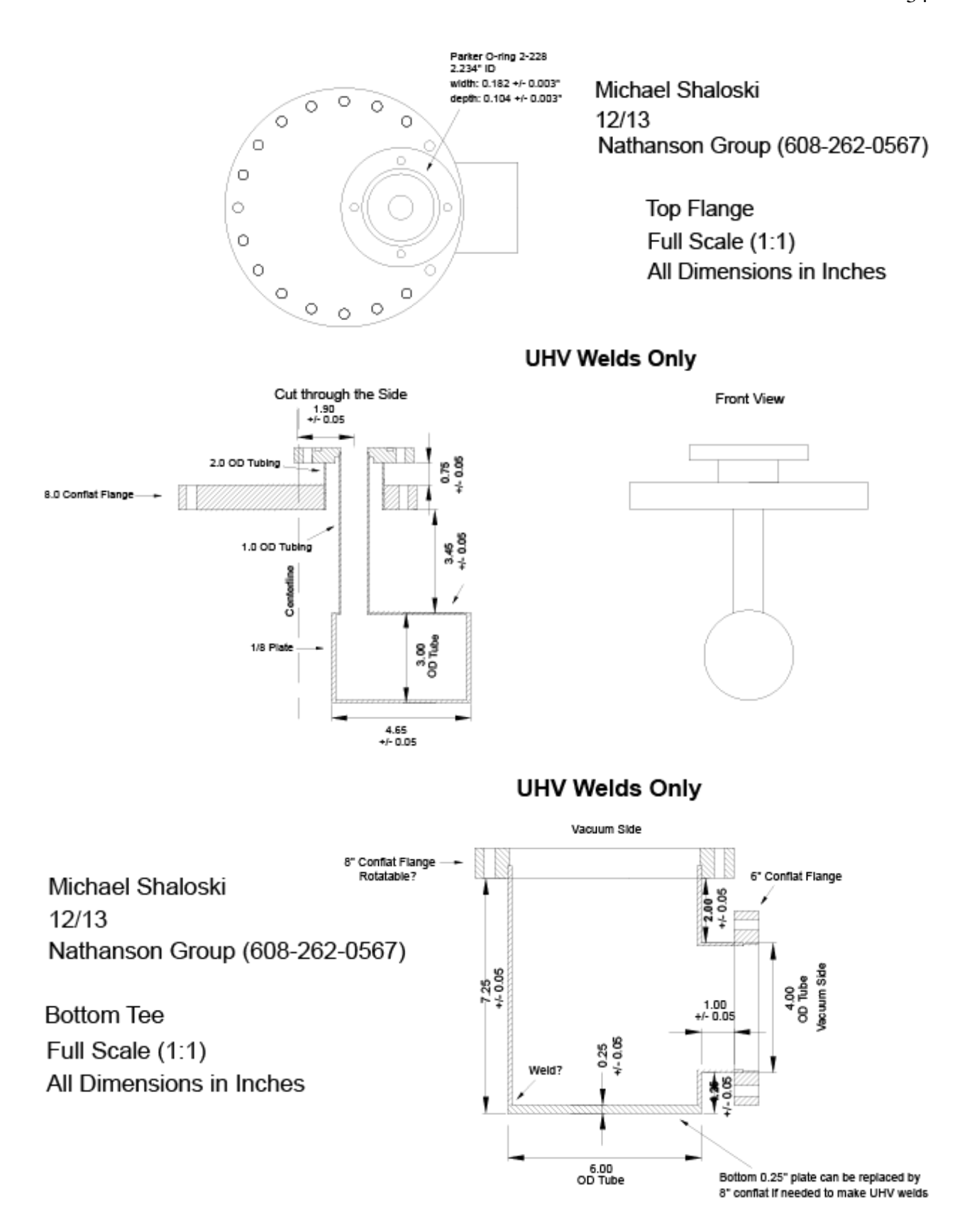
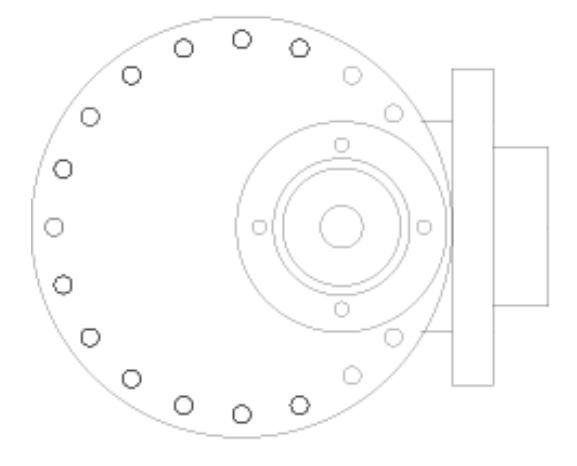
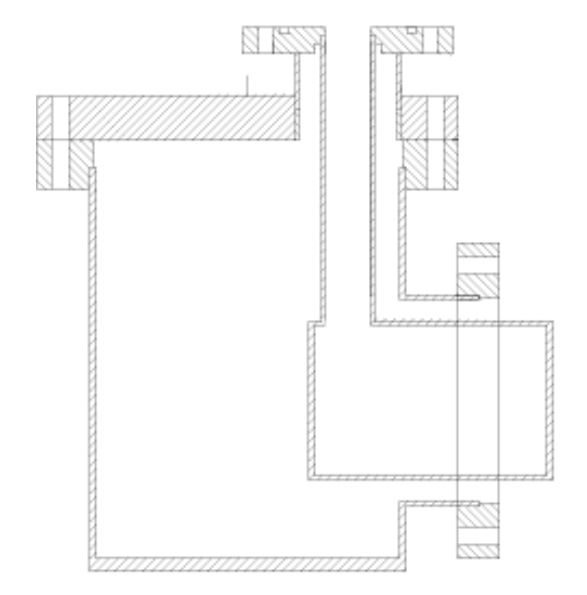


Figure 6. Two Main Pieces of the Detector Cold-Arm.

Top View with Bolthole Arrangement



Cut through the Side



Michael Shaloski 12/13 Nathanson Group (608-262-0567)

Assembly Drawing
Full Scale (1:1)
All Dimensions in Inches

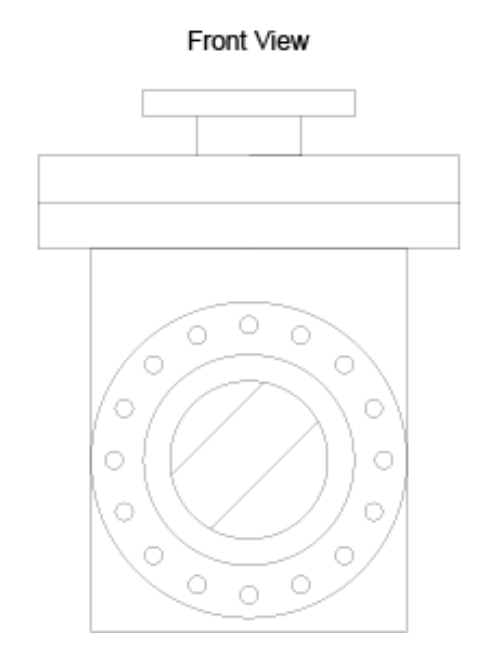


Figure 7. Fully-Assembled Detector Cold-Arm.

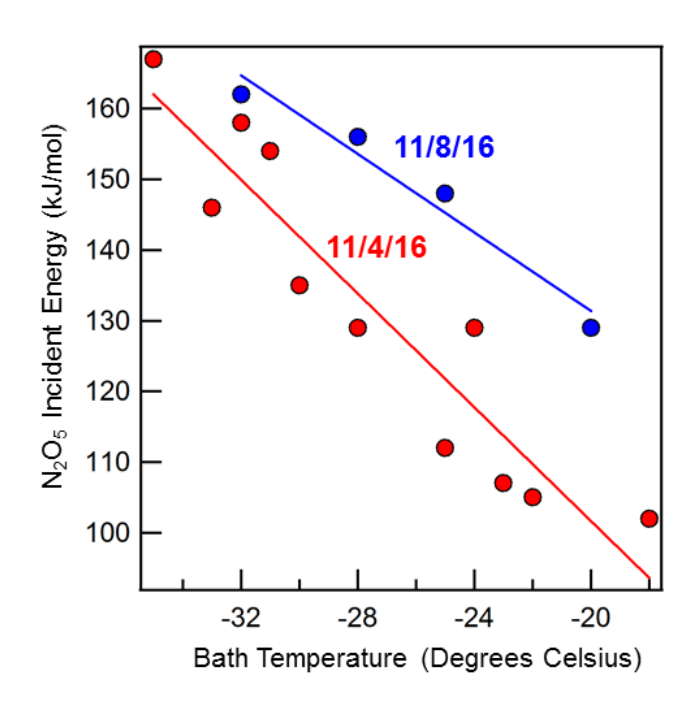


Figure 8. Plot of N_2O_5 incident beam energy vs bath temperature.

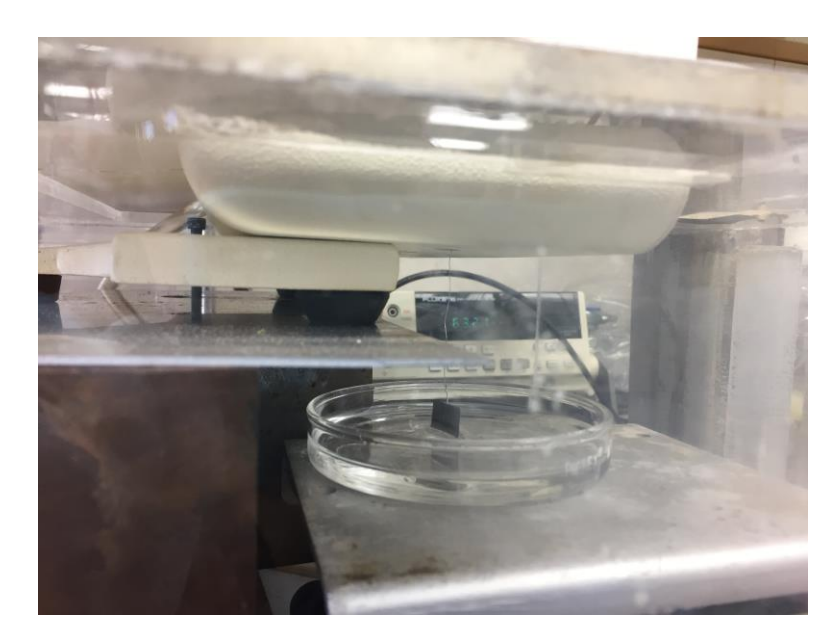




Figure 9. Photos taken of the surface tension apparatus.

| Date | Bath Temp. | Energy | | |
|---------|------------|----------|--|--|
| | (°C) | (kJ/mol) | | |
| 11/4/16 | -35 | 167 | | |
| | -33 | 146 | | |
| | -32 | 158 | | |
| | -31 | 154 | | |
| | -30 | 135 | | |
| | -28 | 129 | | |
| | -25 | 112 | | |
| | -24 | 129 | | |
| | -23 | 107 | | |
| | -22 | 105 | | |
| | -18 | 102 | | |
| 11/8/16 | -32 | 162 | | |
| | -28 | 156 | | |
| | -25 | 148 | | |
| | -20 | 129 | | |

Table 1. Resulting N_2O_5 incident beam energies at various sample bath temperatures for N_2O_5 mixed with H_2 .

| Experiment | Lens/Device Voltage (V | | |
|-------------------------------|------------------------|-------|--|
| DCl | Filament Bias | -72 | |
| | Extractor | 10 | |
| | Grid | 10 | |
| | Entrance Lens | 0 | |
| | 1+3 Lenses | -30 | |
| | 2 Lens | -350 | |
| | Exit Lens | 0 | |
| N ₂ O ₅ | Filament Bias | -74 | |
| | Extractor | 31 | |
| | Grid | 20.3 | |
| | Entrance Lens | 40.1 | |
| | 1+3 Lenses | 4.0 | |
| | 2 Lens | -33.2 | |
| | Exit Lens | 8.8 | |

| Experiment | Parameter | Value | |
|------------|--------------------------------|------------|--|
| DCl | α | 7.0 | |
| N_2O_5 | α | 2.4 | |
| Both | Electronic Offset | 20.5 μs | |
| | Forward- Backward Offset | 0 to -7 μs | |
| | Flight Path 18.9 cm | | |

Table 2. Detector electronic settings and fitting parameters for the DCl and N_2O_5 experiments.

| Solution of Interest | Reference Solution | Low/High Energy | Dates | |
|-----------------------------|-----------------------|--------------------|--|--|
| 30 mM THABr | 2.7 M NaBr | Low | 5/20/16, 6/3/16, 7/12/16 | |
| 30 mM THABr | 2.7 M NaBr | High | 2/4/16, 2/11/16, 5/5/16, 7/29 + 8/01/16 | |
| 10 mM CTAB | 2.7 M NaBr | High | 3/29/16, 3/31/16 | |
| 30 mM THABr + 10 mM SDS | 30 mM THABr | High | 2/29/16 | |
| 30 mM THABr + 0.5 M NaBr | 30 mM THABr | High | 11/26/16 | |
| 30 mM THABr + 0.5 M NaCl | 30 mM THABr | High | 8/1/16 | |
| 30 mM THABr + 2.7 M NaBr | 2.7 M NaBr | High | 2/2/16, 3/4/16 | |

Table 3. Summary of Dates for N_2O_5 Studies.

References

- 1. Antman, M. D. Collisions and Reactions of Inert and Organic Gases. University of Wisconsin Madison, 1998.
- 2. Burden, D. K. The Role of Chain Structure and Functional Group on HCl Entry into Surfactant-Coated Sulfuric Acid. University of Wisconsin Madison, 2010.
- 3. Brauer, G., Handbook of Preparative Inorganic Chemistry. 1963; Vol. 2.
- 4. Davidson, J. A.; Viggiano, A. A.; Howard, C. J.; Dotan, I.; Fehsenfeld, F. C.; Albritton, D. L.; Ferguson, E. E., Rate constants for the reactions of O₂⁺, NO₂⁺, NO₇⁺, NO₇⁺, NO₇⁺, NO₇⁻, and halide ions with N₂O₅ at 300 K. *J. Chem. Phys.* **1978**, *68*, 2085.

Chapter 3

DCl Transport through Dodecyl Sulfate Films on Salty Glycerol: Effects of Seawater Ions on Gas Entry

This chapter is a reproduction of a paper published in the Journal of Physical Chemistry A. Shaloski, M. A.; Sobyra, T. B.; Nathanson, G. M. DCl Transport through Dodecyl Sulfate Films on Salty Glycerol: Effects of Seawater Ions on Gas Entry. J. Phys. Chem. A. 119, 12357 – 12366. DOI: 10.1021/acs.jpca.5b07298

3.1 Summary

Gas-liquid scattering experiments were employed to measure the entry and dissociation of the acidic gas DCl into salty glycerol coated with dodecyl sulfate ions (DS = CH₃(CH₂)₁₁OSO₃⁻). Five sets of salty solutions were examined: 0.25 and 0.5 M NaCl, 0.25 M MgCl₂, 0.25 M CaCl₂, and artificial sea salt. DS bulk concentrations were varied from 0 to 11 mM, generating DS⁻ surface coverages of up to 34% of a compact monolayer, as determined by surface tension and argon scattering measurements. DS surface segregation is enhanced by the dissolved salts in the order $MgCl_2 \approx CaCl_2 > sea salt > NaCl$. We find that DCl penetration through the dodecyl chains decreases at first gradually and then sharply as more chains segregate to the surface, dropping from 70% entry on bare glycerol to 11% for DS⁻ surface concentrations of 1.8 x 10¹⁴ cm⁻². When plotted against DS⁻ surface concentration, the DCl entry probabilities fall within a single band for all solutions. These observations imply that the monovalent Na⁺ and divalent Ca²⁺ and Mg²⁺ ions do not bind differently enough to the ROSO₃⁻ headgroup to significantly alter the diffusive passage of DCl molecules through the dodecyl chains at the same DS⁻ chain density. The chief difference among the salts is the greater propensity for the divalent salts to expel the soluble ionic surfactant to the surface.

3.2 Introduction

Bursting bubbles at the ocean surface generate sea spray aerosols that contain organic molecules scavenged from the top millimeter of the ocean, a region that is rich in organic and biological species. Organic molecules, including carbohydrates, amino acids, and lipids, and segregate to the surface of both the ocean and sea spray droplets, forming a coating that suppresses or enhances the uptake and reactions of ambient gases. Among these organic species are anionic surfactants, including naturally occurring phospholipids and carboxylates and synthetic sulfonates and sulfates from wastewater runoff in coastal regions. In particular, sodium dodecyl sulfate (SDS), CH₃(CH₂)₁₁OSO₃-Na⁺, has been detected as a trace component in seawater, and is often used as a model for oceanic surfactants because of its moderate solubility (8 mM in pure water).

We employ SDS here to address two questions concerning ions in the ocean: how do monovalent cations (Na⁺) and divalent cations (Ca²⁺ and Mg²⁺) influence the adsorption of dodecyl sulfate (DS⁻) at the surfaces of protic liquids, and how do these cations alter the ability of these DS⁻ films to impede the transport of gases into the aqueous subphase? Seawater contains 0.47 M Na⁺ but only 0.05 M Mg²⁺ and 0.01 M Ca²⁺. However, these divalent ions may play an outsized role because they can displace the Na⁺ counterion and bridge adjacent DS⁻ chains.¹⁷⁻²⁰ They have also been found to populate the surfaces of sea spray particles with organic coatings.²¹ Previous studies show that metal chloride salts enhance the adsorption of DS⁻ at the surface of water, and in particular reveal that the divalent ions are more effective than monovalent ions at 10⁻³ M salt concentrations, a specificity that disappears at 10⁻¹ M values.²²⁻²⁴ In this study, we compare the adsorption of DS⁻ with added NaCl, CaCl₂, MgCl₂, and artificial

sea salt in liquid glycerol, and ask whether these ions alter the orientations of the DS⁻ chains in ways that change their porosity.

To gauge the ability of the DS⁻ films to impede gas transport, we measured the uptake of the acidic gas DCl into glycerol containing SDS and NaCl, CaCl₂, or MgCl₂, as well as a sea salt mixture containing all three cations at seawater concentrations. As shown in Figure 1, the deuterated isotope was chosen as the probe gas because DCl molecules that enter the solution undergo DCl \rightarrow HCl exchange and then evaporate as HCl, providing a direct experimental signature of gas entry into protic liquids coated with a non-protic surfactant.^{25,26} Glycerol, HOCH₂CH(OH)CH₂OH, was chosen over water as the subphase because we perform these gasliquid scattering experiments in vacuum, where low volatility liquids minimize gas-vapor collisions and enable the gas molecule to strike the liquid without deflection. Glycerol is a low vapor pressure (4 × 10⁻⁵ Torr at 289 K) and high surface tension (64 mN m⁻¹) protic liquid that is also viscous (2060 cP).²⁷ It shares many of the solvent properties of water, including a high NaCl solubility of ~1.6 M in comparison to 6 M for water.²⁸

The experiments performed here incorporate benchtop surface tension measurements to determine static DS^- surface concentrations and gas-liquid scattering experiments to measure the fraction of impinging DCl molecules that permeate through the monolayer and enter the glycerol subphase. We also use argon scattering to determine the time-dependent surface concentrations of DS^- on glycerol inside the vacuum chamber.²⁹ A key advantage of these vacuum measurements is the absence of gas-phase diffusion, which often limits entry probability measurements to values below $0.1.^{16}$ The experiments collectively indicate that DS^- chains segregate in the order $Mg^{2+} \approx Ca^{2+} > sea$ salt $> Na^+$, but at the *same* DS^- surface concentration, the subphase ions make little or no difference in the permeation of DCl through the chains.

3.3 Experimental Procedure

All chemicals were purchased from Sigma Aldrich. Glycerol (>99%) and crystalline granules of NaCl, MgCl₂(H₂O)₆, and CaCl₂(H₂O)₂ were used without further purification. SDS (99+%), however, contains trace amounts of surface-active contaminants such as dodecanol, ³⁰⁻³³ which were removed in selected tests by recrystallizing SDS from ethanol. ³⁴ Figure A.1 in the Appendix shows that the surface tensions of recrystallized 0−5 mM SDS in 0.25 M NaCl/glycerol were nearly identical to unrecrystallized SDS, in sharp contrast to measurements in water. ³⁵ Additionally, DCl entry probabilities measured with SDS before and after recrystallization changed only from 0.33 to 0.30 for 5 mM SDS in 0.25 M NaCl/glycerol and from 0.214 to 0.206 for 5 mM SDS in 0.25 M MgCl₂/glycerol. Based on the similarities in these measurements, we used unrecrystallized SDS for all other experiments. Each solution was prepared by dissolving salt and SDS into glycerol and stirring with mild heating at 10⁻² Torr to remove dissolved gases and residual water. The sea salt mimic was made from 0.47 M Na⁺, 0.056 M Mg²⁺, 0.010 M Ca²⁺, 0.010 M K⁺, and 0.61 M Cl⁻. Sulfate ions were excluded because they react with H⁺ to make HSO₄⁻ and suppress evaporation of D→H exchanged HCl.

Figure 2 depicts the scattering apparatus and liquid reservoir described in ref 29. For each experiment, 50 mL of the glycerol-salt mixture were added to the aluminum reservoir and cooled to 289 K. Continuously renewed films of glycerol were prepared by rotating a 5.0 cm diameter glass wheel in the solution, which was scraped by a Teflon rod to create a uniform vertical film that was 0.5 mm thick. The incident Ar or DCl beam projected an elliptical $2.4 \text{ mm} \times 1.7 \text{ mm}$ spot when directed at the liquid film at 45° . The exposure time of the liquid film to the incident beam was controlled by the wheel rotation speed to be 0.07 to 0.26 s, and was set at 0.17 s in most experiments.

High-energy (90 kJ mol⁻¹) DCl beams were generated by bubbling a 2.0% HCl mixture in H₂ through 20–50 mL of 98 wt % D₂SO₄ cooled to 0 °C. Lower energy (50 and 10 kJ mol⁻¹) beams were created by seeding DCl in He and N₂, respectively. The DCl gas mixture was then expanded through a 100 μm diameter nozzle heated to 90 °C (to minimize DCl dimer formation) at a backing pressure of 1 bar. The HCl impurity in the DCl beam was typically 10%, but was as high as 50% before the D₂SO₄ solution was replaced.³⁶

DCl and HCl molecules leaving the solution were chopped by an 18 cm diameter post-chopper wheel located 6.2 cm away from the liquid film. The wheel contains four 3.2 mm slots and was spun at 150 Hz. The 38 µs gas pulses then traveled 18.9 cm through a doubly differentially pumped electron-impact ionizer and quadrupole mass spectrometer, where the arrival times of the pulses were recorded as a time-of-flight (TOF) spectrum.

Surface tensions were measured by the Wilhelmy plate method using a 16.5 mm wide by 0.1 mm thick Pt plate within a N₂-purged enclosure. The downward force on the plate was recorded by a microbalance with a precision of 0.1 mg. Each 20-30 mL sample was measured at least 3 times at different salt and SDS concentrations

3.4 Results and Analysis

3.4.1 Surface Tension Measurements and Adsorption of DS on Salty Glycerol.

The interfacial DS⁻ number densities were determined by measurements of the surface tension γ . Figure 3a displays the changes in γ for the different salty glycerol solutions upon addition of SDS. Added salts increase the surface tension of pure glycerol by 0.33, 0.66, 0.68, and 0.68 mN m⁻¹ for 0.25 M NaCl, 0.5 M NaCl, 0.25 M CaCl₂, and 0.25 M MgCl₂, respectively. These increments are slightly smaller than those observed in water.³⁷ As SDS is mixed at concentrations up to 6 mM, γ drops by 13 mN m⁻¹ for 0.25 M NaCl and by 22 mN m⁻¹ for 0.25 M

MgCl₂.

The surface excess of DS⁻ in each mixture is calculated from the Gibbs adsorption equation, which for NaCl/glycerol is³⁸

$$dg = -G_{DS^{-}} dm_{DS^{-}} - G_{Na^{+}} dm_{Na^{+}} - G_{CI^{-}} dm_{CI^{-}}$$
(1)

where G_{DS^-} is the surface excess of DS⁻ with respect to the glycerol solvent, and m_{DS^-} is the chemical potential of DS⁻. Dodecyl sulfate is strongly surface-active and likely segregates to the single outermost layer. In this case, G_{DS^-} is nearly identical to the monolayer surface density $n_{surf}(DS^-)$. Refs 38, 40, and 41 further show that $G_{Na^+}dm_{Na^+}$ and $G_{Cl^-}dm_{Cl^-}$ do not contribute significantly to $d\gamma$ when the fixed NaCl concentration greatly exceeds the added amount of SDS (by a minimum ratio of 50:1 for 5 mM SDS and 0.25 M NaCl). Equation 1 then becomes

$$n_{\text{surf}} (\text{DS}^-) \approx \Gamma_{\text{DS}^-} \approx -\frac{1}{RT} \cdot \frac{\partial \gamma}{\partial \ln c_{\text{SDS}}} \bigg|_{T}$$
 (2)

where $c_{\rm SDS}$ is the bulk SDS concentration. Equation 2 also assumes that the DS⁻ activity coefficient remains constant as SDS is added to each solution. This approximation has been verified for SDS in NaCl-water solutions below the critical micelle concentration. In glycerol, the SDS solutions stay clear for the duration of the experiments, but 5 mM SDS in 0.5 M NaCl thickens during the experiments and is not included in the analysis.

Lastly, we note that eq 1 will contain an additional $G_{Mg^{2+}}dm_{Mg^{2+}}$ or $G_{Ca^{2+}}dm_{Ca^{2+}}$ term for

the divalent salts. These terms will also not contribute significantly because the Ca^{2+} or Mg^{2+} concentration is held fixed during the addition of SDS. For these salts, the Na^+ concentration increases as SDS is added, and eq 2 is valid only if there is little segregation of Na^+ compared to DS^- such that $\left|G_{Na^+}\right|$ is much less than G_{DS^-} . This inequality has been verified by radioactive tracer studies of SDS in $MgCl_2$ /water solutions.²²

Within the assumptions presented above, the DS⁻ surface densities $n_{\text{surf}}(\text{DS}^-)$ are determined from numerical differentiation of the surface tensions in Figure 3a. The results of eq 2 are plotted in Figure 3b for 0.5, 1, 2, and 5 mM SDS. They rise in a Langmuir-like way but approach saturation upon addition of up to 5 mM SDS. As can be seen, DS⁻ segregates to the surface in the order pure glycerol < 0.25 M NaCl < 0.5 M NaCl < sea salt < 0.25 M Mg²⁺ \approx 0.25 M Ca²⁺. Approximate Langmuir fits to the data indicate that a 25% DS⁻ monolayer fraction requires ~3 mM of SDS in 0.25 M NaCl but only ~0.5 mM in 0.25 M MgCl₂. SDS dissolved in artificial sea salt, containing only 1/10 as many Mg²⁺ as Na⁺, segregates at a value midway between pure Na⁺ and Mg²⁺.

Table 1 shows that the highest surface concentration reached for 5 mM SDS in MgCl₂ or CaCl₂ is $1.56 \pm 0.08 \times 10^{14}$ cm⁻². Additional measurements around 10.9 mM SDS in 0.25 M MgCl₂ yield $n_{\text{surf}} = 1.81 \pm 0.06 \times 10^{14}$ cm⁻². This surface density corresponds to a molecular area of 55 Å², nearly three times the minimum area of 19.3 Å² based on SDS crystal packing.⁴³ It is noteworthy that SDS is more surface active in salty water than in salty glycerol: for 0.5 mM SDS in 0.5 M NaCl/water, the DS⁻ surface concentration is 2.2×10^{14} cm⁻², roughly 3 times larger than for 0.5 M NaCl/glycerol.²² Intriguingly, 0.1 M NaCl and 0.1 M MgCl₂ in water cause nearly equal SDS segregation at SDS concentrations below 0.5 mM SDS (where micelles form in the MgCl₂ solution). Our measurements indicate that salty glycerol solutions extend this pre-

micelle range to at least 11 mM SDS in 0.25 M MgCl₂ over the several-day time period of the experiments, perhaps because DS⁻ is more soluble in glycerol or because micelles form so slowly in the viscous solution (~3200 cP). These benchtop surface tension measurements provide an anchor for the measurements below of DS⁻ surface concentrations in vacuum.

3.4.2 High-Energy Argon Scattering as a Probe of DS Surface Coverage.

The packing of the DS⁻ chains on the glycerol-coated wheel in the vacuum chamber can be gauged by the scattering of high-energy argon atoms.^{29,44} Figure 4a shows TOF spectra of 90 kJ mol⁻¹ Ar atoms scattering from 0–11 mM SDS in 0.25 M MgCl₂/glycerol at 289 K. The narrow component at early arrival times (high average exit energies of ~30 kJ mol⁻¹) is composed of Ar atoms that scatter directly from the surface in one or a few bounces and lose on average 2/3 of their energy (labeled inelastic or impulsive scattering, IS). The broad component at later arrival times (low average energies of $2RT_{liq} = 5 \text{ kJ mol}^{-1}$) arises from Ar atoms that dissipate all of their excess energy and become momentarily trapped before desorbing in a Maxwell-Boltzmann distribution at the 289 K glycerol temperature (labeled thermal desorption, TD). The spectra in Figure 4a reveal that, as more DS⁻ chains populate the surface region at higher SDS concentrations, the TD component grows while the IS component shrinks and shifts to longer arrival times. These changes likely occur because the surface DS⁻ chains do not pack tightly, making the surface rougher and less dense than bare glycerol. Ar atoms striking the alkyl chains transfer more energy per impact, leading to lower exit energies in the IS channel, and undergo more collisions, resulting in more frequent thermalization.

We used high-energy Ar collisions to calibrate the coverage of DS⁻ at the surface of the glycerol-coated wheel, whose rotation speed generates a 0.91 s delay between scraping by the Teflon bar and exposure to the Ar beam (as illustrated in the inset in Figure 4b). This 0.91 s

replenishment time ($t_{\text{replenish}}$) does not allow dissolved DS⁻ to fully diffuse to the surface and reach coverages obtained by the longtime surface tension measurements in Figure 3. A characteristic time required to asymptotically populate a fresh surface can be estimated from $\tau = K^2/D$ for surface segregation during quiescent diffusion, where D is the surfactant diffusion coefficient and K is the longtime surface-to-bulk concentration ratio, equal to $n_{\text{surf}}(t\to\infty)/c_{\text{bulk}}$. For 2 mM DS⁻ in 0.25 M MgCl₂/glycerol, $n_{\text{surf}}(t\to\infty) = 1.5 \times 10^{14} \text{ cm}^{-2}$, $D \approx 5 \times 10^{-9} \text{ cm}^2 \text{ s}^{-1}$, and τ is computed to be 4 s. This segregation time is longer than the 0.91 s replenishment time of the rotating wheel and generates lower surface coverages that increase as the coated wheel is spun more slowly. These variations are shown in Figure 4b for $t_{\text{replenish}} = 0.34 \text{ s}$ (red), 0.91 s (green), and 1.36 s (blue). The shortest replenishment time in red generates the highest IS and smallest TD components, corresponding to the smallest DS⁻ segregation. We chose $t_{\text{replenish}} = 0.91 \text{ s}$ for most experiments because the liquid films occasionally drain and become spotty when $t_{\text{replenish}}$ is set to 1.36 s.

The actual DS⁻ monolayer coverages on the glycerol-covered wheel (at $t_{\text{replenish}}$ = 0.91 s) were determined by comparing impulsive Ar scattering of the solution with scattering from a bare solution and a reference solution with a known monolayer coverage, n_{surf} (ref):

$$n_{\text{surf}}(t_{\text{replenish}}) \gg \frac{I_{\text{bare}} - I(t_{\text{replenish}})}{I_{\text{bare}} - I_{\text{ref}}} n_{\text{surf}}(\text{ref})$$
 (3)

where I_{bare} , I_{ref} , and $I(t_{\text{replenish}})$ are the integrated fluxes of Ar atoms scattering impulsively from the bare salty solution, the reference SDS solution, and a SDS solution at $t_{\text{replenish}}$. We chose 10.9 mM SDS in 0.25 M MgCl₂ as the reference solution because the characteristic diffusion time τ is

only 0.2~s for this system. In this case, the predicted monolayer coverage is 97% of its equilibrium value of $1.81\times10^{14}~cm^{-2}$, 45 as determined by the surface tension measurements above. This method has been shown to yield correct surface concentrations in experiments involving alcohol and carboxylic acid surfactants at the surface of sulfuric acid to within statistical uncertainties of $\pm~10\%$. 29,44 All DS $^{-}$ surface concentrations measured by Ar scattering are listed in Table 1 in comparison with those obtained from the surface tension data. They range from 28% of the equilibrium value for 0.5 mM SDS in 0.25 M MgCl₂ to 89% for the 5 mM SDS in 0.25 M CaCl₂. The surface concentrations from Ar scattering are taken to be the actual concentrations on the rotating wheel and will be used below to investigate how the DCl entry probabilities vary with the density of DS $^{-}$ surface chains.

3.4.3 $DCl \rightarrow HCl$ Exchange and DCl Entry.

Figure 5 shows that high-energy DCl molecules, like Ar atoms, scatter directly (short arrival times) or become momentarily trapped and then thermally desorb (long arrival times). In addition, impinging DCl molecules can undergo D→H exchange and evaporate as HCl (red spectra). We have shown previously that these HCl molecules arise from DCl that thermally equilibrate in the interfacial region and then dissociate into D⁺ and Cl⁻, followed by statistical exchange of D⁺ for H⁺ provided by glycerol -OH groups.²⁷ At low DCl fluxes, the Cl⁻ and D→H exchanged H⁺ dissolve in solution for long times and only slowly recombine and evaporate as HCl. A key difference in the present experiments is the large 0.5 M excess of Cl⁻ ions in solution, which rapidly combine with the D→H exchanged H⁺ and force essentially all HCl to evaporate within the 0.2 s observation time of the mass spectrometer.⁴⁶ In this way, each DCl molecule that dissociates into D⁺ and Cl⁻ is detected as evaporating HCl. The fraction f_{exch} of thermally equilibrated DCl molecules that undergo D→H exchange can then be calculated

from:25,44

$$f_{\text{exch}} = \frac{I_{\text{TD}}(\text{HCl})}{I_{\text{TD}}(\text{HCl}) + I_{\text{TD}}(\text{DCl})}$$
(4)

where $I_{TD}(DCl)$ and $I_{TD}(HCl)$ are the integrated fluxes of unreacted DCl molecules and D \rightarrow H exchanged HCl molecules that thermally desorb in a Maxwell-Boltzmann distribution.

The calculation of f_{exch} is illustrated in Figure 5, which shows spectra of unreacted DCl (blue) and D \rightarrow H exchanged HCl (red) following collisions of DCl at different incident energies with bare 0.5 M NaCl (panels a and b) and 5 mM SDS in 0.5 M NaCl (panels c and d). The sharp DCl and HCl signals at early arrival times arise from impulsive scattering of DCl and impurity HCl in the incident beam and are subtracted from the spectra before calculating f_{exch} . Importantly, the spectra in each row show that f_{exch} does not depend on the incident DCl energy: panels a and b are recorded at $\langle E_{\text{inc}} \rangle = 90$ and 10 kJ mol⁻¹, yielding $f_{\text{exch}} = 0.70$ and 0.67, and panels c and d at 90 and 50 kJ mol⁻¹, yielding $f_{\text{exch}} = 0.45$ each. The only difference between the left and right panels is the reduction in impulsive scattering at lower incident DCl energies, which reflects the increase in DCl trapping probability p_{trap} as the collision energy decreases.

The decoupling of f_{exch} from E_{inc} implies that DCl dissolution is a two-step process. First, impinging DCl molecules either recoil directly or dissipate their excess energy and thermally equilibrate at the surface through multiple bounces with probability p_{trap} . Second, a fraction f_{exch} of these momentarily trapped molecules enter the solution, while the remaining fraction of DCl molecules desorb back into the gas phase. The DCl entry probability p_{enter} then equals the product $p_{\text{trap}} \bullet f_{\text{exch}}$. The nearly absent inelastic scattering channel in Figure 5b further

implies that p_{trap} approaches one at low collision energies of 10 kJ mol⁻¹, such that f_{exch} can be equated with the DCl entry probability at the even lower average thermal energy of $2RT_{\text{liq}} = 4.8$ kJ mol⁻¹. We still use the higher 90 kJ mol⁻¹ beam energy in most experiments to measure f_{exch} because the DCl flux is ~4 times higher than at 10 kJ mol⁻¹, which reduces signal averaging time, and because the IS and TD channels can be separated more clearly.

The resulting DCl \rightarrow HCl exchange measurements are plotted against the DS⁻ surface concentration in Figure 6. The error bars represent 90% confidence intervals, as listed in Table 1. This figure reveals three trends: 1) f_{exch} is nearly constant at 0.70 ± 0.03 for the different bare NaCl, CaCl₂, and MgCl₂ solutions;⁴⁷ 2) f_{exch} drops at first gradually and then sharply as SDS is added to the different salt solutions, and reaches its lowest value of 0.11 ± 0.05 for 10.9 mM SDS in 0.25 M MgCl₂; and 3) the f_{exch} values coalesce into a single narrow band, apparently independent of cation identity, when plotted against DS⁻ monolayer coverage. These trends are discussed below.

3.5 Discussion

3.5.1 DCl Entry into SDS-Coated Salty Glycerol.

Our key observations are summarized in Figure 6, which shows that DCl \rightarrow HCl exchange decreases steadily with dodecyl chain packing in a similar fashion for the different Na⁺, Ca²⁺, and Mg²⁺ subphase ions. As described above, these $f_{\rm exch}$ values can be equated with the entry probability of DCl into glycerol under thermal collision conditions. Figure 6 shows that these entry probabilities range from 0.70 for bare salty glycerol to 0.11 for a DS⁻ surface concentration of 1.76×10^{14} cm⁻², equal to ~34% of the maximum monolayer coverage of 8×10^{14} cm⁻² inferred from crystalline SDS.⁴³ The constant values for the bare salty solutions imply that the Na⁺, Mg²⁺, and Ca²⁺ cations do not alter DCl entry, most likely because of their low mole

fractions relative to glycerol (50:1 glycerol:cation for 0.25 M cation) and because these ions likely lie below the outermost layer of glycerol molecules where ionization begins to occur.⁴⁷ Previous simulations predict that impinging HCl molecules achieve significant ionic character within 5 ps of the collision with surface glycerol molecules and within a 5 Å depth, equal to one monolayer.⁴⁸ Simulations of facile HCl ionization at the surface of pure water are in accord with this picture, beginning with formation of interfacial H⁺/Cl⁻ contact ion pairs.⁴⁹⁻⁵¹

The adsorption of SDS at the surface of water has been visualized by Rideg et al. through molecular dynamics simulations. Side- and top-view snapshots are reproduced in Figure 7 at low and high surface densities corresponding to 0.6×10^{14} cm⁻² (170 Å²/chain) and 2.4×10^{14} cm⁻² (42 Å²/chain), in comparison with 1.8×10^{14} cm⁻² (55 Å²/chain) for the most compact DS-film we investigated on glycerol. The simulations reveal numerous entangled and bent dodecyl chains that become more organized and cover more of the surface at the higher chain density. The sulfate head groups appear to be well solvated, and additional studies indicate that the closest 1-4 CH₂ groups are also often submerged in these porous monolayers. We note that the 46% coverage snapshot in Figure 7 is close to the maximum SDS concentration on pure water before micelles begin to form. Significantly at speeds comparable to the underlying water molecules.

Figure 6 shows the trends in DCl entry at different areas A per DS⁻ chain. The DCl entry probabilities change little at DS⁻ surface areas greater than 100 Å² but decrease sharply as the monolayer becomes more compact. We imagine that the DS⁻ chains adopt a wide range of configurations when the average area exceeds ~100 Å² (roughly five times the cross-sectional area of crystalline SDS), including chains that lie flat along the surface. Even in this case, DCl

molecules striking the chains first will likely bounce a second time and make contact with the bare glycerol surface, where the entry probability is high. Figure 6 suggests that this mechanism is replaced near 100 Å^2 by more tortuous pathways of DCl moving between the DS $^{-}$ chains. This linear regime has also been observed for N₂O₅ transport through butanol and hexanol monolayers in the same coverage region, 58 and should eventually depend exponentially on surface coverage for much smaller molecular areas and when the surfactant chains are longer. $^{7.59}$ In our experiments, the lowest entry probability of 0.11 is attained when the average surface area per chain is roughly 55 Å^2 . The average distance between alkyl chains is then approximately 7.4 Å, or about 3 Å greater than the 4.4 Å separation in crystalline SDS. This average gap is close to the $\sim 3.7 \text{ Å}$ diameter of a DCl molecule, based on a molecular volume of 51 Å^3 per molecule. Our measurements imply that this gap, over the length of the CH₃(CH₂)₁₁ alkyl chain, is sufficient to stop 90% of the impinging DCl molecules from reaching the underlying glycerol subphase and dissociating. The remaining 10% may be captured by glycerol OH groups in bare patches or that poke through the DS $^{\circ}$ chains (shown in Figure 7). 53,54,60

The coalescence of entry probabilities into a narrow band in Figure 6 suggests that DCl entry is primarily controlled by the dodecyl chain density, such that conformational changes or binding to the sulfate headgroup caused by the subphase Na^+ , Ca^{2+} , and Mg^{2+} cations do not significantly perturb the chain conformations at the same chain density. This might be expected for long entangled chains, where the effect of sulfate headgroup orientation is lost over the methyl and 11 methylene groups. Figure 3 and Table 1, however, indicate that SDS surface segregation is promoted in the order $Na^+ < Ca^{2+} \approx Mg^{2+}$. Specifically, for 2 mM SDS, the DS-surface concentration ratios are 0.73:0.98:1.0 for the 0.25 M salts NaCl:CaCl₂:MgCl₂. This divalent effect persists in mixtures of Mg^{2+} and Na^+ , as reflected in the sea salt measurements:

the addition of 0.05 M MgCl₂ to 0.5 M NaCl raises the DS⁻ surface concentration by 11% for 2 mM SDS. Although this increased coverage does not produce a significant change in DCl entry, it may suppress gas transport more substantially when the packing density is higher, an effect we hope to investigate in the future.

Lastly, molecular dynamics simulations by Chen et al. provide a microscopic perspective on the effect of adding divalent salts to SDS in water. They show that Mg²⁺ and Ca²⁺, mostly accompanied by their tightly bound solvation shells, replace Na⁺ ions bound directly to DS⁻ and enhance bridging between neighboring DS⁻ headgroups; Ca²⁺ and Mg²⁺ also enhance bridging in SDS micelles 17,19. Additionally, Chen et al. predict that water molecules situated between DS⁻ and Ca²⁺/Mg²⁺ actually roughen the surface of the SDS-coated solution, creating *more* surface area and therefore more disordered and loosely packed DS⁻ chains for the *same* nominal surface areas of 40 Å²/chain. This roughening creates surface areas that are 10% greater for 0.5 M MgCl₂ and 5% greater for 0.5 M CaCl₂ than for the bare surface and for 1.0 M NaCl, which had no effect. Our DCl uptake measurements are performed at higher DS⁻ surface areas of 57 Å²/chain and may not be sensitive to these small changes, but it would be intriguing to measure gas permeation through more tightly packed monolayers, where this ion-induced roughening may generate fluctuating holes in the DS⁻ film.

3.5.2 Implications for Gas Uptake into the Ocean and into Sea Spray

The observed reductions in DCl entry from $p_{\text{enter}} = 0.7$ on bare salty glycerol to 0.1 on 11 mM SDS in 0.25 M MgCl₂ will not limit the entry of HCl into the ocean when compared to gasphase diffusion, but they can limit DCl entry into submicron sea spray particles. These consequences may be inferred from the relation between the flux J of dissolving molecules and the overall resistance r to gas transport, where $J = n_{\text{gas}}/r$ and r = r(air) + r(monolayer). Over

distances within 10 m above the ocean, the global average for r(air) is roughly 1 s cm⁻¹ at a global average wind speed of 7 m s⁻¹.⁶¹ This can be compared to the much smaller resistance of the monolayer itself, given by $r(\text{monolayer}) = 4/(\langle v \rangle p_{\text{enter}})$, where $\langle v \rangle = (8RT/\pi m)^{1/2}$ is the average DCl velocity.⁶² The monolayer resistances range from 1.4×10^{-4} s cm⁻¹ for $p_{\text{enter}} = 0.7$ to 1.0×10^{-3} s cm⁻¹ for $p_{\text{enter}} = 0.1$. These monolayer resistances are negligible compared to the 1 s cm⁻¹ diffusion barrier on the airside of the ocean; p_{enter} must drop to 1×10^{-4} to equal this diffusion resistance through the air layer. Such low monolayer resistances can generally be attained only for compact monolayers of longer chain alcohols and carboxylic acids under pristine conditions.^{7,26,59,63}

The gas-phase diffusion region around aerosol particles is much thinner because of their smaller size. This diffusional resistance may be estimated from the Fuchs-Sutegin equation $r(\text{air}) \approx (a/D_{\text{HCl}})(1-0.62/(1+a/\lambda))$, where a is the particle radius, D_{HCl} is the HCl gas-phase diffusion coefficient, and λ is the HCl mean free path. At a pressure of one atmosphere, D_{HCl} is $\sim 0.1 \text{ cm}^2 \text{ s}^{-1}$, λ is $\sim 70 \text{ }\mu\text{m}$, and r(aerosol) is calculated to be 5×10^{-6} , 8×10^{-5} , and $1 \times 10^{-3} \text{ s}$ cm⁻¹ for particle radii of 0.01, 0.1, and $1 \text{ }\mu\text{m}$, respectively. Thus, our lowest measured entry probability of 0.1 imposes a higher resistance ($1 \times 10^{-3} \text{ s cm}^{-1}$) than gas-phase diffusion for particles with radii smaller than $1 \text{ }\mu\text{m}$. A substantial fraction of nascent sea spray radii fall within the $1 \text{ }\mu\text{m}$ range, implying that even porous films can reduce the entry of gases into fine aerosol droplets, and affect the rapid and near-surface hydrolysis of N_2O_5 as well. Indeed, the 7-fold decrease we observe for DCl permeation through SDS on glycerol is close to the 10-fold decrease observed by McNeill et al. for N_2O_5 permeation through SDS on seawater.

Although SDS in coastal ocean regions has been attributed to leakage from wastewater, 12 it is not likely to be plentiful with respect to other surfactants such as long-chain carboxylic

acids.^{5,66} In particular, the total dissolved organic carbon in the ocean is generally below 0.1 mM in the bulk, much lower than the SDS concentrations used here.^{1,4} Aerosol particles, however, may be highly enriched in both organic species and ions, as reviewed in ref 1. Our goal in forthcoming studies is to use the data in Figure 6 as an "SDS permeation scale" against which we can compare DCl entry through surface-active species found in the ocean and in sea spray. We hope that these measurements may be particularly valuable for entry probabilities between 0.1 and 1, a range that is not easily accessible by non-vacuum techniques limited by gas-phase diffusion.

3.6 Acknowledgments

This research was supported by the National Science Foundation via the Center for Aerosol Impacts on Climate and the Environment, a Center for Chemical Innovation (NSF CHE1305427). We thank Tim Bertram, Ellen Adams, Heather Allen, Francesco Paesani, Vicki Grassian, and Kim Prather for many useful discussions throughout this project. We also thank Keaten Kappes for assisting with the surface tension measurements and the authors of refs 52 and 53 for permission to use Figure 7.

3.7 Appendix

Figure A.1 shows surface tension measurements of as-received SDS (Sigma Alrich 99%+) and SDS recrystallized once from ethanol. In water, the surface tension of as-received SDS dips at 6 mM concentration, attributed to the presence of the impurity, dodecanol.³⁰⁻³³ This curve diminishes after one recrystallization in ethanol, as shown in the figure. In glycerol, the stock and recrystallized SDS have nearly identical surface tensions up to the 5 mM concentration

using in most of our experiments. Based on the similarity of the surface tensions and the DCl entry probabilities, we used the as-received SDS for all of our studies.

Table 1. DS Surface Concentrations and $f_{\rm exch}$ Values^a

| Salt Solution (M) | SDS Conc (mM) | n_{surf} Surf Tens $(\times 10^{14} \text{cm}^{-2})$ | n_{surf} Ar Scatt $(\times 10^{14} \text{cm}^{-2})$ | n _{surf} Ratio (Ar/ST) | $f_{ m exch}$ | # Trials |
|------------------------|-------------------|--|---|---------------------------------|-----------------|----------|
| Pure Glycerol | 5.0 | 0.52 ± 0.02 | - | - | - | - |
| 0.5 NaCl | 0 | 0 | 0 | - | 0.69 ± 0.02 | 12 |
| | 0.5 | 0.69 ± 0.03 | 0.44 ± 0.08 | 0.64 | 0.68 ± 0.02 | 7 |
| | 2.0 | 1.21 ± 0.02 | 1.02 ± 0.06 | 0.84 | 0.54 ± 0.01 | 4 |
| | 5.0 | 1.53 ± 0.10 | 1.53 ± 0.05 | 1.00 | 0.45 ± 0.02 | 9 |
| 0.25 NaCl | 1.0 | 0.88 ± 0.04 | 0.90 ± 0.06 | 1.02 | 0.58 ± 0.03 | 4 |
| | 2.0 | 1.19 ± 0.04 | - | - | - | - |
| | 5.0 | 1.37 ± 0.07 | 1.27 ± 0.12 | 0.93 | 0.32 ± 0.03 | 4 |
| 0.25 CaCl ₂ | 0 | 0 | 0 | - | 0.71 ± 0.02 | 4 |
| | 2.0 | 1.43 ± 0.13 | 0.92 ± 0.09 | 0.64 | 0.55 ± 0.05 | 3 |
| | 5.0 | 1.57 ± 0.01 | 1.35 ± 0.19 | 0.86 | 0.21 ± 0.03 | 4 |
| 0.25 MgCl ₂ | 0 | 0 | 0 | - | 0.71 ± 0.01 | 4 |
| | 0.5 | 1.23 ± 0.11 | 0.35 ± 0.05 | 0.28 | 0.70 ± 0.02 | 4 |
| | 2.0 | 1.46 ± 0.03 | 1.12 ± 0.06 | 0.77 | 0.50 ± 0.03 | 4 |
| | 5.0 | 1.56 ± 0.08 | 1.39 ± 0.10 | 0.89 | 0.21 ± 0.02 | 12 |
| | 10.9 ^b | 1.81 ± 0.06 | 1.76 ± 0.05 | 0.97 | 0.11 ± 0.05 | 4 |
| Sea Salt | 2.0 | 1.34 ±0.03 | 0.99 ± 0.07 | 0.74 | 0.53 ± 0.02 | 3 |

^a Error bars correspond to \pm 1 standard deviation for n_{surf} (surface tension), the uncertainty in fitting the TOF spectra for n_{surf} (Ar scattering), and 90% confidence intervals for f_{exch} for the indicated number of measurements.

^b Determined from a Langmuir fit instead of a numerical derivative.

References and Notes

- 1. Quinn, P. K.; Collins, D. B.; Grassian, V. H.; Prather, K. A.; Bates, T. S. Chemistry and Related Properties of Freshly Emitted Sea Spray Aerosol. *Chem. Rev.* **2015**, *115*, 4383-4399.
- 2. Cunliffe, M.; Engel, A.; Frka, S.; Gašparovíc, B.; Guitart, C.; Murrell, J. C.; Salter, M.; Stolle, C.; Upstill-Goddard, R.; Wurl, O. Sea Surface Microlayers: A Unified Physicochemical and Biological Perspective of the Air-Ocean Interface. *Prog. Oceanogr.* **2013**, *109*, 104-116.
- 3. Verdugo, P. Marine Microgels. Ann. Rev. Mar. Sci. 2012, 4, 375-400.
- 4. van Pinxteren, M.; Muller, C.; Iinuma, Y.; Stolle, C.; Herrmann, H. Chemical Characterization of Dissolved Organic Compounds from Coastal Sea Surface Microlayers (Baltic Sea, Germany). *Environ. Sci. Tech.* **2012**, *46*, 10455-10462.
- 5. Marty, J. C.; Saliot, A.; Buat-Menard, P.; Chesselet, R.; Hunter, K. A. Relationship between the Lipid Concentrations of Marine Aerosols, the Sea Surface Microlayers and Subsurface Water. *J. Geophys. Res.*, *C: Ocean Atmos.* **1979**, *84*, 5707-5716.
- 6. Donaldson, D. J.; Vaida, V. The Influence of Organic Films at the Air-Aqueous Boundary on Atmospheric Processes. *Chem. Rev.* **2006**, *106*, 1445-1461.
- 7. Cosman, L. M.; Knopf, D. A.; Bertram, A. K. N₂O₅ Reactive Uptake on Aqueous Sulfuric Acid Solutions Coated with Branched and Straight-Chain Insoluble Organic Surfactants. *J. Phys. Chem. A* **2008**, *112*, 2386-2396.
- 8. Park, S.-C.; Burden, D. K.; Nathanson, G. M. Surfactant Control of Gas Transport and Reactions at the Surface of Sulfuric Acid. *Acc. Chem. Res.* **2009**, *42*, 379 387.
- 9. Griffith, E. C.; Tuck, A. F.; Vaida, V. Ocean-Atmosphere Interactions in the Emergence of Complexity in Simple Chemical Systems. *Acc. Chem. Res.* **2012**, *45*, 2106-2113.
- 10. Ryder, O. S.; Ault, A. P.; Cahill, J. F.; Guasco, T. L.; Reidel, T. P.; Caudra-Rodriguez, L. A.; Gaston, C. J.; Fitzgerald, E.; Lee, C.; Prather, K. A.; Bertram, T. H. On the Role of Particle Inorganic Mixing State in the Reactive Uptake of N₂O₅ to Ambient Aerosol Particles. *Environ. Sci. Tech.* **2014**, *48*, 1618-1627.
- 11. Larsson, K.; Odham, G.; Södergren, A. On Lipid Surface Films on the Sea. I. A Simple Method for Sampling and Studies of Composition. *Mar. Chem.* **1974**, *2*, 49-57.
- 12. Lara-Martín, P. A.; Gómez-Parra, A.; González-Mazo, E. Development of a Method for the Simultaneous Analysis of Anionic and Non-Anionic Surfactants and Their Carboxylated Metabolites in Environmental Samples by Mixed-Mode Liquid Chromatography-Mass Spectrometry. *J. Chromatogr. A* **2006**, *1137*, 188-197.

- 13. Li, Z.; Williams, A. L.; Rood, M. J. Influence of Soluble Surfactant Properties on the Activation of Aerosol Particles Containing Inorganic Solute. *J. Atmos. Sci.* **1998,** *55*, 1859-1866.
- 14. McNeill, V. F.; Patterson, J.; Wolfe, G. M.; Thornton, J. A. The Effect of Varying Levels of Surfactant on the Reactive Uptake of N₂O₅ to Aqueous Aerosol. *Atmos. Chem. Phys.* **2006**, *6*, 1635-1644.
- 15. Frinak, E. K.; Abbatt, J. P. D. Br₂ Production from the Heterogeneous Reaction of Gas-Phase OH with Aqueous Solutions: Impacts of Acidity, Halide Concentration, and Organic Surfactants. *J. Phys. Chem. A* **2006**, *110*, 10456-10464.
- 16. Davies, J. F.; Haddrell, A. E.; Miles, R. E.; Bull, C. R.; Reid, J. P. Bulk, Surface, and Gas-Phase Limited Water Transport in Aerosol. *J. Phys. Chem. A* **2012**, *116*, 10987-10998.
- 17. Yan, H.; Yuan, S. L.; Xu, G. Y.; Liu, C. B. Effect of Ca²⁺ and Mg²⁺ Ions on Surfactant Solutions Investigated by Molecular Dynamics Simulation. *Langmuir : the ACS journal of surfaces and colloids* **2010**, *26*, 10448-10459.
- 18. Chen, M.; Lu, X.; Liu, X.; Hou, Q.; Zhu, Y.; Zhou, H. Specific Counterion Effects on the Atomistic Structure and Capillary-Waves Fluctuation of the Water/Vapor Interface Covered by Sodium Dodecyl Sulfate. *J. Phys. Chem. C* **2014**, *118*, 19205-19213.
- 19. Sammalkorpi, M.; Karttunen, M.; Haataja, M. Ionic Surfactant Aggregates in Saline Solutions: Sodium Dodecyl Sulfate (SDS) in the Presence of Excess Sodium Chloride (NaCl) or Calcium Chloride (CaCl₂). *J. Phys. Chem. B* **2009**, *113*, 5863-5870.
- 20. Pandey, S.; Bagwe, R. P.; Shah, D. O. Effect of Counterions on Surface and Foaming Properties of Dodecyl Sulfate. *J. Coll. Interface Sci.* **2003**, 267, 160-166.
- 21. Ault, A. P.; Moffet, R. C.; Baltrusaitis, J.; Collins, D. B.; Ruppel, M. J.; Cuadra-Rodriguez, L. A.; Zhao, D.; Gausco, T. L.; Ebben, C. J.; Geiger, F. M.; Bertram, T. H.; Prather, K. A.; Grassian, V. H. Size-Dependent Changes in Sea Spray Aerosol Composition and Properties with Different Seawater Conditions. *Environ. Sci. Tech.* **2013**, *47*, 5603-5612.
- 22. Matuura, R.; Kimizuka, H.; Yatsunami, K. The Study of the Adsorption of Detergents at a Solution-Air Interface by Radiotracer Method. III. The Effect of Inorganic Electrolytes on the Adsorption of Sodium Dodecyl Sulfate. *Bull. Chem. Soc. Japan* **1959**, *32*, 646-650.
- 23. Giribabu, K.; Reddy, M. L. N.; Ghosh, P. Coalescence of Air Bubbles in Surfactant Solutions: Role of Salts Containing Mono, Di, and Trivalent Ions. *Chem. Eng. Comm.* **2008**, *195*, 336-351.

- 24. Cross, A. W.; Jayson, G. G. The Effect of Small Quantities of Calcium on the Adsorption of Sodium Dodecyl Sulfate and Calcium at the Gas-Liquid Interface. *J. Coll. Interface Sci.* **1994**, *162*, 45-51.
- 25. Morris, J. R.; Behr, P.; Antman, M. D.; Ringeisen, B. R.; Splan, J.; Nathanson, G. M. Molecular Beam Scattering from Supercooled Sulfuric Acid: Collisions of HCl, HBr, and HNO₃ with 70 wt % D₂SO₄. *J. Phys. Chem. A* **2000**, *104*, 6738-6751.
- 26. Acidic gas entry and dissociation have also been measured using an acid-base indicator. See Gilman, J. B.; Vaida, V. Permeability of Acetic Acid Through Organic Films at the Air-Aqueous Interface *J. Phys. Chem. A* **2006**, *110*, 7581-7587.
- 27. Ringeisen, B. R.; Muenter, A. H.; Nathanson, G. M. Collisions of HCl, DCl, and HBr with Liquid Glycerol: Gas Uptake, D→H Exchange, and Solution Thermodynamics. *J. Phys. Chem. B* **2002**, *106*, 4988-4998.
- 28. Miner, C. S., *Glycerol*. Reinhold Publishing Corporation: New York, 1953.
- 29. Lawrence, J. R.; Glass, S. V.; Nathanson, G. M. Evaporation of Water through Butanol Films at the Surface of Supercooled Sulfuric Acid. *J. Phys. Chem. A* **2005**, *109*, 7449-7457.
- 30. Mysels, K. J. Surface Tension of Solutions of Pure Sodium Dodecyl Sulfate. *Langmuir*: the ACS journal of surfaces and colloids **1986**, 2, 423-428.
- 31. Hines, J. D. The Preparation of Surface Chemically Pure Sodium *n*-Dodecyl Sulfate by Foam Fractionation. *J. Colloid Interface Sci.* **1996,** *180*, 488-492.
- 32. Prosser, A. J.; Franses, E. I. Adsorption and Surface Tension of Ionic Surfactants at the Air-Water Interface: Review and Evaluation of Equilibrium Models. *Colloids Surf.*, *A* **2001**, *178*, 1-40.
- 33. Kralchevsky, P. A.; Danov, K. D.; Kolev, V. L.; Broze, G.; Mehreteab, A. Effect of Nonionic Admixtures on the Adsorption of Ionic Surfactants at Fluid Interfaces. 1. Sodium Dodecyl Sulfate and Dodecanol. *Langmuir: the ACS journal of surfaces and colloids* **2003**, *19*, 5004-5018.
- 34. Nguyen, A. V.; Nguyen, K. T. *In Situ* Investigation of Halide Co-Ion Effects on SDS Adsorption at Air-Water Interfaces. *Soft Matter* **2014**, *10*, 6556-6563.
- 35. Arias, C.; Gómez-Excalonilla, I.; Rueda, C.; Molina, C. Influence of the Purification of Sodium Dodecyl Sulfate on the Physical Properties of Solutions and O/W Emulsions. *Drug. Develop. Ind. Pharm.* **1998**, *24*, 95-100.

- 36. When HCl is present in the DCl incident beam, eq 4 becomes $f_{\text{exch}}(\text{true}) = [f_{\text{exch}}(\text{observed}) g_{\text{HCl}}]/[1 g_{\text{HCl}}]$, where g_{HCl} is the fraction of HCl in the incident beam.
- 37. Marcus, Y. Surface Tension of Aqueous Electrolytes and Ions. *J. Chem. Eng. Data* **2010**, 55, 3641-3644.
- 38. Chattoraj, D. K.; Birdi, K. S., *Adsorption and the Gibbs Surface Excess*. Plenum Press: 1984.
- 39. In the monolayer model, $n_{\text{surf}}(DS^-) = \Gamma(DS^-) + n^{2D}(Cl^-) [1 A(DS^-) (DS^-)]$, where $n^{2D}(Cl^-)$ is the surface concentration in the absence of segregation or depletion, and A is the molecular area. For dilute surfactant solutions, $n^{2D}(Cl^-)$ is roughly $[DS^-]/([gly]A(gly))$, which is $3x10^{11}$ cm⁻² for 11 mM SDS. This term is less than 1% of $\Gamma(DS^-)$.
- 40. Sasaki, J.; Tajima, K.; Sasaki, T. Adsorption of Sodium and Calcium Dodecyl Sulfates at the Surface of Their Aqueous Solutions. *Bull. Chem. Soc. Japan* **1972**, *45*, 348-351.
- 41. Tajima, K. Radiotracer Studies on Adsorption of Surface Active Substance at Aqueous Surface. III. The Effects of Salt on the Adsorption of Sodium Dodecylsulfate. *Bull. Chem. Soc. Japan* **1971**, *44*, 1767-1771.
- 42. Cutler, S. G.; Meares, P.; Hall, D. G. Ionic Activities in Sodium Dodecyl Sulphate Solutions from Electromotive Force Measurements. *J. Chem. Soc.*, *Faraday Trans.* **1978**, *1*, 1758-1767.
- 43. Smith, L. A.; Hammond, R. B.; Roberts, K. J.; Machin, D.; McLeod, G. Determination of the Crystal Structure of Anhydrous Sodium Dodecyl Sulphate Using a Combination of Synchrotron Radiation Powder Diffraction and Molecular Modelling Techniques. *J. Molec. Struct.* **2000**, *554*, 173-182.
- 44. Burden, D. K.; Johnson, A. M.; Nathanson, G. M. HCl Uptake through Films of Pentanoic Acid and Pentanoic Acid/Hexanol Mixtures at the Surface of Sulfuric Acid. *J. Phys. Chem. A* **2009**, *113*, 14131-14140.
- 45. Ferri, J. K.; Stebe, K. J. Which Surfactants Reduce Surface Tension Faster? A Scaling Argument for Diffusion-Controlled Adsorption. *Adv. Colloid Interface Sci.* **2000**, *85*, 61-97.
- 46. The characteristic time for production of HCl(g) from dissolved H⁺ and Cl⁻ in excess Cl⁻ can be estimated from the relation $\mathcal{T}_{\text{HCl}} = D_{\text{HCl}} (4K_{\text{HCl}} RT/f_{\text{exch}} < v > g^{\pm} [\text{Cl}^{-}])^2$. In this equation, $D_{\text{HCl}} \sim 10^{-8} \, \text{cm}^2 \, \text{s}^{-1}$ is the joint H⁺ + Cl⁻ diffusion coefficient, $K_{\text{HCl}} = 2000 \, \text{M}^2$ atm⁻¹ is the equilibrium constant for HCl(g) = H⁺(gly) + Cl⁻(gly), g^{\pm} is the HCl activity coefficient, and $< v > = (8RT/\pi \, \text{m}_{\text{HCl}})^{1/2} = 4 \times 10^4 \, \text{cm s}^{-1}$. For the worst case of [Cl⁻] = 0.5 M, $f_{\text{exch}} = 0.1$, and $g^{\pm} = 0.3$ for 11 mM SDS in 0.25 M MgCl₂, \mathcal{T}_{HCl} is 0.001 s. For this short time, essentially all HCl desorbs from the glycerol film during the 0.1 s beam

- exposure and mass spectrometer observation time of the rotating wheel. The equation for \mathcal{F}_{HCl} may be derived from eq 2 of ref 27 by noting that $H = K_{HCl}/(g^{\pm}[Cl^{-}])$ and $[Cl^{-}]$ is constant.
- 47. We have previously investigated distinct near-interfacial and bulk-phase DCl⊕HCl exchange in salty glycerol without a common Cl⁻ ion. In the case here of a large Cl⁻ excess, the distinction between interfacial and bulk-phase exchange becomes blurred because Cl⁻ ions are distributed throughout the near-surface region. The overall entry probability 0.7 measured here on bare salty glycerol is lower than the value predicted by our earlier studies of ~0.9. This may be due to errors in the earlier analysis, which involved a complex complex comparison of absolute uptake measurements and TOF spectra. For details, see Muenter, A. H.; DeZwaan, J. L.; Nathanson, G. M. Collisions of DCl with Pure and Salty Glycerol: Enhancement of Interfacial D→H Exchange by Dissolved NaI. *J. Phys. Chem. B* **2006**, *110*, 4881-4891.
- 48. Chorny, I.; Benjamin, I.; Nathanson, G. M. Scattering, Trapping, and Ionization of HCl at the Surface of Liquid Glycerol. *J. Phys. Chem. B* **2004**, *108*, 995-1002.
- 49. Ardura, D.; Donaldson, D. J. Where Does Acid Hydrolysis Take Place? *Phys. Chem. Chem. Phys.* **2009**, *11*, 857-863.
- 50. Wick, C. D. HCl Accommodation, Dissociation, and Propensity for the Surface of Water. *J. Phys. Chem. A* **2013**, *117*, 12459-12467.
- 51. Baer, M. D.; Tobias, D. J.; Mundy, C. J. Investigation of Interfacial and Bulk Dissociation of HBr, HCl, and HNO₃ Using Density Functional Theory-Based Molecular Dynamics Simulations. *J. Phys. Chem. C* **2014**, *118*, 24912-29420.
- 52. Rideg, N. A.; Darvas, M.; Varga, I.; Jedlovszky, P. Lateral Dynamics of Surfactants at the Free Water Surface: A Computer Simulation Study. *Langmuir: the ACS journal of surfaces and colloids* **2012**, 28, 14944-14953.
- 53. Abranko-Rideg, N.; Horvai, G.; Jedlovszky, P. Structure of the Adsorption Layer of Various Ionic and Non-Ionic Surfactants at the Free Water Surface, as Seen from Computer Simulation and ITIM Analysis. *J. Mol. Liq.* **2015**, *205*, 9-15.
- 54. Abrankó-Rideg, N.; Darvas, M.; Horvai, G.; Jedlovszky, P. Immersion Depth of Surfactants at the Free Water Surface: A Computer Simulation and ITIM Analysis Study. *J. Phys. Chem. B* **2013**, *117*, 8733-8746.
- 55. Wilson, A.; Epstein, M. B.; Ross, J. The Adsorption of Sodium Lauryl Sulfate and Lauryl Alcohol at the Air-Liquid Interface. *J. Colloid Sci.* **1957**, *12*, 345-355.
- 56. Nilsson, G. The Adsorption of Tritriated Sodium Dodecyl Sulfate at the Solution Surface Measured with a Windowless, High Humidity Gas, Flow Proportional Counter. *J. Phys. Chem.* **1957**, *61*, 1135.

- 57. Persson, C. M.; Jonsson, A. P.; Bergström, M.; Eriksson, J. C. Testing the Gouy–Chapman Theory by Means of Surface Tension Measurements for SDS–NaCl–H2O Mixtures. *J. Colloid Interface Sci.* **2003**, *267*, 151-154.
- 58. Lawrence, J. R.; Glass, S. V.; Park, S.-C.; Nathanson, G. M. Surfactant Control of Gas Uptake: Effect of Butanol Films on HCl and HBr Entry into Supercooled Sulfuric Acid. *J. Phys. Chem. A* **2005**, *109*, 7458-7465.
- 59. Barnes, G. T. Permeation through Monolayers. *Colloids Surf.*, A **1997**, 126, 149-158.
- 60. Sakaguchi, S.; Morita, A. Mass Accommodation Mechanism of Water through Monolayer Films at Water/Vapor Interface. *J. Chem. Phys.* **2014**, *137*, 184703.
- 61. Johnson, M. T. A Numerical Scheme to Calculate Temperature and Salinity Dependent Air-Water Transfer Velocities of Any Gas. *Ocean Sci.* **2010**, *6*, 913-932.
- 62. Shi, Q.; Davidovits, P.; Jayne, J. T.; Worsnop, D. R.; Kolb, C. E. Uptake of Gas-Phase Ammonia. 1. Uptake by Aqueous Surfaces as a Function of pH. *J. Phys. Chem. A* **1999**, *103*, 8812-8823.
- 63. Barnes, G. T. The Potential for Monolayers to Reduce the Evaporation of Water from Large Water Storages. *Agric. Water Manag.* **2008**, *95*, 339-353.
- 64. Pokkunuri, P.; Nissenson, P.; Dabdub, D. Impact of the Knudsen Number and Mass-Transfer Expression on Multi-Phase Kinetic Modeling. *Atmos. Environ.* **2010**, *44*, 153-163.
- 65. Fuchs, N. A.; Sutugin, A. G., *Highly Dispersed Aerosols*. Ann Arbor Science Publishers: Ann Arbor, 1970; Ch. 3.8.
- 66. Tervahattu, H.; Juhanoja, J.; Kupiainen, K. Identification of an Organic Coating on Marine Aerosol Particles by TOF-SIMS. *J. Geophys. Res.-Atmos.* **2002**, *107*, D16-4319.

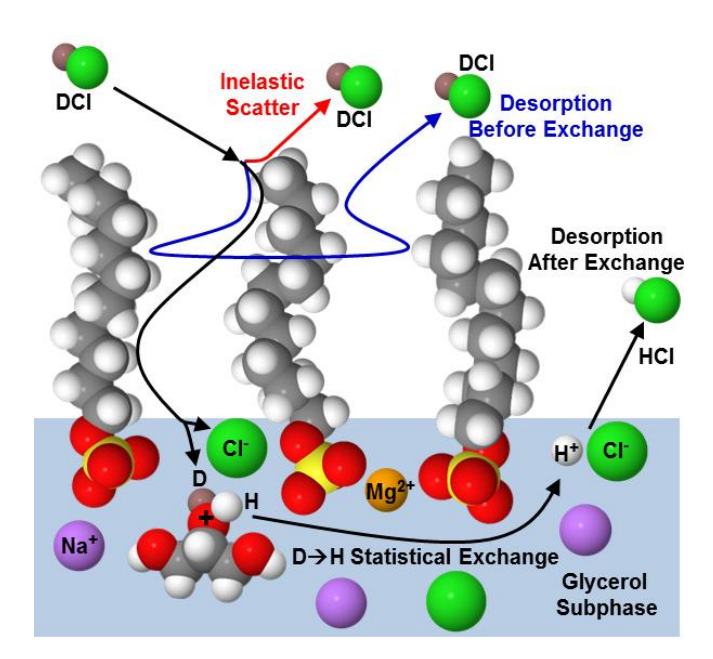


Figure 1. Collisions of gas-phase DCl with sodium dodecyl sulfate ($CH_3(CH_2)_9OSO_3^-$) at the surface of a MgCl₂/glycerol solution. The DCl entry probability is equal to the fraction of thermally equilibrated DCl molecules that undergo $D^+ \rightarrow H^+$ exchange and produce HCl, which then desorb from solution.

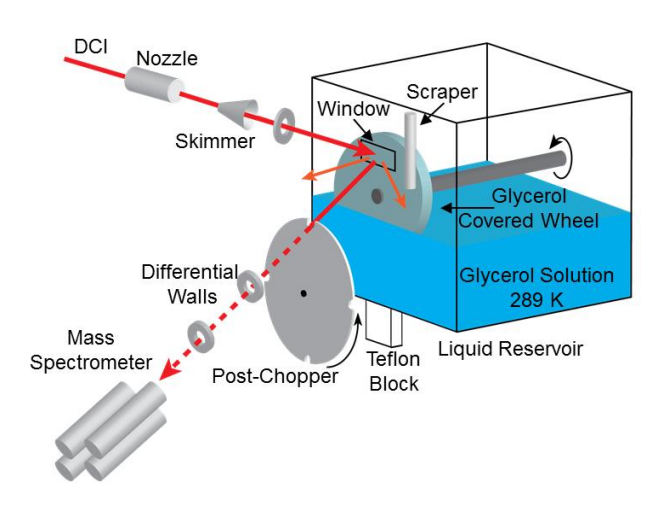


Figure 2. Experimental Setup. The liquid reservoir is enclosed except for a $0.8 \text{ cm tall} \times 1.2 \text{ cm}$ wide hole in the front face, which allows DCl molecules to enter at 45° and collide with the rotating glycerol-coated wheel. DCl and HCl exiting from the liquid at 45° are detected by the mass spectrometer.

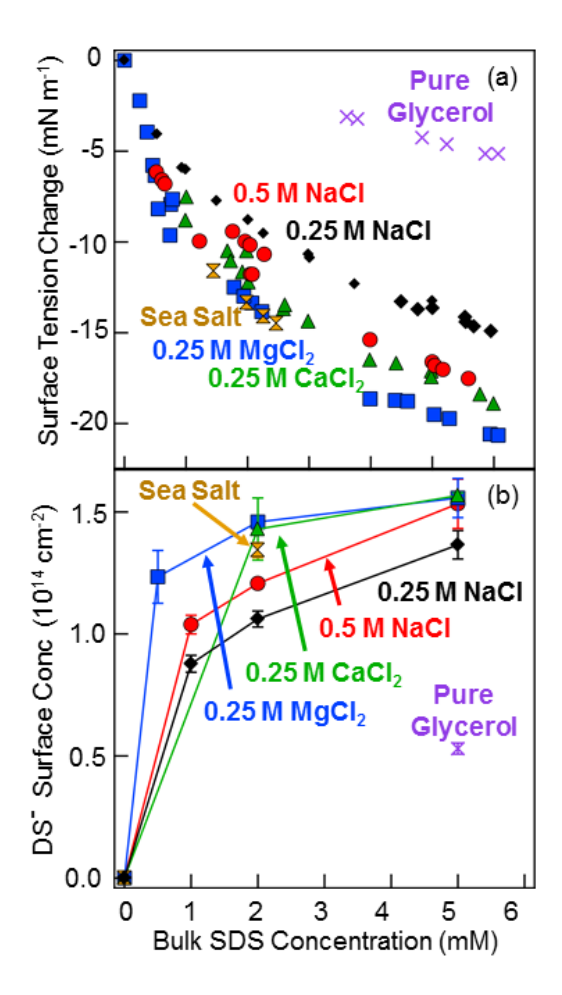


Figure 3. (a) Reduction in surface tension of 0–6 mM SDS in glycerol solutions of 0.25 M NaCl (black diamonds), 0.5 M NaCl (red circles), 0.25 M CaCl₂ (green triangles), 0.25 M MgCl₂ (blue squares), and no salt (purple x). 2 mM SDS in sea salt is represented by the tan hourglass. (b) DS⁻ surface concentration determined from the surface tension measurements at selected concentrations. DS⁻ segregates to the surface in the order 0.25 M MgCl₂ \approx 0.25 M CaCl₂ > sea salt > 0.50 M NaCl > 0.25 M NaCl.

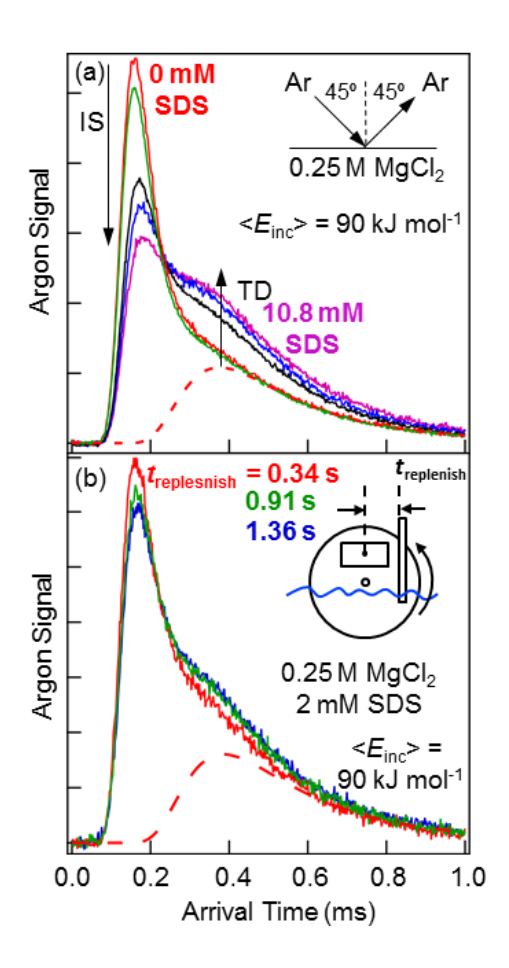


Figure 4. (a) High-energy argon scattering from 0.25 M MgCl₂/glycerol containing no SDS (red) and 0.5 (green), 2.0 (black), 5.0 (blue) and 10.9 (purple) mM SDS. The decrease in inelastic scattering (IS) with increasing SDS concentration is used to gauge DS⁻ surface concentrations. (b) Changes in Ar scattering caused by spinning the glycerol-coated wheel at different speeds, creating different replenishment times between scraping and exposure to the Ar beam.

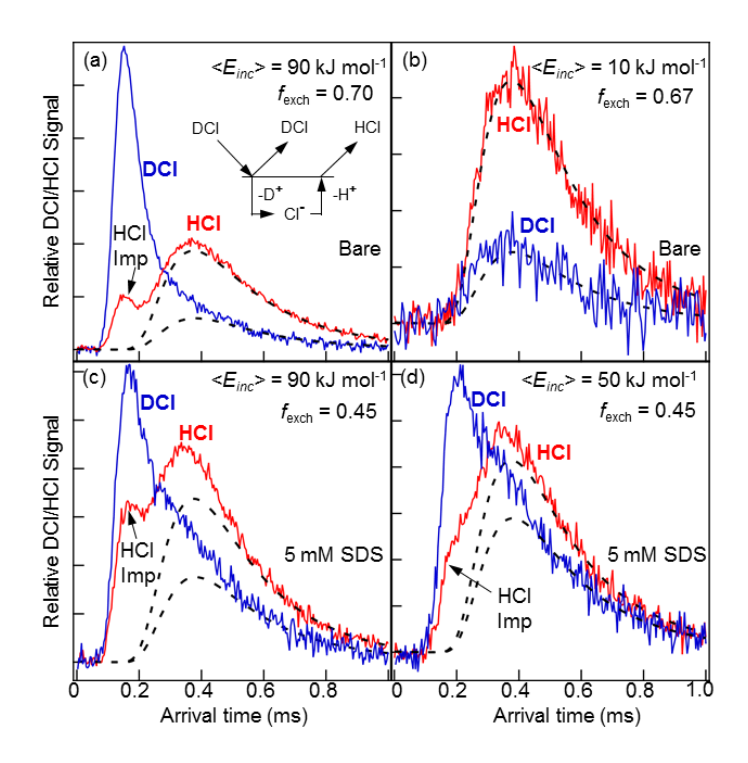


Figure 5. High and low-energy DCl scattering from bare and SDS-coated 0.50 M NaCl/glycerol solutions. Bare glycerol: (a) $\langle E_{\rm inc} \rangle = 90 \text{ kJ mol}^{-1}$ and b) $\langle E_{\rm inc} \rangle = 10 \text{ kJ mol}^{-1}$. 5 mM SDS: c) $\langle E_{\rm inc} \rangle = 90 \text{ kJ mol}^{-1}$ and (d) $\langle E_{\rm inc} \rangle = 50 \text{ kJ mol}^{-1}$. Similar D \rightarrow H exchange values are measured at different energies for the same system. "HCl imp" refers to impurity HCl in the DCl beam.

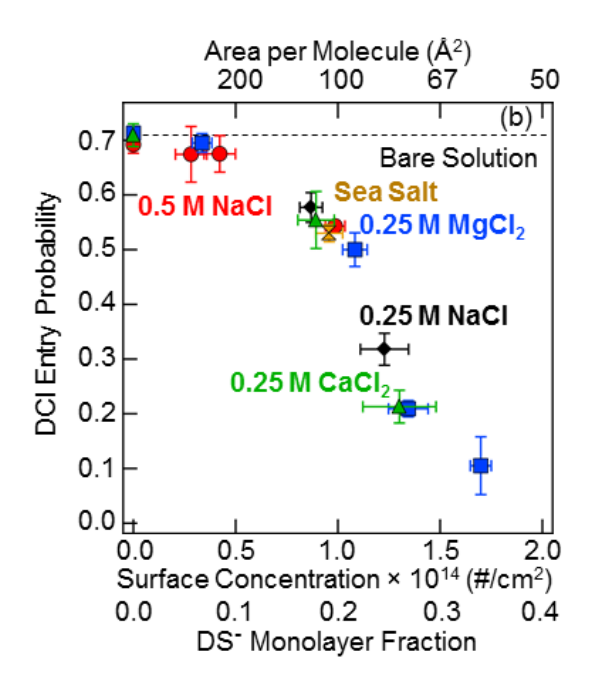


Figure 6. Fraction of thermally equilibrated DCl molecules that enter into salty glycerol (DCl entry probability) versus DS⁻ surface concentration. The DS⁻ surface coverages are based on a maximum packing of 5.2×10^{14} cm⁻².

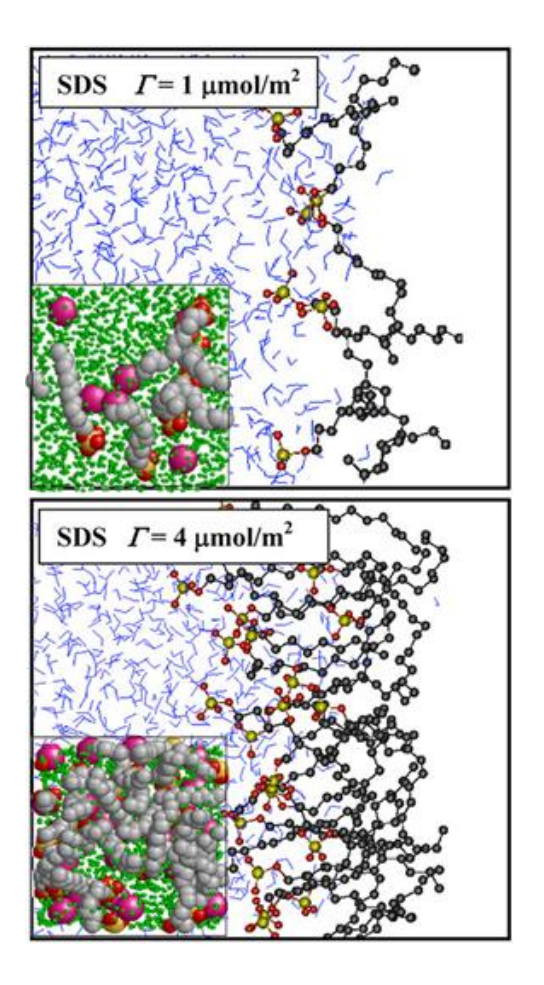


Figure 7. Molecular dynamics snapshots of SDS on water by Rideg et al (refs 52 and 53). The surface concentrations correspond to (a) 6×1013 cm-2 (12% monolayer fraction) and (b) 2.4×1014 cm-2 (46% monolayer fraction). Reproduced with permission from ref 52, copyright 2012 by the American Chemical Society, and ref 53, copyright 2105 by Elsevier.

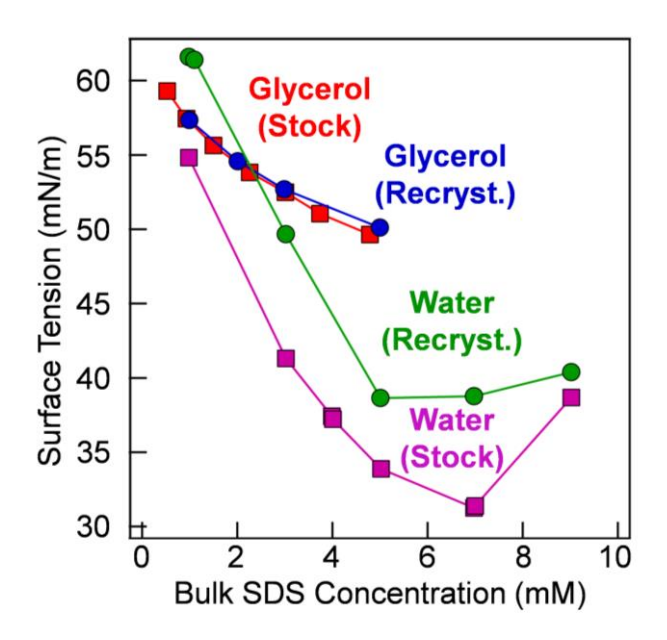


Figure A.1. Surface tensions of as-received SDS (stock) and recrystallized SDS (recryst.) in glycerol and in water.

Chapter 4

N₂O₅ Reactions at the Salty Glycerol Surface: Effects of Tetrahexylammonium Bromide (THABr)

4.1 Introduction

Nitrogen oxides have tremendous impact on the troposphere. NO₂ is considered to be the dominant anthropogenic source of tropospheric ozone,¹ while NO_x (= NO + NO₂) as well as its reservoir species can activate halides to form reactive halogen species.²⁻³ Activation of bromine has been connected to the sudden depletion of O₃ in the arctic, often referred to as the "bromine explosion."⁴⁻⁵ Chloride ions present in sea spray particles can be activated through the production of ClNO₂ generated within sea spray and then emitted into the atmosphere.²⁻³ Once emitted, ClNO₂ photolyzes and generates chlorine atoms. These Cl atoms readily react with organic molecules by hydrogen abstraction and lead their removal from the atmosphere.^{1, 6}

 N_2O_5 is a nighttime reservoir for NO_x that is quickly photolyzed during the day to produce NO_2 and NO_3 , ultimately leading to ozone production via photodissociation of NO_2 into NO + O and $O + O_2 \rightarrow O_3$. Nighttime removal of N_2O_5 is considered to be a major sink for NO_x through its reaction with water in aqueous aerosols to form HNO_3 .⁷⁻⁹ Modeling by Macintyre et al. (see Chapter 1, Figure 4) indicates that the reactive uptake of N_2O_5 by aerosols can have significant impacts on global tropospheric concentrations of O_3 (12% reduction), OH (18% reduction), and CH_4 (2 year enhanced lifetime).⁹ The removal of N_2O_5 from the atmosphere during the night means that there is less NO_2 during the day, and therefore fewer O_3 molecules are produced. In turn, fewer O_3 are available to photolyze to $O(^1D)$, and therefore fewer OH radicals are produced by $O(^1D) + H_2O \rightarrow 2$ OH. Lastly, the lower concentrations of OH imply a longer lifetime for CH_4 because of a lower reaction rate for $OH + CH_4 \rightarrow H_2O + CH_3$. The

uptake of N_2O_5 into sea spray droplets is therefore a crucial step in tropospheric chemistry. Sea spray, generated by breaking waves on the ocean, is one of the most significant sources for atmospheric particles. They are also chemically diverse, and this diversity presents a challenge in determining which of their characteristics control N_2O_5 hydrolysis and other multiphase reactions.¹⁰

Wave breaking and jet droplet formation (described in Chapter 1) can enrich sea spray aerosols in organic molecules, including species such as carbohydrates, 11 saturated and unsaturated fatty acids, phospholipids, organosulfates, and sulfates. 12 These molecules often act as surfactants, coating the surface of the aerosol particles.¹³ These coatings in turn may control the entry of N_2O_5 and other gases into the particle or even catalyze reactions or provide additional reaction sites. For example, hexanoic acid has been shown to effectively reduce N₂O₅ reactivity by a factor of 3-4 at a monolayer coverage with artificial sea spray aerosols.³ The hydrolysis of N₂O₅ to HNO₃ was also reduced when adding hexanol or butanol to 60 – 68 wt % at 213 K.¹⁴ At a 0.6 ML coverage, N₂O₅ hydrolysis was reduced by 60%. Generally surfactants reduce reactivity by coating the surface and blocking gas transport to the aqueous subphase. This blocking occurs because long alkyl chains pack tightly enough to provide a tortuous diffusion path for the incoming gas molecule. Some headgroups can open new pathways and alter the overall reactivity of the aerosol particle. For example, DCl entry into 60 - 68 wt % sulfuric acid, is enhanced by the of small amounts hexanol and butanol.¹⁴ In this case, the ROH groups appear to add additional sites for interfacial protonation, allowing DCl molecules to more easily dissociate near the surface of the acid.

 Cl_2 reactions with Br^- have also been shown to be enhanced by the surfactant tetrahexylammonium bromide (THABr). ¹⁵ THA⁺ ions at the surface of glycerol appear to draw

in and polarize Cl₂, stabilizing the formation of Cl₂Br⁻. Cl₂Br⁻ can then react with an additional Br⁻ to form Br₂. When compared with a NaBr solution with a similar Br⁻ surface coverage, the Cl₂ reactivity was nearly three times greater with THABr than with NaBr. Surfactant reactivity appears to have a "sweet spot" in coverage in some cases, where the surface concentration is not too high to block entry but high enough to provide additional reaction sites. This behavior is observed for HCl reactions with both pentanoic acid and hexanol on sulfuric acid. ¹⁶ Cationic surfactants have been detected in aerosols and the sea surface microlayer in coastal regions, though not as abundantly as anionic surfactants. ¹⁷⁻¹⁸ Didodecyldimethylammonium chloride in particular has been identified in seawater. ¹⁹

Our objective is to investigate reactions of N_2O_5 with a catalytic or reactive surfactant that does not simply block gas transport. We wish to explore whether N_2O_5 reactions with halide ions can be enhanced by the presence of a surfactant and whether there is an optimal surfactant concentration for halogen activation. N_2O_5 certainly reacts with B_1^- when no surfactant is present, forming B_1^- and perhaps $B_1^ B_1^-$ We find below, however, that B_1^- is formed even more efficiently in the presence of THA_1^+ , a common phase-transfer catalyst. THA_1^+ was chosen because of its previously established ability to enhance the reaction of Cl_2 with B_1^- to generate B_1^- . In particular, we combine THA_1^+ with L_1^+ with L_2^+ with L_1^+ with L_2^+ with L_2^+

Our vacuum-based scattering experiments employ liquid glycerol as a solvent because of its low, 10⁻⁴ Torr vapor pressure. A comparison between glycerol and water is provided in Table

1. Glycerol is a protic liquid with a surface tension similar to that of water and a high dielectric constant roughly half that of water. It dissolves alkali halides, but not to the extent that water does. However, it is an even better solvent for organic surfactants such as THABr, whose solubility is at least twice as high in glycerol as in water. The use of glycerol can also be motivated by its combination of both protic (-OH) group and its hydrocarbon (C-C-C) backbone. This dual character makes salty and surfactant-coated glycerol a potential surrogate for the interfacial region of the sea surface microlayer and nascent sea spray aerosols which, as mentioned above, contain a wide variety of organic molecules and salts. Glycerol, however, is not water, and we hope to perform parallel experiments soon using water microjets for comparison.

Figure 1 depicts a possible reaction scheme showing the conversion of N₂O₅ to Br₂ using THABr. The experiments below indeed demonstrate that THA⁺ catalyzes the conversion of N₂O₅ and Br⁻ to Br₂. The ammonium headgroup, buried within a hydrophobic pocket formed by its four hexyl chains, may facilitate the formation of an N₂O₅Br⁻ complex or enhance the ionization of N₂O₅ to NO₃⁻ and NO₂⁺, leading to NO₂Br. The addition of 0.5 M NaCl or NaBr salt to THABr is found to increase the THA⁺ surface concentration to a point where the reactivity diminishes. In parallel, the addition of SDS also reduces Br₂ production, mostly likely because the dodecyl sulfate chains substitute for some THA⁺ at the surface. The ability of ammonium cations to enhance interfacial reactivity is also demonstrated by the more conversion of N₂O₅ to Br₂ by CTAB present in solution at only 10 mM. Despite its hexadecyl chains, CTA⁺ must not pack tightly enough to fully block N₂O₅ transport. These experiments are described below.

4.2 Experimental Procedure

4.2.1 Sample Preparation and Scattering Apparatus

Glycerol (≥99.0%), NaCl (≥99.0%), NaBr (≥99.5%), tetrahexylammonium bromide (THABr, 99%), sodium dodecyl sulfate (SDS, ≥99.0%), and hexadecyltrimethylammonium bromide (CTAB, ≥99%) were purchased from Sigma Aldrich and used without further purification. The salts were dissolved in glycerol by stirring and mild heating under a 10 mTorr vacuum in order to remove dissolved gases.

Figure 2 depicts the gas-liquid scattering apparatus. Two liquid reservoirs were used to quickly compare signals and minimize signal fluctuations in the incident N_2O_5 beam: one reservoir was typically filled with 50 mL of the THABr solution while the other contained another salt and/or surfactant solution. Both reservoirs were then cooled to 289 K under vacuum. In each reservoir, a rotating 5.0 cm dia glass wheel was coated by the liquid and then scraped by a Teflon rod to generate a continuously renewed 0.5 mm thick glycerol film. Incident beams of Ar or N_2O_5 were directed at one of the coated-wheels at a 45° angle. Each beam projects a 6.6 mm by 9.3 mm ellipse onto the glycerol film through a 8 mm x by 12 mm window. The 0.125 Hz rotation speed of the wheel exposes the film to the gas beam for 0.64 s. Exposure times as long as 6.4 s with a very slowly rotating wheel were used in selected experiments.

 N_2O_5 beams were generated by mixing N_2O_5 vapor with Ar or H_2 and expanding the mixture through a 100 μ m glass nozzle heated to 90 °C. N_2O_5 samples were kept between -15 and -35 °C, with estimated vapor pressures of 1–5 Torr. Incident beam measurements for H_2 mixtures yield energies of 110–160 kJ mol⁻¹. This wide range in translational energies is a consequence of the changing N_2O_5 sample surface area and H_2 -vapor mixing time within the N_2O_5 trap. This range shows the extent the beam energy might drift between experiments.

Consequently the N_2O_5 experiment can drift during the experiment but is accounted for by swapping between reservoirs every ~15 minutes. N_2O_5 mixtures seeded in Ar produced beam energies close to 10 kJ/mol. High-energy, 90 kJ mol⁻¹ Ar beams were produced from 2% Ar seeded in H_2 carrier gas.

Argon, N₂O₅, and Br₂ reagents and products desorbing or scattering from the glycerol film at 90° from the incident beam are chopped into 38 μs gas pulses by a spinning slotted wheel. These pulses traverse a flight path of 18.9 cm through a doubly differentially pumped chamber and are ionized by electron impact. The ions are then filtered by a quadrupole mass spectrometer and their arrival times are recorded as a time-of-flight (TOF) spectrum.

4.2.2 N_2O_5 Synthesis, Handling, and Characterization

 N_2O_5 was synthesized using the procedure described by Davidson et al.²² In the first step, NO gas was oxidized to N_2O_5 by a flow of O_3/O_2 from a Welsbach ozonator. The N_2O_5 then passed through a P_2O_5 glass trap to reduce impurity HNO₃ before being collected and stored in a glass trap using a dry ice/acetone bath. During the scattering experiments, the N_2O_5 trap was stored in an ethylene glycol/water bath cooled by dry ice. To further reduce the HNO₃ content in the molecular beam, the N_2O_5 vapor passed through a P_2O_5 trap and a trap filled with nylon mesh just before entering the glass nozzle. Final sample purity was assessed by scattering N_2O_5 from a Teflon block in vacuum. The resulting 46 m/z (NO_2^+) TOF spectra were analyzed by fitting to dual Maxwell-Boltzmann distributions that correspond to HNO₃ and N_2O_5 . These fits yield an HNO₃ impurity of ~15% in the N_2O_5 molecular beam.

4.2.3 Chemical Ionization Mass Spectrometry (CIMS)

For the CIMS measurements, N_2O_5 was made *in situ* via a process described by Bertram et al.²³ O_2 was first irradiated by a mercury UV lamp to produce O_3 via photolysis. The O_3/O_2

flow was then mixed with an excess of NO₂, resulting in a N₂O₅ vapor pressure of 8×10^{-5} torr and a total pressure of 1 atm. The N₂O₅ gas was sent through a 6.3 mm OD Teflon tube at 100 standard cm³ min⁻¹ and then over a 15.4 cm \times 1.3 cm PFA trough (modelled after Roberts et al.²⁴ filled with a glycerol solution. The exit gases were then mixed with a wet N₂ flow before entering the CIMS, which utilizes $\Gamma \cdot (H_2O)_n$ as the reagent ion.²⁵ This wet flow increases the relative humidity and $\Gamma \cdot (H_2O)_n$ adduct concentration. N₂O₅ was detected as the Γ adduct ($\Gamma \cdot N_2O_5$) at 234.7 m/z. Similarly, ClNO₂ was detected at both 207.5 m/z ($\Gamma \cdot CINO_2$) and at 209.5 m/z ($\Gamma \cdot CINO_3$) and at 209.5 m/z ($\Gamma \cdot CINO_3$) are separate ⁸¹Br natural abundance combinations), and BrNO₂ at 253 m/z ($\Gamma \cdot BrNO_2$). Mononitroglycerin (MNG), C₃H₇O₃NO₂, was detected as two different adducts, $\Gamma \cdot MNG$ and $\Gamma \cdot MNG(H_2O)$ at 263.1 m/z and 281.2 m/z. Dinitroglycerin (DNG), C₃H₆O₃(NO₂)₂, was detected as $\Gamma \cdot DNG$ at 307.7 m/z and at 325.8 m/z as $\Gamma \cdot DNG(H_2O)$.

Quantum calculations of the binding enthalpy for the I⁻ adducts indicate that the CIMS sensitivity to Br₂ (31 kcal/mol binding energy) MNG (27 kcal/mol), and DNG (29 kcal/mol), and BrNO₂ (25 kcal/mol) should be comparable as I⁻ forms strongly bound adducts, sufficient for transmission through the CIMS.²⁶⁻²⁷ In contrast ClNO₂ forms a much weaker adduct (17 kcal mol⁻¹), resulting in reduced sensitivity in the CIMS.

4.2.4 Surface Tension Measurements

The surface tensions of the solutions were determined using the Wilhelmy plate method. The downward force of a 16.5×0.1 mm Pt plate was measured within a N₂-purged enclosure by a microbalance with a precision of 0.1 mg. The surface tension of a 20 mL sample of a dewatered and degassed solution was measured six times and averaged for each reported data point. The waiting time during each measurement was approximately 10 minutes.

4.3 Results and Analysis

We investigated reactions of N_2O_5 with six glycerol solutions containing Br⁻: 2.7 M NaBr, 30 mM THABr, 30 mM THABr + 0.5 M NaBr, 30 mM THABr + 0.5 M NaCl, 30 mM THABr + 10 mM SDS, and 10 mM CTAB. Three types of measurements were made for most systems: surface tension, argon scattering, and Br₂ production following N_2O_5 collisions. CIMS measurements were also performed for N_2O_5 reactions with pure glycerol, 2.7 M NaBr, and 30 mM THABr + 0.5 M NaCl.

4.3.1 Surface Tension Measurements.

The surface activities of the THABr and CTAB solutions were estimated from measurements of the surface tension γ using a Wilhelmy plate. These measurements were analyzed according to an approximate form of the Gibbs adsorption equation:

$$n_{\text{surf}} \text{ (chain)} \approx \Gamma_{\text{chain}} = -\frac{1}{mRT} \left(\frac{\partial \gamma}{\ln c_{\text{chain}}} \right)_T$$
 (1)

where n_{surf} (chain) is the THA⁺ or CTA⁺ surface concentration (# chains/area), which is assumed to be equal to the surface excess Γ_{chain} at the low surfactant bulk concentrations c_{chain} of 0 to 30 mM for THABr and 0 to 10 mM for CTAB. The THABr and CTAB activity coefficients f^{\pm} multiplying c_{chain} were assumed to be near 1 and constant. In eq (1), m is the number of surfactant species, equal to two for THA⁺ and Br⁻ in pure glycerol because both species must segregate equally to the interfacial region to maintain electroneutrality. However, m is assumed to be one for THA⁺ in the presence of excess Br⁻ supplied by 0.5 M NaBr. It is also assumed to be one for THABr in 0.5 M NaCl, where Br⁻ mixes with a 17-fold greater number of Cl⁻ ions.

These *m* values follow from studies in water of dodecyltrimethylammonium with NaBr and NaCl.²⁸ For the THABr solutions, we focused on measurements at 15 and 25 mM in order to obtain good estimates of the slopes in this region; 30 mM and higher values were avoided because the solutions become cloudy in the presence of small amounts of dissolved water, presumably due to formation of THABr micelles. Table 2 shows the slopes of between 15 mM and 25 mM THABr as well as the number of measurements.

Figure 3 displays the surface tensions for the different surfactant solutions, all of which decrease with increasing surfactant concentration. Our previous measurements indicate that the 2.7 M NaBr and 30 mM THABr solutions have similar interfacial Br⁻ concentrations of 7 and 8 × 10^{13} cm⁻², respectively, with equal interfacial concentrations of THA⁺ and Br⁻ for 30 mM THABr. The present THABr measurements duplicate the results found in the earlier study, where measurements were made even closer to 30 mM.²⁹ This interfacial region must be thick enough to be charge neutral, and it therefore encompasses both THA⁺ and Br⁻, since surface tension measurements alone cannot measure their relative positions with respect to the surface. As shown below, Ar scattering measurements confirm that THA⁺ resides in the outermost layer. Similarly, measurements of CTAB yield a surface coverage of CTA⁺ and Br⁻ of 6 × 10^{13} cm⁻² at 10 mM, reflecting its greater surface activity of the hexadecyl chain.

Figure 3 shows that, near 20 mM, the surface tensions of THABr and THABr + 0.5 M NaBr solutions have similar slopes. However, the interfacial THA⁺ concentration is predicted to be nearly twice as large for THABr + 0.5 M NaBr $(1.4 \times 10^{14} \text{ cm}^{-2})$ as pure THABr $(8 \times 10^{13} \text{ cm}^{-2})$ because at high NaBr concentrations m is set to one at high NaBr concentrations, and without salt m is two. This higher THA⁺ surface segregation is likely driven by the large excess of Na⁺ and Br⁻, which effectively "salt out" the hydrophobic tetrahexyl cation.

Measurements for 30 mM THABr + 0.5 M NaCl solutions are more complicated to analyze because of the presence of 4 distinct ions in solution. The behavior of an analogous CTAB-NaCl aqueous solution (hexadecyltrimethylammonium and Br $^-$ in NaCl/H₂O), has been investigated by several groups and is summarized by Morgan et al.³⁰ They find that the ion selectivity constant, [$c_{surf}(Br^-)/c_{bulk}(Br^-)$]/[$c_{surf}(Cl^-)/c_{bulk}(Cl^-)$], is equal to 3.0 in water. We do not know if this Br $^-$ /Cl $^-$ segregation also occurs in glycerol. However, high precision He $^+$ scattering measurements by Krebs and Morgner of NaI in glycerol reveal that I $^-$ does *not* segregate to the surface.³¹ This lack of surface activity by the large and polarizable I $^-$ ion, typically considered to be the most surface-active halide, suggests that there should be little difference in segregation between Br $^-$ and Cl $^-$ in glycerol. Within this assumption, THA $^+$ is statistically surrounded by Cl $^-$ over Br $^-$ by 500 mM/30 mM = 17:1. The data below hint that this assumption may not be correct, and that THA $^+$ may selectively bind to Br $^-$. In either case, the surface tension measurements again indicate that the THA $^+$ surface concentration in the NaCl solution is 1.4×10^{14} cm $^{-2}$, essentially equal to that of THABr in the NaBr solution.

Lastly, the surface tensions of SDS + THABr solutions were measured but the changes were too small to discern a trend. Argon scattering measurements shown below do confirm that SDS reaches the surface.

4.3.2 High-Energy Argon Scattering.

High-energy argon scattering can be used to gauge the presence of hydrocarbon molecules at the surface of glycerol because long alkyl chains increase gas-surface energy transfer and the probability of Ar atom thermalization. Figure 4 shows TOF spectra of Ar atoms following collisions at 80 kJ mol⁻¹ with 2.7 M NaBr, 30 mM THABr, and 30 mM THABr + 0.5 M NaCl. In each case, the narrow component at early arrival times corresponds to impulsive

scattering (IS) and arises from Ar atoms that undergo one or a few collisions and retain a substantial fraction of their initial translational energy (~30 kJ/mol). The broader component at later arrival times corresponds to thermal desorption (TD) and arises from Ar atoms that fully dissipate their excess translational energy through multiple collisions before desorbing in a Maxwell-Boltzmann distribution at the 289 K liquid temperature. Figure 4 indicates that Ar atoms striking THABr-glycerol thermalize more often and scatter less often than from glycerol containing just NaBr. In contrast, the addition of 0.5 M NaCl to THABr only slightly changes the scattering pattern. Only small deviations were observed for the TD components of THABr + NaCl, THABr + NaBr, and CTAB relative to THABr alone (Table 2). The adsorbed alkyl chains of THA⁺ and CTA⁺ likely do not pack well and roughen the surface, promoting additional collisions that dissipate the incident energy of the Ar atoms. The Ar scattering patterns complement the surface tension measurements by showing that the alkyl chains dominate the outermost region. A significant change was observed with the addition of 10 mM SDS to 30 mM THABr, increasing the TD component by 19%. This was confirmed by N₂O₅ scattering measurements that showed a similar 19% increase in TD. The SDS/THABr mixture must further roughen the surface, perhaps because of differences in the packing of the single dodecyl and four hexyl chains per ammonium ion.

4.3.3 Conversion of N_2O_5 to Br_2 in 2.7 M NaBr versus 30 mM THABr.

Allan Bertram and coworkers have measured the fraction of N_2O_5 collisions that react with pure glycerol to be 0.0008 using a rotating wall flow cell coupled to a CIMS.³² This low reactivity makes it impossible for us to detect reactions of N_2O_5 by depletion of the incident beam, as shown by our attempt in Figure 5 to compare the loss of N_2O_5 upon exposing pure

glycerol and 30 mM THABr to N₂O₅ at a low collision energy of 10 kJ/mol. The two spectra appear to be statistically identical.

Upon the suggestion of Tim Bertram, we added Br⁻ ions into solution with the hope that this ion would react with N₂O₅ that is momentarily present in the interfacial or deeper regions of the solution before it evaporates. Our studies show that this indeed occurs: N₂O₅ reacts with every glycerol solution containing Br⁻ to produce Br₂. As depicted in Figure 1, the mechanism is presumed to be Br⁻ attack on molecular N₂O₅ or ionized NO₂⁺/NO₃⁻, leading to formation of BrNO₂ and NO₃⁻. Despite intensive searches, BrNO₂ was not detected in the gas phase and is instead hypothesized to react quickly with a second Br⁻ to produce NO₂⁻ and Br₂, which then evaporates from solution. Br₂ was not detected when exposing N₂O₅ to pure glycerol and does not spontaneously evaporate from Br⁻-containing solutions.

We first compared the formation of Br₂ from 2.7 M NaBr and 30 mM THABr using the dual liquid reservoirs in Figure 2 and low incident energy N_2O_5 ($\langle E_{inc} \rangle \sim 10$ kJ/mol), where nearly all impinging N_2O_5 molecules dissipate their energy and become momentarily trapped in the interfacial region. TOF spectra of the desorbing Br₂ are shown in Figure 6a; the 30 mM THABr solution produces more Br₂ by a factor of 1.46 ± 0.15 over the 2.7 M NaBr solution (90% confidence interval for 4 trials). This 1.46 ratio, however, is not equal to the relative reaction probabilities because the average solvation (or residence) time of Br₂ is very different in the two solutions. The characteristic Br₂ residence time in 2.7 M NaBr was measured to be 10^{-5} s in previous experiments in our lab.³³ This is very short relative to the 0.70 s N_2O_5 exposure and observation time of the solution. In this case, essentially all dissolved Br₂ molecules evaporate from solution in this 0.70 s time window. In contrast, the residence time of Br₂ in 30 mM THABr is much longer, measured in previous pulsed-beam experiments to exceed 0.1 s, mostly

likely because THA⁺ stabilizes the Br₃⁻ complex formed by Br₂ + Br⁻. This long residence time implies that a large fraction of Br₂ molecules remain in solution and do not evaporate over the 0.70 s exposure time. To account for the fraction of Br₂ molecules that remain in solution, we measured the Br₂ evaporation signal at the longest controllable exposure time of 7.0 s, ten times longer than our typical exposure and observation time of the rotating film-covered wheel. This longer time allowed more Br₂ to evaporate and increased the enhancement ratio from 1.46 to 2.70. We have made this correction in every solution containing THABr, but this will be verified in experiments following the thesis defense. Preliminary experiments suggest that not all Br₂ molecules have evaporated even within this 7.0 second window, and therefore the present ratio of 2.70 may still underestimate the enhancement by THABr.

In an effort to reduce signal averaging times and minimize fluctuations in the N_2O_5 beam intensity, we increased the beam flux 14-fold by seeding N_2O_5 in H_2 carrier gas, which accelerates N_2O_5 to high speeds and focuses it along the beam centerline. This substitution of H_2 for Ar as the seed gas also increases the N_2O_5 collision energy from 10 kJ mol⁻¹ (4 RT_{liq}) to ~140 kJ mol⁻¹ (30 RT_{liq}). At this high collision energy, only a fraction of the impinging molecules are expected dissipate enough energy to become momentarily trapped at the surface, a likely prerequisite for reaction. The thermalization probability depends on surface composition, and is higher for a surface covered with loosely packed alkyl chains, as noted above for Ar scattering. When these ~140 kJ mol⁻¹ N_2O_5 molecules are substituted for 10 kJ mol⁻¹ N_2O_5 , the observed ratio of Br_2 signals from 30 mM THABr and 2.7 M NaBr rises from 1.46 \pm 0.15 to 2.63 \pm 0.36 before residence time corrections. This increase implies that N_2O_5 thermalizes 1.8 times as often on the THABr solution as on the NaBr solution. This nearly two-fold increase reflects the kinematics of the collision, which favors energy transfer to the poorly packed hexyl chains that

likely promote multiple collisions. The chains also possess low-frequency vibrational and librational modes that should be readily excited upon impact. As shown in Table 3, the TD components in the TOF spectra of solutions containing surfactant are all within 6% except for 30 mM THABr + 10 mM SDS. Other than the SDS solution, these similar TD components imply similar thermalization probabilities of high-energy Ar atoms among the different solutions. We then assume that these similar TD ratios imply similar thermalization probabilities for N_2O_5 as well, since this molecule is heavier and will dissipate its excess collision energy even more effectively.³⁴ The exception of the SDS/THABr solution will be discussed later.

4.3.4 Salt Mixtures: 30 mM THABr + 0.5 M NaCl and 30 mM THABr + 0.5 M NaBr

Surface tension measurements in Figure 3 and Table 2 indicate that 0.5 M NaBr and NaCl cause additional THA⁺ to adsorb to the surface, which increases both the number and packing of interfacial THA⁺ cations. To explore the role of this packing and the presence of Br⁻, Cl⁻, and Na⁺ ions in Br₂ production, we directed high incident energy N₂O₅ at solutions containing 30 mM THABr + 0.5 M NaCl and 30 mM THABr + 0.5 M NaBr. In both cases, we see a significant decrease in the observed Br₂ signal, as shown in Figure 6b and Table 4. Surprisingly, the addition of 0.5 M NaBr did not increase the Br₂ signal, as might be expected from the higher Br⁻ bulk concentration, but lowered Br₂ production to 0.64 ± 0.04 compared with THABr alone. Furthermore the addition of 0.5 M NaCl to 30 mM THABr reduced the Br₂ signal even further to 0.46 ± 0.07 relative to THABr. However this signal is still large and suggests that Br⁻ still is preferred at the surface despite the much larger (17:1) bulk Cl⁻ concentration. We had expected a substantially lower reaction rate between N₂O₅ with Br⁻ since Cl⁻:Br⁻ ion ratio is 17:1. Previously mentioned He⁺ scattering experiments indicate that I⁻ does not segregate in glycerol when using NaI as the source of iodide. However, it may be that THA⁺ preferentially

binds to Br⁻ over Cl⁻, selectively dragging it to the surface. It would be fascinating to investigate this segregation further using He⁺ ion scattering or X-ray photoelectron spectroscopy.³⁵

4.3.5 Surfactant Effects: 30 mM THABr + 10 mM SDS and 10 mM CTAB

Different surfactant headgroups and alkyl chain lengths may alter the interfacial conversion of N_2O_5 and Br^* to Br_2 by eliminating catalytic sites and by blocking access to surface Br^* ions. To explore these possibilities, we added 10 mM of SDS to a 30 mM THABr solution as a means to introduce unreactive sulfate headgroups to the surface. The resulting solution was clear and did not produce micelles; however, surface tension studies were too insensitive to determine the extent to which dodecyl sulfate anions (DS^*) replaces THA^+ at the surface. Ar scattering (Table 3) does show a significant change in IS and TD components, suggesting SDS does reach the surface. The resulting Br_2 signal did decrease to 0.42 ± 0.05 , falling below that of both 0.5 M NaBr + 30 mM THABr and 0.5 M NaCl + 30 mM THABr. This value was obtained after lowering the Br_2 signal from THABr + SDS to counteract the 19% increase in thermalization, as directly measured by Ar and N_2O_5 scattering. The lower Br_2 production rate may arise for two reasons: the DS^* ions provide alkyl chains that can block entry, while the anionic headgroup can also potentially bind tightly with the cationic headgroup of the THABr and neutralize it.

We also measured Br_2 production from N_2O_5 reacting with a 10 mM CTAB solution, producing a 6×10^{13} cm⁻² film of hexadecyltrimethylammonium ions. This film brings slightly less Br^- to the surface (8×10^{13} cm⁻² for THABr) but has a significantly reduced relative signal of only 0.08 ± 0.02 . This reduction is likely due to the long 16-carbon chain that can prevent gas entry. Additionally, the methyl groups that surround the headgroup may not create the kind of hydrophobic pocket postulated for the tetrahexylammonium cation. We note that the small Br_2

production rate using CTAB has not yet been corrected for the potentially long residence time of Br_2 in solution. This effect will be measured soon, but even a doubling of the Br_2 signal would still leave the relative rate of 0.16 well below the value for the other systems.

4.3.6 Chemical Ionization Mass Spectrometric detection of reaction products

The scattering experiments rely on electron-impact ionization of the gas-phase molecules in the mass spectrometer. This method is not appropriate for detecting evaporating ClNO₂ or BrNO₂ because the parent ions immediately fragment and detection is possible only at 35 m/z (Cl⁺) and 81 m/z (Br⁺). These m/z values are unfortunately obscured by dissociative ionization of evaporating glycerol molecules, by Br⁺ from Br₂, and by evaporating HCl and HBr created upon acidification of the surface region by HNO₃ impurity in the incident N₂O₅ beam. Additionally, we were not able to identify the products of the reaction of N₂O₅ with pure glycerol.

In contrast to electron impact ionization, CIMS can identify these and other species as I adducts without fragmentation. N_2O_5 was exposed to solutions of pure glycerol, 0.5 M NaCl + 30 mM THABr, and 2.7 M NaBr glycerol in a static boat, as described in the Experimental Section. As shown in Figure 7, we observe mononitroglycerine and dinitroglycerine as the larger and smaller products of N_2O_5 with pure glycerol, which are found to evaporate slowly from solution. This nitration is analogous to the aqueous reaction $N_2O_5 + H_2O \rightarrow 2HNO_3$.

The reaction product Br₂ was also identified from both Br⁻ solutions upon exposure to N₂O₅, with three times smaller yield from the THABr/NaCl solution. Only a trace amount of ClNO₂ could be identified for the THABr +NaCl mixture, but its low binding enthalpy to I⁻ may mean that it is present in significant yield. No BrNO₂ product could be detected in the gas phase in any experiment, confirming its absence in the scattering experiments.

4.4 Discussion

Our key findings are summarized by the bar graphs in Figure 6. The production of Br_2 from N_2O_5 is heavily influenced by the presence of surfactant and salt. In particular, 0.03 M THABr enhances Br_2 production over 2.7 M NaBr by 2.7 \pm 0.3, despite similar surface concentrations of bromide ions of 7 and 8 x 10^{13} cm⁻². In every instance that salt or surfactant is added to 30 mM THABr, the resulting Br_2 production is reduced to values close to that of 2.7 M NaBr, effectively shutting off the enhancement. CIMS detection confirms the presence of Br_2 as well as additional reaction products, including mononitroglycerin, dinitroglycerin, and ClNO₂.

Faust et al. have previously shown that 0.03 M THABr enhances Cl₂ to Br₂ conversion by a factor of 3.3 when compared to 2.7 M NaBr.¹⁵ Following studies of Margerum and coworkers of Cl₂ in Br solutions in water, it was assumed that Cl₂ first reacts with Br to form Cl₂Br, which then reacts with Br to form ClBr₂, and then dissociates to Br₂ and Cl. The product Br₂ molecules then react reversibly with an additional Br to create Br₃ in competition with Br₂ evaporation. Faust et al postulated that the enhancement is caused by interactions between Cl₂ and THA⁺. Based on simulations of tetrabutylammonium iodide, THA⁺ likely orients itself such that one hexyl chain is in the bulk while the other three lie along the interface to minimize unfavorable interactions. This creates a charged hydrophobic pocket that can polarize Cl₂ and attract Br to form Cl₂Br. Similarly, this same hydrophobic pocket could impact the reaction of N₂O₅. One possibility is that the charged pocket can polarize N₂O₅, capturing it for longer times near the surface. This positively-charged pocket may also draw in Br to form N₂O₅Br, which then reacts with a second Br in a direct displacement of NO₃:

$$N_2O_5 + Br^- \rightarrow N_2O_5Br^-$$

$$N_2O_5Br^- + Br^- \rightarrow NO_2Br_2^- + NO_3^-$$

From here the reaction could continue to Br₂ by direct dissociation:

$$NO_2Br_2^- \rightarrow NO_2^- + Br_2$$

Alternatively, $NO_2Br_2^-$ could fall apart into $BrNO_2 + Br^-$, followed by attack of Br^- to displace NO_2^- :

$$NO_2Br_2^- \rightarrow BrNO_2 + Br^-$$

$$BrNO_2 + Br^- \rightarrow NO_2^- + Br_2$$

The existence of a BrNO₂ intermediate in glycerol remains hypothetical. Although we did not detect evaporating BrNO₂ using either electron impact or CIMS detection, we note that past studies have identified gas-phase BrNO₂ when passing N₂O₅ over solid NaBr using IR and UV spectroscopy.³⁶⁻³⁷

The mechanisms above rely on attack of Br^- on intact, molecular N_2O_5 . However, glycerol is a protic solvent that may support N_2O_5 ionization as contact ion pairs or solvent-separated ion pairs, followed by reaction of NO_2^+ with Br^- . This process may be aided by the high charge density in the THA^+ pocket:

$$N_2O_5 \rightarrow NO_2^+ + NO_3^-$$

$$NO_2^+ + Br^- \rightarrow BrNO_2$$

$$Br^- + BrNO_2 \rightarrow Br_2 + NO_2^-$$

 N_2O_5 is believed to undergo ionization in reactions in salty water;³⁸ however, the lower dielectric constant of glycerol (47 vs 80)³⁹ may allow both direct Br⁻ attack on molecular N_2O_5 and N_2O_5 pre-ionization to occur in solution. This change in mechanism is analogous to a shift from an S_N2 synchronous exchange of Br⁻ and NO_2 ⁻ to S_N1 attack of Br⁻ on NO_2 ⁺. A potential way to investigate this possibility is to simulate reactions of Br⁻ with N_2O_5 in a continuum solvent in

which the dielectric constant can be varied, both in the absence and presence of a hydrophobic cation. We hope to carry out these calculations in collaboration with Benny Gerber and his group.

We can conjecture on the timing and interfacial nature of the N₂O₅ + Br⁻ reaction. In our previous studies of Cl₂ with 2.7 M NaBr/glycerol solutions, we measured the residence time of Cl₂ to be less than a few microseconds using microsecond pulsed beams of Cl₂, implying that the initial Br⁻ attack must occur within this time. The products BrCl and Br₂ appeared within 10 µs and 30 µs, respectively. The short 1 µs initial reaction time corresponds to a diffusion depth of less than 5 Å. These studies were followed by pulsed beam experiments of Cl₂ with 30 mM THABr, again revealing that the initial attack on Cl₂ occurs within a few microseconds, corresponding to a similar ~5 Å reaction depth. In both cases, the initial Cl₂ reaction occurs within an interfacial region whose thickness is 1-2 glycerol monolayers.

We did not perform pulsed beam experiments due to the very challenging nature of these experiments, but we can still surmise that the reaction must be an interfacial one. This conjecture is based on the greater reactivity of the 30 mM THABr solution with respect to the 2.7 M NaBr solution, which have similar interfacial Br⁻ concentrations but bulk concentrations that favor NaBr by 90:1. Electroneutrality demands that THA+ and Br- reside closely together, such that surface THA⁺ drag Br⁻ toward the surface as well, in contrast to the Br- in NaBr that is distributed throughout the solution. This interfacial reactivity was expected on the basis of previous studies in our group and by others. In particular, Seong-Chan Park used pulsed beam experiments to determine reaction times of N₂O₅ with 60 wt % H₂SO₄ at 213 K of less than 2 microseconds, corresponding to a reaction depth smaller than 10 Å. Tim Bertram and coworkers have also explored surfactant control of N2O5 reactions. They found that the addition of 8 mM

phenol to 0.5 M ClNO₂ the conversion of N_2O_5 to ClNO₂ from 0.8 to 0.4.⁴⁰ The concentration of phenol was enhanced by a factor of 100 showing that the interfacial species strongly influenced reaction products. Gaston et al. have also investigated the reactive uptake of N_2O_5 into NaCl aerosols. They analyzed their data within a reaction-diffusion model and found that reactions occurred within 2-5 nm of the surface and were independent of particle size.³⁸

4.4.2 Influence of the addition of salt to THABr.

Previous students in our group have investigated the change in uptake and reactivity with addition of salt to a surfactant. Faust et al. found that adding 0.6 M NaCl to 0.03 M THABr reduced the reactive uptake of Cl₂ from 79% to 46%. This is attributed to excess Cl⁻ displacing Br⁻ from the interface. Clearly Cl⁻ is not effective at displacing interfacial Br⁻ ions since the reaction probability is by less than half, despite Cl⁻ outnumbering Br⁻ by 20:1. My own research exploring DCl entry through DS⁻ covered glycerol demonstrated a dramatic change in surface concentration and gas entry with the addition of salt. For example, the addition of 0.25 M NaCl to 5 mM SDS changed the surface concentration from 0.5×10^{14} cm⁻² to 1.37×10^{14} cm⁻². An enhancement is also observed when replacing cations, such as when Mg²⁺ is switched for Na⁺. This can be seen when 0.5 M NaCl is replaced by 0.25 M MgCl₂ in 2 mM SDS, which causes the DS⁻ surface concentration to increase from 1.2 to 1.5×10^{14} cm⁻². Increased surface concentrations led to a decrease in gas entry, the lowest being 11% at a surface concentration of 1.8×10^{14} cm⁻² from the addition of 0.25 M MgCl₂ to 10.9 mM SDS.

In this current study, the addition of both 0.5 M NaCl and NaBr to 30 mM THABr reduces the enhancement of N_2O_5 conversion to Br_2 . However in both cases the Br_2 production rate is still greater than 2.7 M NaBr. This is in agreement with the results of Faust et al., as they observed a 2.0 enhancement of Cl_2 reactivity over 2.7 M NaBr even after adding 0.6 M NaCl to

30 mM THABr. The decrease in Br₂ production can only partly be due to the displacement of Br by Cl because we also observe a decrease in Br₂ production with the addition of 0.5 M NaBr. This comparison suggests that there must also be another factor. Our surface tension studies indicate that the addition of 0.5 M NaCl or 0.5 M NaBr raises the surface concentration of THA⁺ from 0.8×10^{14} cm⁻² to 1.4×10^{14} cm⁻². It is possible that the THA⁺ ions that enhance N₂O₅ reactivity at lower coverages become too closely packed at higher coverages, blocking N₂O₅ contact with the ammonium group and subphase glycerol molecules and Br ions as the hexyl chains come close together. Based on an estimated van der Waals radius of $THA^+ = 4.7 \text{ Å}$, the THA⁺ cross sectional area is 70 Å². The maximum packing is therefore about 1.4 \times 10¹⁴/cm² in the case in which THABr forms a tight double layer of THA⁺ and Br⁻. This number density decreases to 9×10^{13} for an equally distributed surface monolayer of THA⁺ and Br⁻ using a Br⁻ van der Waals radius of 1.3 Å. Although there is uncertainty in these radii, it is remarkable that the upper van der Waals limit to the surface density corresponds to just the measured THA⁺ surface concentrations in the presence of NaCl or NaBr. This similarity provides support for the hypothesis that the THA⁺ hexyl chains are closely packed and can provide a tortuous path for N₂O₅ to reach the underlying suphase, reducing the production of Br₂.

A second possibility pertains to the role of the additional Cl^- and Br^- ions themselves. At large excess, these anions may flood the positively charged hydrophobic pocket and bind to the ammonium cation, deactivating it and reducing its effectiveness in ionizing or polarizing N_2O_5 . It may be possible to test this idea by adding SO_3^{2-} , a doubly-charged and surface-inactive anion that could bind particularly strongly to the ammonium cation.

4.4.3 Surfactant Control of N₂O₅ Reactivity.

Cationic/anionic surfactant mixtures have been well-studied for their cooperative effects. Electrostatic attractions between the headgroups can lead to changes in micelle formation, foaming, and surface adsorption. A study performed by Sohrabi et al. explored the change in surface excess when mixing CTAB and SDS, two soluble surfactants in water with oppositely charged headgroups. 41 Their findings suggest that the addition of oppositely-charged surfactants reduces electrostatic repulsion and increases the total surface concentration of surfactants. In our experiments, we investigated the addition of 10 mM SDS to a 30 mM THABr solution. Attempts were made to measure the change in surface tension when adding SDS to THABr, but little change was seen at the SDS concentrations used. One reason is that 0.01 M SDS + 30 mM THABr becomes slightly cloudy once mixed, implying the formation of subphase micelles that steal away any additional surfactant added to solution. Additionally, SDS may simply displace THABr at the surface, causing the surface tension to remain roughly constant. Although we were unable to discern surface tension differences, the Ar scattering reported in Table 2 shows that Ar atoms thermalize 19% more often on the surface of the SDS/THABr solution than on pure THABr, implying that some DS ions have added to or displaced THA⁺ at the surface.

The observed decrease in Br₂ production upon adding SDS could arise from at least two factors. Due to anionic/cationic interactions, the surface layer is likely more compact, just as when 0.5 M NaCl or NaBr is added to THABr solutions. The negatively charged sulfate group of the DS⁻ ion most likely occupies positions adjacent to THA⁺, and could then preoccupy the positively charged hydrophobic pocket, preventing it from interacting with the impinging N₂O₅. The dodecyl chains of DS⁻ ions are also much longer than the hexyl chains of THA⁺, potentially

imposing a greater barrier for N_2O_5 transport through the monolayer and into the liquid, as we previously observed in our DCl/SDS studies.

As we have discussed, we suspect that THABr provides a hydrophobic pocket that helps induce the reaction of N_2O_5 , similar to Cl_2 . CTAB is a surfactant that similarly has an ammonium headgroup and brings a Br^- ion with it to the surface region. 10 mM CTAB generates a surface concentration close to that of 30 mM THABr (6×10^{13} cm⁻² versus 8×10^{13} cm⁻²). The Br_2 produced from a 10 mM CTAB is only a small fraction (0.08 ± 0.02) of that produced by 30 mM THABr. This value has not yet been corrected for the finite residence time of Br_2 in solution and may potentially double. It is possible that the structure of the ammonium headgroup does not provide a charged hydrophobic region due to the long alkyl chain paired with three small methyl groups. Additionally, the long hexyl chain can produce a tangled pathway for the N_2O_5 to reach the surface. The maximum surface excess for CTAB on water has been determined to be 1.9×10^{14} cm⁻². Our 10 mM CTAB solution instead creates a coverage of This indicates we are achieving a coverage of 6×10^{13} cm⁻², or ~ 32 % of maximum coverage. This submonolayer coverage may therefore only partially block N_2O_5 entry, as observed in our studies.

4.4.4 Detection of ClNO₂, Br₂, MNG, and DNG: CIMS versus Molecular Beam Scattering.

The detection of ClNO₂, MNG, and DNG illustrates the advantage of chemical ionization over electron-impact ionization, which is used for the scattering studies. Attempts were made to detect ClNO₂ from 1.4 molal NaCl and 30 mM THACl glycerol using electron impact ionization in the scattering experiments, but without success. However, CIMS was able to detect the presence of at least trace quantities of ClNO₂ in a 30 mM THABr + 0.5 M NaCl solution. This suggests another reason for the reduction of Br_2 signal for 30 mM THABr + 0.5 M NaCl in the

scattering experiments: some of the N_2O_5 may react to form $ClNO_2$ instead. $ClNO_2$ was difficult to detect through electron-impact ionization because of the instability of the parent ion $ClNO_2^+$. Instead we relied on detecting $ClNO_2$ at Cl^+ ion mass at 35 m/z. Unfortunately both glycerol and HCl (from acidification of the solution by HNO_3 beam impurity) fragment at this m/z value, overwhelming the $ClNO_2$ signal. We estimate that the reaction probability of N_2O_5 forming $ClNO_2$ would need to be as high as 0.01 to be within our detection limit.

Unsuccessful attempts were made to detect MNG during the scattering experiments. Based on the CIMS measurements, MNG and DNG are the dominant products of the reaction with glycerol. The fragmentation of MNG and DNG is broad and has only one significant channel for detection at 76 m/z. Its dominant channel at 46 m/z could not be used due to fragmentation of unreactive N₂O₅. Additionally MNG and DNG are both soluble within glycerol and would have long residence times greater the time scale of the moving wheel. Stopped wheel studies were also performed but without success. The coated wheel was stopped for 30 minutes allowing MNG and DNG to evaporate into the detector even if their residence time was on the order of tens of minutes. However, the only signal detected at 76 m/z was from glycerol. We believe the glycerol background at this mass channel overwhelmed the MNG and DNG signals that would be present there.

The detection of MNG and DNG and trace amounts of ClNO₂ provide valuable insight into the reactions products following collisions of N₂O₅ with salty and surfactant-coated glycerol. A key unanswered question is whether these ions and surfactants actually enhance the reaction probability of N₂O₅. We are greatly frustrated by our inability to measure a depletion in the reflected N₂O₅ molecules upon collision with pure glycerol and 30 mM THABr shown in Figure 5. The similarities in the signals are in stark contrast with our earlier studies of Cl₂

collisions, where the uptake ranged from 23% for 2.7 M NaBr to 79% for 30 mM THABr. ¹⁵ The substantial noise in the TOF spectra in Figure 5 limit observations of reaction probabilities to a few percent. This is unfortunately larger than the 0.0008 probability measured by Alan Bertram for pure glycerol. This low reaction probability made our experiments extremely challenging. If we continue with these studies, we will reconstruct the machine to reduce the distance between molecular beam nozzle and film-covered wheel, and thereby increase the signal by a factor of ten.

4.4.5 Atmospheric Implications

While THA⁺ has not been specifically identified in the sea surface microlayer or sea spray aerosols, cationic surfactants have been detected and efforts have been made to detect quaternary ammonium surfactants in seawater, such as didodecyldimethylammonium chloride. Trimethyl ammonium groups are also present in lipids such as dipalmitoylphosphatidylcholine (DPPC). These surfactants have much longer hydrophobic chains than then the hexyl chains of THABr, and they likely do not present as exposed of a hydrophobic pocket at the surface. CTAB however has a similar alkyl chain but still manages to produce Br₂, showing that reactions can occur despite the long length of the single alkyl chain.

The oceanic concentration of Br⁻ is only 0.8 mM, roughly 700 times smaller than the 0.55 M Cl⁻ concentrations. Our 30 mM THABr and 0.5 M NaCl mixture also used Cl⁻ as the majority component, though at a much smaller ratio of ~17:1 Cl⁻:Br⁻. Despite this ratio, we still observed a significant Br₂ signal and only a decrease of 36% in signal relative to 30 mM THABr without salt. This indicates that THA⁺ is able to activate Br⁻ even when it is immersed within a 17-fold excess of Cl- ions. As postulated earlier, this effect may arise from preferential binding of Br- to THA+. Although we cannot extrapolate these results to oceanic concentrations, it is intriguing to

speculate that Br- may be more present at greater than a 1:700 Br-:Cl- ratio through the segregation of cationic surfactants, potentially allowing Br⁻ to be reactive even at oceanic concentrations.

Overall, the addition of oceanic levels of salt (~ 0.5 M) reduced the production of Br₂ in the molecular beam studies. Added salts raise the surface concentration of THA⁺ and flood the headgroup with Cl⁻ or Br⁻, thus preventing favorable interactions with N₂O₅. This is not the first time that surfactant packing has influenced N₂O₅ reactivity. Cosman et al. showed that reactive uptake of N₂O₅ on 60 wt % H₂SO₄ can be greatly influenced by the surface concentration and tail of the surfactant. In their studies, compact layers of surfactants with unbranched alkyl chains (1-hexadecanol, 1-octadecanol, stearic acid) could pack tightly and reduce reactive uptake by a factor of 17 to 61. However, the branched surfactant phytanic acid (C₁₉H₃₉COOH) was not able to pack tightly and did not reduce N₂O₅ reactive uptake within uncertainty.

Similarly our study shows that the loosely-packed THA⁺ overall does not inhibit production of Br₂ from N₂O₅ but once made more compact by the addition of 0.5 M salt, the production of Br₂ is reduced. The addition of SDS likely had a similar effect, increasing the surface concentration through anionic/cationic attraction and shielding. The compactness we observed for the salty solutions (\sim 80 Å²/THA⁺) was less dense than the phytanic acid compactness (\sim 45 Å²/phytanic acid); however, we still were able to see changes in reactivity at these low surface concentrations.

4.4.6 Conclusion

Our findings show that N_2O_5 reactivity is enhanced in the presence of THA⁺ when comparing solutions with similar Br⁻ surface concentrations (30 mM THABr vs 2.7 M NaBr). Furthermore our surface tension studies showed that the addition of 0.5 M salt to 30 mM THABr

increases the surface concentration of THA $^+$ from 8.0×10^{13} to 1.4×10^{14} cm $^{-2}$. The increased packing disrupts the interactions between THA $^+$ and N_2O_5 , reducing the observed Br $_2$ signal. Similarly the addition of 10 mM SDS to 30 mM THABr likely increases surface packing through cationic/anionic interactions of the headgroups and also decreases the observed Br $_2$ signal. Despite higher surface packing, all solutions containing THA $^+$ still produced more Br $_2$ than 2.7 M NaBr. 10 mM CTAB was also studied and despite its long hexadecyl chain, still produced observable Br $_2$ signals, though much smaller than the other solutions. `

References

- 1. Finlayson-Pitts, B. J.; Pitts, J. M., *Upper and Lower Atmosphere: Theory, Experiments, and Applications*. 1999.
- 2. Finlayson-Pitts, B. J.; Ezell, M. J.; Pitts, J. N., Formation of Chemically Active Chlorine Compounds by Reactions of Atmospheric NaCl Particles with Gaseous N₂O₅ and ClONO₂. *Nature* **1989**, *337*, 241-244.
- 3. Thornton, J. A.; Abbatt, J. P. D., N2O5 Reaction on Submicron Sea Salt Aerosol: Kinetics, Products, and the Effect of Surface Active Organics. *J. Phys. Chem. A* **2005**, *109*, 10004-10012.
- 4. Simpson, W. R.; von Glasow, R.; Riedel, K.; Anderson, P.; Ariya, P.; Bottenheim, J.; Burrows, J.; Carpenter, L. J.; Frie, U.; Goodsite, M. E.; Heard, D.; Hutterli, M.; Jacobi, H.-W.; Kaleschke, L.; Neff, B.; Plane, J.; Platt, U.; Richter, A.; Roscoe, H.; Sander, R.; Shepson, P.; Sodeau, J.; Steffen, A.; Wagner, T.; Wolff, E., Halogens and Their Role in Polar Boundary-Layer Ozone Depletion. *Atmos. Chem. Phys.* **2007**, *7*, 4375-4418.
- 5. McConnell, J.; Henderson, G.; Barrie, L.; Bottenheim, J.; Niki, H.; Langford, C. a. T., E., Photochemical Bromine Producation Implicated in Arctic Boundary-Layer Ozone Depletion. *Nature* **1992**, *355*, 150-152.
- 6. Oum, K. W.; Lakin, M. J.; Dehaan, D. O.; Brauers, T.; Finlayson-Pitts, B. J., Formation of Molecular Chlorine from the Photolysis of Ozone and Aqueous Sea-Salt Particles. *Science* **1998**, *279*, 74-76.
- 7. Dentener, F. J.; Crutzen, P. J., Reaction of N₂O₅ on Tropospheric Aerosols' Impact on the Global Distributions of NO_x, O₃, and OH *Journal of Geophysical Research* **1993**, 98, 7149-7163.
- 8. Jacob, D. J.; Evans, M. J., Impact of New Laboratory Studies of N₂O₅ Hydrolysis on Global Model Budgets of Tropospheric Nitrogen Oxides, Ozone, and OH. *Geophysical Research Letters* **2005**, *32*, L09813.
- 9. Macintyre, H. L.; Evans, M. J., Sensitivity of a Global Model to the Uptake of N₂O₅ by Tropospheric Aerosol. *Atmos. Chem. Phys.* **2010**, *10*, 7409-7414.
- Prather, K. A.; Bertram, T. H.; Grassian, V. H.; Deane, G. B.; Stokes, M. D.; DeMott, P. J.; Aluwihare, L. I.; Palenik, B. P.; Azam, F.; Seinfeld, J. H.; Moffet, R. C.; Molina, M. J.; Cappa, C. D.; Geiger, F. M.; Roberts, G. C.; Russell, L. M.; Ault, A. P.; Baltrusaitis, J.; Collins, D. B.; Corrigan, C. E.; Cuadra-Rodriguez, L. A.; Ebben, C. J.; Forestieri, S. D.; Guasco, T. L.; Hersey, S. P.; Kim, M. J.; Lambert, W. F.; Modini, R. L.; Mui, W.; Pedler, B. E.; Ruppel, M. J.; Ryder, O. S.; Schoepp, N. G.; Sullivan, R. C.; Zhao, D. F., Bringing the Ocean into the Laboratory to Probe the Chemical Complexity of Sea Spray Aerosol. *Proc. Natl. Acad. Sci. USA* 2013, 110 (19), 7550-7555.

- Jayarathne, T.; Sultana, C.; Lee, C.; Malfatti, F.; Cox, J. L.; Pendergraft, M. A.; Moore, K. A.; Azam, F.; Tivanski, A. V.; Cappa, C. D.; Bertram, T. H.; Grassian, V. H.; Prather, K. A.; Stone, E. A., Enrichment of Saccharides and Divalent Cations in Sea Spray Aerosol During Two Phytoplankton Blooms. *Environ. Sci. Technol.* 2016, 50, 11511-11520.
- 12. Cochran, R. E.; Laskina, O.; Jayarathne, T.; Laskin, A.; Laskin, J.; Lin, P.; Sultana, C.; Lee, C.; Moore, K. A.; Cappa, C. D.; Bertram, T. H.; Prather, K. A.; Grassian, V. H.; Stone, E. A., Analysis of Organic Anionic Surfactants in Fine and Coarse Fractions of Freshly Emitted Sea Spray Aerosol. *Environ. Sci. Technol.* **2016**, *50*, 2477-2486.
- 13. Oppo, C.; Bellandi, S.; Innocenti, N. G.; Stortini, A. M.; Loglio, G.; Schiavuta, E.; Cini, R., Surfactant Components of Marine Organic Matter as Agents for Biogeochemical Fractionation and Pollutant Transport via Marine Aerosols. *Mar. Chem.* **1999**, *63*, 235-253.
- 14. Park, S.; Burden, D. K.; Nathanson, G. M., The Inhibition of N₂O₅ Hydrolysis in Sulfuric Acid by 1-Butanol and 1-Hexanol Surfactant Coatings. *J. Phys. Chem. A* **2007**, *111*, 2921-2929.
- 15. Faust, J. A.; Dempsey, L. P.; Nathanson, G. M., Surfactant-Promoted Reactions of Cl₂ and Br₂ with Br⁻ in Glycerol. *J. Phys. Chem. B* **2013**, *117*, 12602-12612.
- 16. Burden, D. K. The Role of Chain Structure and Functional Group on HCl Entry into Surfactant-Coated Sulfuric Acid. University of Wisconsin Madison, 2010.
- 17. Gerard, V.; Noziere, B.; Baduel, C.; Fine, L.; Frossard, A. A.; Cohen, R. C., Anionic, Cationic, and Nonionic Surfactants in Atmospheric Aerosols from the Baltic Coast at Askö, Sweden: Implications for Cloud Droplet Activation. *Environ. Sci. Technol.* **2016**, 50, 2974-2982.
- 18. Alsalahi, M. A.; Latif, M. T.; Ali, M. M.; Magam, S. M.; Wahid, N. B. A.; Khan, M. F.; Suratman, S., Distribution of Surfactants along the Estuarine Area of Selangor River, Malaysia. *Marine Pollution Bulletin* **2014**, *80*, 344-350.
- 19. Bassarab, P.; Williams, D.; R., D. J.; Ludkin, E.; Perry, J. J., Determination of Quaternary Ammonium Compounds in Seawater Samples by Solid-Phase Extraction and Liquid Chromatography-Mass Spectrometry. *J Chromatogr A* **2011**, *1218*, 673-677.
- 20. Finlayson-Pitts, B. J.; Livingston, F. E.; Berko, H. N., Ozone Destruction and Bromine Photochemistry at Ground Level in the Arctic Spring. *Nature* **1990**, *343*, 622-625.
- 21. George, C.; Mirabel, P.; Schweitzer, F., Multiphase Chemistry of N₂O₅, ClNO₂, and BrNO₂. *J Phys. Chem. A* **1998**, *102*, 3942-3952.

- 22. Davidson, J. A.; Viggiano, A. A.; Howard, C. J.; Dotan, I.; Fehsenfeld, F. C.; Albritton, D. L.; Ferguson, E. E., Rate constants for the reactions of O₂⁺, NO₂⁺, NO₇⁺, NO₇⁺, NO₇⁻, and halide ions with N₂O₅ at 300 K. J. Chem. Phys. **1978**, 68, 2085.
- 23. Bertram, T. H.; Thornton, J. A.; Riedel, T. P., An experimental technique for the direct measurement of N₂O₅ reactivity on ambient particles. *Atmos Meas Tech* **2009**, *2* (1), 231-242.
- 24. Roberts, J. M.; Osthoff, H. D.; Brown, S. S.; Ravishankara, A. R.; Coffman, D.; Quinn, P.; Bates, T., Laboratory Studies of Products of N₂O₅ Uptake on Cl Containing Substrates. *Geophys. Res. Lett.* **2009**, *36*, L20808.
- 25. Kercher, J. P.; Riedel, T. P.; Thornton, J. A., Chlorine activation by N2O5: simultaneous, in situ detection of ClNO2 and N2O5 by chemical ionization mass spectrometry. *Atmos Meas Tech* **2009**, *2* (1), 193-204.
- 26. Iyer, S.; Lopez-Hilfiker, F.; Lee, B. H.; Thornton, J. A.; Kurten, T., Modeling the Detection of Organic and Inorganic Compounds Using Iodide-Based Chemical Ionization. *J Phys Chem A* **2016**, *120* (4), 576-587.
- 27. Lopez-Hilfiker, F. D.; Iyer, S.; Mohr, C.; Lee, B. H.; D'Ambro, E. L.; Kurten, T.; Thornton, J. A., Constraining the sensitivity of iodide adduct chemical ionization mass spectrometry to multifunctional organic molecules using the collision limit and thermodynamic stability of iodide ion adducts. *Atmos Meas Tech* **2016**, *9* (4), 1505-1512.
- 28. Okuda, H.; Ikeda, S., Preferential Adsorption of Ions on Aqueous Surfaces of NaCl Solutions of Dodecyldimethylammonium Bromide *J. Colloid Interface Sci.* **1988**, *131*, 333-348.
- 29. Brastad, S. M.; Albert, D. R.; Huang, M.; Nathanson, G. M., Collisions of DCl with a Solution Covered with Hydrophobic and Hydrophilic Ions: Tetrahexylammonium Bromide in Glycerol. *J. Phys. Chem. A* **2009**, *113*, 7422-7430.
- 30. Morgan, J. D.; Napper, D. H.; Warr, G. G.; Nicol, S. K., Measurement of the Selective Adsorption of Ions at Air/Surfactant Solution Interfaces *Langmuir* **1994**, *10*, 797-801.
- 31. DeZwaan, J. L.; Brastad, S. M.; Nathanson, G. M., The Roles of Salt Concentration and Cation Charge in Collisions of Ar and DCl with Salty Glycerol Solutions of NaI and CaI₂. *J Phys. Chem. C* **2008**, *112*, 3008-3017.
- 32. Gross, S.; Iannone, R.; Xiao, S.; Bertram, A. K., Reactive Uptake Studies of NO₃ and N₂O₅ on Alkenoic Acid, Alkanoate, and Polyalcohol Substrates to Probe Nighttime Aerosol Chemistry. *Phys. Chem. Phys.* **2009**, *11*, 7792-7803.

- 33. Dempsey, L. P.; Faust, J. A.; Nathanson, G. M., Near-Interfacial Halogen Atom Exchange in Collisions of Cl₂ with 2.7 M NaBr–Glycerol. *J Phys. Chem. B* **2012**, *116*, 12306-12318.
- 34. King, M. E.; Saecker, M. E.; Nathanson, G. M., The Thermal Roughening of Liquid Surfaces and Its Effect on Gas-Liquid Collisions. *J. Chem. Phys.* **1994**, *101*, 2539-2547.
- 35. Pohl, H.; Morgner, H.; Andersson, G., Energy-Loss Straggling of Helium Projectiles at Low Kinetic Energies: Deconvolution of Concentration Depth Profiles of Inorganic Salt Solutes in Aqueous Solutions. *Phys. Rev. A* **2008**, 78, 032904.
- 36. Finlayson-Pitts, B. J.; Livingston, F. E.; Berko, H. N., Synthesis and Identification by Infrared Spectroscopy of Gaseous Nitryl Bromide, BrNO₂. *J Phys. Chem.* **1989**, *93*, 4397-4400.
- 37. Frenzel, A.; Scheer, V.; Sikorski, R.; George, C.; Behnke, W.; Zetzsch, C., Heterogeneous Interconversion Reactions of BrNO₂, ClNO₂, Br₂, and Cl₂. *J. Phys. Chem. A* **1998**, *102*, 1329-1337.
- 38. Gaston, C. J.; Thornton, J. A., Reacto-Diffusive Length of N₂O₅ in Aqueous Sulfate- and Chloride-Containing Aerosol Particles. *J. Phys. Chem. A* **2016**, *120*, 1039-1045.
- 39. CRC Handbook of Chemistry and Physics, 91th Ed. . 2010.
- 40. Ryder, O. S.; Campbell, N. R.; Shaloski, M. A.; Al-Mashat, H.; Nathanson, G. M.; Bertram, T. H., Role of Organics in Regulating ClNO₂ Production at the Air–Sea Interface. *J. Phys. Chem. A* **2015**, *119*, 8519-8526.
- 41. Sohrabi, B.; Gharibi, H.; Tajik, B.; Javadian, S.; Hashemianzadeh, M., Molecular Interactions of Cationic and Anionic Surfactants in Mixed Monolayers and Aggregates. *J. Phys. Chem. B* **2008**, *112*, 14869-14876.
- 42. Szymczyk, K.; Janczuk, B., The Adsorption at Solution–Air Interface and Volumetric Properties of Mixtures of Cationic and Nonionic Surfactants. *Colloids Surf.*, A **2007**, 293, 39-50.
- 43. Bertram, A. K.; Knopf, D. A.; Cosman, L. M., N₂O₅ Reactive Uptake on Aqueous Sulfuric Acid Solutions Coated with Branched and Straight-Chain Insoluble Organic Surfactants. *J. Phys. Chem. A* **2008**, *112*, 2386-2396.



Figure 1. Schematic of the formation of Br_2 from the reaction of N_2O_5 and Br^- . THA^+ may help in either the ionization of N_2O_5 or help by polarizing N_2O_5 and enhancing the capture of Br^- .

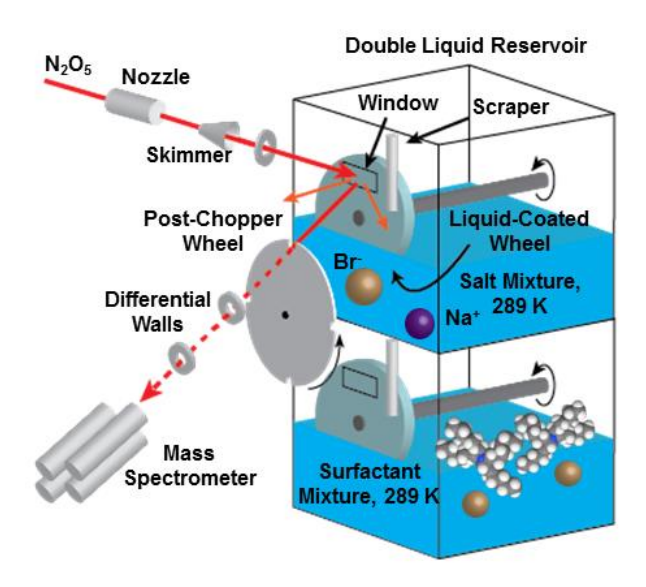


Figure 2. Experimental Setup. The liquid reservoirs are enclosed except for a 0.7-0.8 cm tall \times 1.2 cm wide hole in the front face, which allows N_2O_5 molecules to enter at 45° and collide with the rotating glycerol-coated wheel. The dual reservoir setup allows for quick comparisons of two solution to avoid drifts in signals due to beam fluctuations.

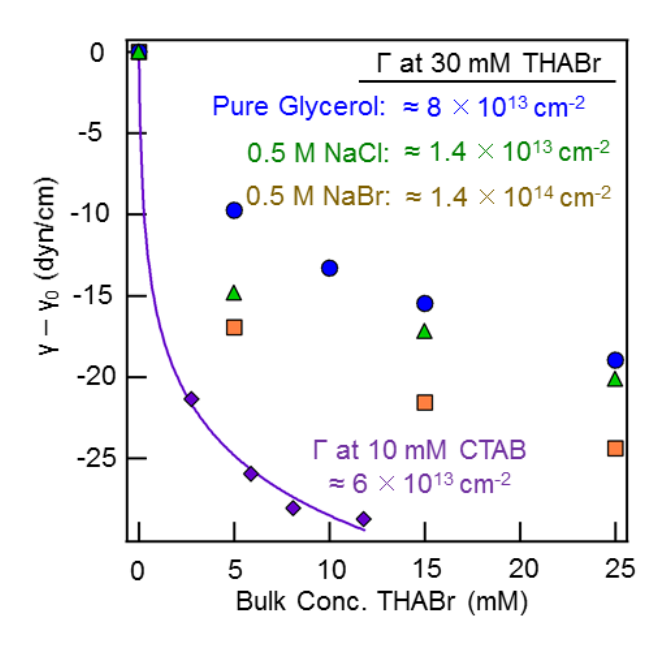


Figure 3. Summary of surface tension measurements. All analyses were performed using the slopes between 15 and 25 mM THABr, except for CTAB (purple) which used a Langmuir fit to determine surface concentration.

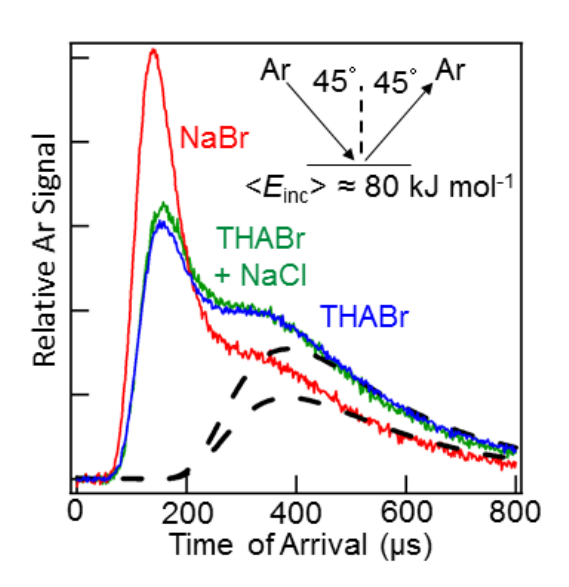


Figure 4. High-energy argon scattering from glycerol solution. Addition of surfactant corresponds to a decrease in IS and increase in TD.

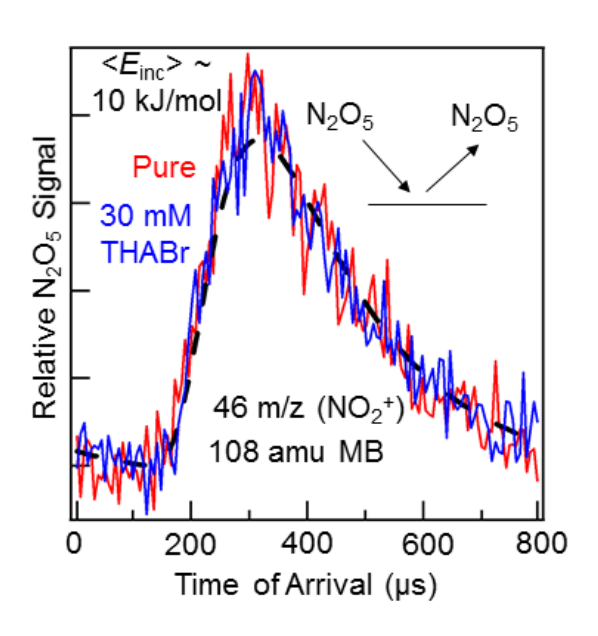


Figure 5. Low-energy N_2O_5 scatter from pure and 30 mM THABr glycerol. The signals are statistically identical preventing an analysis of reactive uptake of N_2O_5 .

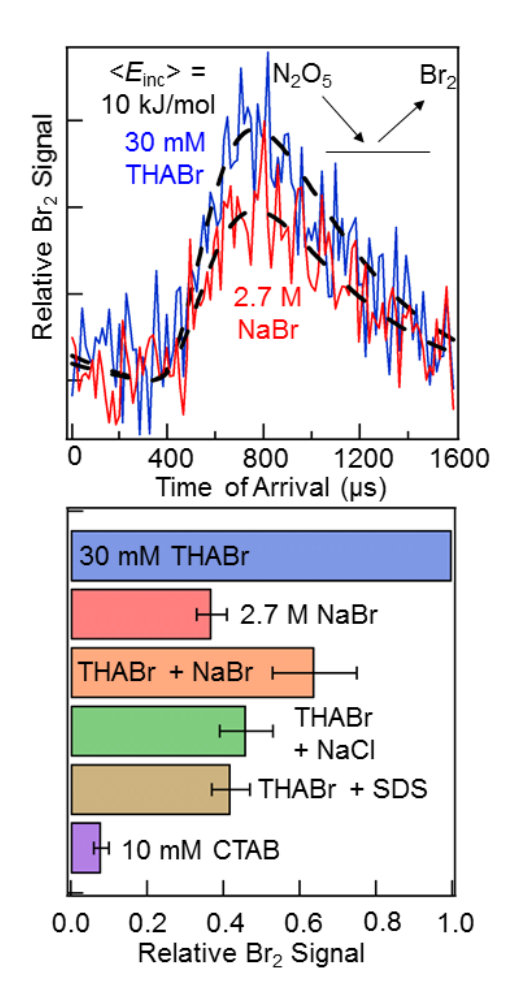


Figure 6. (Top) Br_2 signal comparison resulting from low-energy N_2O_5 scatter with 30 mM THABr and 2.7 M NaBr. 30 mM THABr shows a 1.46 ± 0.15 enhancement over 2.7 M NaBr. (Bottom) A summary of relative Br_2 production rates..

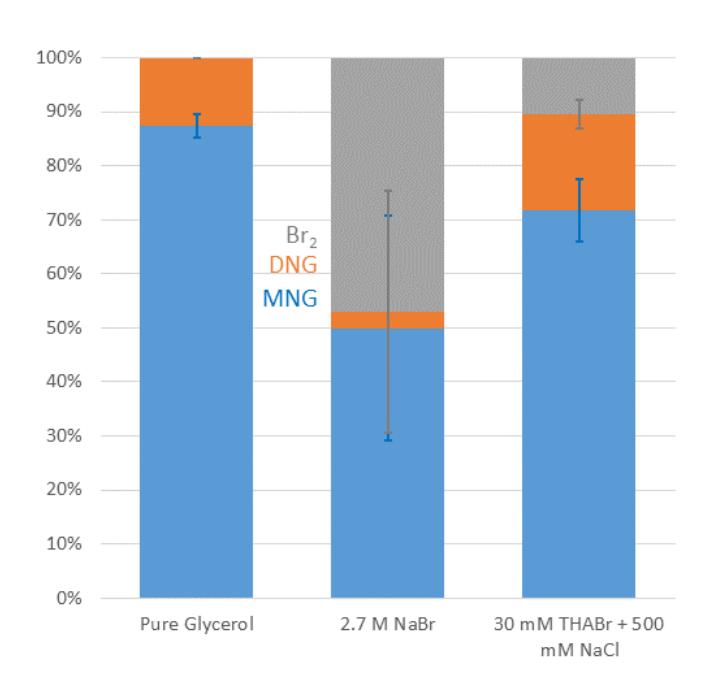


Figure 7. Product distributions from the reaction of N_2O_5 with various solutions as determined by CIMS. (MNG = mononitroglycerin, DNG = dinitroglycerin)

| Property | Glycerol (293 K, 1 bar) | Water (293 K, 1 bar) |
|---|----------------------------|----------------------|
| Surface Tension (dyn cm ⁻¹) | 63 | 73 |
| Dielectric Constant | 44 | 80 |
| Viscosity (cP) | 1400 | 1 |
| Vapor Pressure (Torr) | 1×10^{-4} | 18 |

Table 1. Comparison of important properties between glycerol and water.

| Solution | $\Delta\gamma$ | # of Trials | Surf. Conc. |
|--------------------------|---|-------------|--------------------|
| | $(\gamma_{25~\text{mM}} - \gamma_{15~\text{mM}})$ | # Of Titals | $(\#/\text{cm}^2)$ |
| 30 mM THABr | 3.3 ± 0.1 | 14 | 8.0×10^{13} |
| 30 mM THABr + 0.5 M NaBr | 2.8 ± 0.3 | 13 - 14 | 1.4×10^{14} |
| 30 mM THABr + 0.5 M NaCl | 2.9 ± 0.2 | 6 | 1.4×10^{14} |
| 10 mM CTAB | - | - | 6×10^{13} |

^{*}Uncertainties are presented as a 90% Confidence Interval

| Solution | $\Delta\gamma$ $(\gamma_{25~mM}-\gamma_{15~mM})$ | # of Trials | Surf. Conc. (#/cm ²) |
|--------------------------|--|-------------|----------------------------------|
| 30 mM THABr | 3.3 ± 0.1 | 14 | 8.0×10^{13} |
| 30 mM THABr + 0.5 M NaBr | 2.8 ± 0.3 | 13 - 14 | 1.4×10^{14} |
| 30 mM THABr + 0.5 M NaCl | 2.9 ± 0.2 | 6 | 1.4×10^{14} |
| 10 mM CTAB | - | - | 6×10^{13} |

^{*}Uncertainties are presented as a 90% Confidence Interval

Table 2. Summary of surface tension results and slopes from Figure 3.

| Solution | $< E_{THABr} > - < E_{Solution} >$ | Relative TD | Relative IS |
|----------------------------|------------------------------------|------------------------------|------------------------------|
| | (kJ/mol) | $(TD_{THABr}/TD_{Solution})$ | $(IS_{THABr}/IS_{Solution})$ |
| 30 mM THABr | 0 | 1 | 1 |
| 2.7 M NaBr | -6.1 ± 0.5 | 0.74 ± 0.04 | 1.53 ± 0.03 |
| 30 mM THABr + 0.5 M NaBr | -1.3 ± 0.4 | 1.03 ± 0.04 | 1.12 ± 0.02 |
| 30 mM THABr + 0.5 M NaCl | 1.3 ± 0.3 | 0.94 ± 0.03 | 1.05 ± 0.01 |
| 30 mM THABr + 10 mM SDS | 1.1 ± 0.3 | 1.19 ± 0.03 | 1.01 ± 0.02 |
| 10 mM CTAB | 3.7 ± 0.3 | 1.03 ± 0.03 | 0.83 ± 0.02 |

Table 3. Summary of high-energy scattering results. Second column shows the difference in IS energy after collision with the surface. A negative value suggests that less energy is loss upon collision with the solution than with 30 mM THABr. Third and fourth columns compare integrated IS and TD components relative to 30 mM THABr.

| C alustian | Relative Br ₂ Signal | |
|---------------------------|---------------------------------|--|
| Solution | (Solution / 30 mM THABr) | |
| 30 mM THABr | 1.00 | |
| 2.7 M NaBr | 0.37 ± 0.04 | |
| 30 mM THABr + 0.5 M NaBr | 0.64 ± 0.11 | |
| 30 mM THABr + 0.5 M NaCl | 0.46 ± 0.07 | |
| 30 mM THABr + 10 mM SDS | 0.42 ± 0.05 | |
| 10 mM CTAB | 0.04 ± 0.02 | |

Table 4. Summary of relative Br₂ signals. Solution signals have been estimated using the slowest wheel speed possible (1.5 Hz), giving an exposure time of 7.0 s.